Precision and limits of human vision

How visual resolution depends on ocular optics and spatiotemporal sampling characteristics of the foveolar photoreceptor mosaic

Doctoral thesis

to obtain a doctorate (PhD)

from the Faculty of Medicine

of the University of Bonn

Jenny Lorén Witten, née Reiniger

from Herzberg (Elster), Germany

Bonn, 2025

Written with authorization of

the Faculty of Medicine of the University of Bonn

First reviewer: Dr. Wolf M. Harmening

Second reviewer: Prof. Dr. Henning Boecker

Day of oral examination:

From the Clinic and Policlinic for Ophthalmology

Table of Contents

List of abbreviations

2AFC	Two-alternative-forced-choice
4AFC	Four-alternative-forced-choice
AMD	Age related macular degeneration
AO	Adaptive optics
AOSLO	Adaptive optics scanning laser ophthalmoscope
AOM	Acousto-optic modulator
$arcmin$	Minutes of arc (1/60 degree)
$arcsec$	Seconds of arc (1/3600 degree)
BCE	Before the Common Era
CDC	Cone density centroid
D	Diopter
deg	degree
FEM	Fixational eye movements
Hz	Hertz
HOA	Higher order aberrations
IR	Infrared
ISOA	Isoline Area
KHz	Kilohertz
LGN	Lateral geniculate nucleus
LOA	Lower order aberrations
logMAR	Logarithm of the minimum angle of resolution
MAR	Minimum angle of resolution
MHz	Megahertz
μm	Micrometer
nm	Nanometer
OCT	Optical coherence tomography
PCD	Peak cone density
PMT	Photomultiplier tube
PRL	Preferred retinal locus of fixation

PSF	Point spread function
QUEST	Quick estimate by sequential testing
RMS	Root-mean-square
RP	Retinopathia pigmentosa
SD	Standard deviation
SLO	Scanning laser ophthalmoscope
VA	Visual acuity
V1	Human primary visual cortex
V2	Secondary visual cortex
V3	Tertiary visual cortex

1 Abstract

The human ability to perceive fine spatial details, known as visual resolution, requires combined capacities of both the eye and the brain. Research in anatomy, physiology, and psychophysics has extensively studied the biological structures responsible for visual resolution and identified numerous optical, retinal, and cortical factors that affect its limits. However, the direct observation of small retinal structures is obstructed by optical aberrations, and postreceptoral connectivity in humans *in vivo* remains unexamined. By integrating psychophysical experiments, advanced imaging techniques, and retinal physiology, this thesis investigated the factors that define the limits of human vision and the mechanisms that optimize visual performance. I focused on the interplay between optical properties of the human eye, the anatomical structure and transient signals due to fixational eye movements which result in neural processes that shape our ability to perceive fine spatial details.

Inherent imperfections of the eye's optics such as defocus, astigmatism (known as LOA), and higher-order aberrations (HOA), affect the quality of the retinal image. Corrective measures, like spectacles and contact lenses address the LOA, but HOA remain more challenging to compensate for, thereby influencing the ultimate limits of optical image quality in natural vision. The first study evaluated the impact of habitual HOA on visual resolution and discrimination thresholds. The results showed that resolution acuity decreased significantly with stronger image degradation, while hyperacuity was not affected by HOA of the eye.

A key element for a deepened understanding of the underlying mechanisms within the visual system is the knowledge of the individual cell structure within the foveola, the central 1 degree of the retina. The foveola is densely packed with cone photoreceptors, whose spacing and organization are crucial for resolving fine spatial details. By correcting the individual optical aberrations in real-time, adaptive optics scanning laser ophthalmoscopy (AOSLO) achieves cellular-level image resolution in the living human retina. By employing AOSLO retinal imaging and micro-stimulation with a fixation target, the second study revealed a systematic displacement of the retinal locus preferably used for fixation and the topographical center of cone distribution. Given the high precision with which the eye

comes back to the same few hundreds of cones in a fixational task over a period of multiple years and the highly individual cell topography of the central retina, this demonstrated a close interplay during developmental processes of the foveolar photoreceptor arrangement and visual behavior.

In the third study, the visual demand was changed from the fixation task to a resolution task to study the impact of photoreceptor packing density and fixation behavior on visual acuity. The spacing between foveolar cones has long been assumed to be the limiting factor for visual acuity when optical aberrations are bypassed. This study showed for the first time that resolution acuity is highly correlated with the cone density at the retinal location that samples the stimulus. By precisely recording the eye motion across the cone resolved foveola, the extend of ocular drift as well as it's direction could be shown to be finely tuned to the task within only a few hundreds of milliseconds. The fixation behavior approached stimulus sampling with the most densely packed cones. This combination of quickly adaptable fixational eye motion and precise AO corrected stimulus display allowed for resolution thresholds about 18 % below the theoretical static sampling limit.

In summary, by integrating high-resolution imaging with psychophysical testing, the study results offer detailed insights into the role of the foveolar photoreceptor mosaic and the dynamics of fixational eye movements. These findings deepen the understanding of the human visual system's spatiotemporal processing and contribute to the broader fields of vision science and ophthalmology.

2 Introduction and aims with references

Human vision, with its optimization for high-acuity daytime vision, is one of the best among species (Caves et al. 2018). Only a few bird species can resolve even finer stimuli, whereas other visual systems work particularly well, for example, under low light conditions or under water, adapted to their respective habitat and habits. From a neuroethological point of view, the human sensory organs are adapted to the behavior of a mainly diurnal, socially centered generalist. The ability to see small details is essential to many demands in our daily routine (e.g. reading small text or identifying distant faces). Research in the fields of anatomy, physiology, and psychophysics has meticulously described the biological structures responsible for visual resolution, and identified many optical, retinal, and cortical factors that influence the limits of visual resolution. However, the direct view of small retinal structures is hindered by optical aberrations and the postreceptoral connectivity is not yet examinable in humans *in vivo*. In this thesis I aimed to scrutinize small-scale influences of ocular optics, photoreceptor mosaic and eye movements, thereby approaching the ultimate limit of visual resolution.

The following introduction will provide a general background of the human visual system and the applied methods. First, optical, neural, and dynamic components of the human visual system are outlined. Second, insights into the historical evolution and implications of retinal imaging and especially high-resolution imaging are given to emphasize the great need of being able to examine small anatomical structures of the retina. The third subsection introduces the field of psychophysics and two measurement methods that were applied in the studies. The last part of the introduction is then pointing out the aims of the three main research projects of my doctorate. The following three first-authorship publications, which resulted from the investigation of those research questions, form the central part of my thesis. As the final part, the general discussion provides an overview of the gained insights in the context of current literature, thereby summarizing and extending the specific discussions of the three publications.

2.1 Human visual system

The human visual system is a marvel of biological engineering, enabling us to perceive and interpret the world around us. It operates through a series of highly coordinated steps, transforming electromagnetic waves into meaningful visual experiences.

The light that enters the eye is focused by the cornea and lens on the central retina. In the retina, a thin layer of neural tissue at the back of the eye, photoreceptor cells convert the light energy into electrical signals, which are processed by intermediate retinal neurons before reaching the ganglion cells. The axons of the ganglion cells converge to form the optic nerve, which carries the signals to the brain. The optic nerves from both eyes meet at the optic chiasm, where fibers partially cross over to ensure that visual information from the left field of view is processed in the right hemisphere of the brain, and vice versa. From the optic chiasm, ten percent of neurons project to the superior colliculus (SC), which has an important role in controlling eye movements (Gilbert 2013; Opstal 2023). It is involved in controlling large and fast eye motions (Bergeron et al. 2003; Hafed et al. 2009), but at the same time plays a crucial role in modulating smaller roaming eye movements in a feedback loop to sensory inputs (Chen et al. 2019; Hafed et al. 2021). The majority of optic tract fibers (ninety percent) travel from the optic chiasm to the lateral geniculate nucleus (LGN) of the thalamus, a relay station that organizes and refines the visual information. Some LGN neurons have receptive field centers which are fed by a single photoreceptor (Derrington and Lennie 1984; McMahon et al. 2000; Sincich et al. 2009), a connectivity that is required to also retain fine spatial information throughout the processing stages. The fibers further project to the primary visual cortex (V1), which contains a "map of visual space" (Hubel and Wiesel 1974; Schira et al. 2007). Here, basic features such as edges and orientation are analyzed. This information is then distributed to higher visual areas in the brain, including the dorsal ("where") pathway, which processes spatial location and motion, and the ventral ("what") pathway, which identifies objects and their attributes. At this stage, the brain integrates visual information with data from other sensory modalities, prior experiences, and contextual cues. This results in the conscious perception of objects, allowing us to recognize shapes, colors, textures, and spatial relationships.

2.1.1 Optical quality of the eye - Cornea, lens and pupil

The ocular optics, mainly cornea and lens, relay photons reflected from, or emitted by, physical objects in the visual field onto a phototransductive surface, the retina. The retina must be at the precisely right plane to receive the relayed image in crisp focus (emmetropia). Extensive work has been done on characterizing the precision of ocular image formation and it's consequences to perception (for a review, see Westheimer 2006). For a mature eye (by an age of 13) with a flat lens (non-accommodating) the axial length is roughly 23 mm, which corresponds to an emmetropic refractive power of 59 diopters (D) (Larsen 1971; Kiely et al. 1982). If the relationship between optical power and axial eye length is not perfectly tuned, discrepancies result in one of two types of image defocus, myopia (image focused in front of the retina) or hyperopia (image focused behind the retina).

These optical errors are called wavefront aberrations, as rays of a point object are not perfectly focused at the same retinal location. As first recognized by Helmholtz, these aberrations can be visualized by observing a small point light source. Under low light conditions it would not appear as a small circle but rather as a star shaped spot, depending on the exact aberrations of the individual eye (Helmholtz 1867). The distribution of light in the retinal image can be mathematically described by the point spread function (PSF), it depends on and is inversely related to the pupil size (Williams and Hofer 2003). It's exact form is the reason why we see an individually different star shape when looking at a small point light source in the dark. The underlying wavefront aberrations are typically quantified by sets of Zernike polynomials that represent the closest approximation to the actually measured wavefront of the eye (Born and Wolf 1989).

The most commonly described ocular imperfections are defocus and astigmatism (2^{nd} order Zernike polynomials). Those lower order aberrations (LOA) are today routinely measured and corrected by glasses or contact lenses. The earliest refractive correction spectacles were crafted in the 14th century to correct presbyopia (age-related farsightedness), as other refractive errors had not yet been recognized. Correction of myopia was first recorded around 1500, while it wasn't until another 200 years later that it became commonplace (Rubin 1986). Only in the 19th century, the astigmatic component in ocular refraction has been described for the first time (Young 1801), which set the basis for the

sphero-cylindrical correction that is common optometric routine up to this day.

Thus, it is well known that the eyes optics are far from perfect, which impacts our visual perception. The source of most of the eyes aberrations are imperfections in the cornea and lens (Roorda and Glasser 2004), with the lens partially compensating for some of the corneal aberrations, resulting in a higher optical quality of the entire eye than either element attains on its own (Artal et al. 2006). The eyes monochromatic aberrations are on average composed of 85 % LOA and 15 % higher order aberrations (HOA) (Jayabalan and Bille 2019). Even when successfully compensating for LOA, the more complex HOA can also lead to noticeable retinal image distortions as HOA introduce multiple focus points of an observed object. Out of the HOA, the 3^{rd} and 4^{th} order of Zernike polynomials (especially coma, trefoil and spherical aberrations) are known to have the biggest impact on the wavefront function (Iskander et al. 2001). The coma shape is like an offset pimple which is a consequence of a displacement between cornea apex, lens center and the optical axis. Spherical aberrations arise due to the aspherical shape of the cornea. It occurs when light rays passing through the center of cornea and lens have a slightly different focus than those passing through the periphery. Thus, there can be strong inter-individual differences in the general optical quality of eyes.

At the same time, the effective impact of LOA and HOA is highly dependent on the size of the finely adjustable dynamic aperture in front of the lens, the pupil. The musculus sphincter pupillae and dilatator pupillae adjust its size in response to varying light conditions, thereby regulating the amount of light that reaches the retina with an effective light ratio of 1:28. Acting similarly to a camera's aperture, the pupil also controls the depth of field and sharpness of the image projected onto the retina. When the pupil constricts in bright light, it reduces the amount of wavefront aberrations and increases the depth of field which enhances the sharpness and clarity of the image while at the same time introducing a strong effect of diffraction. Conversely, in low-light conditions, the pupil dilates to allow more light to reach the retina, which results in a reduced effect of diffraction but an increased amount of ocular wavefront aberrations which can reduce image sharpness. In a perfect (diffraction-limited) eye, the incoming plane wavefront would be converted to a spherical one and focused to a point on the retina (Westheimer 2006), which is also possible to be achieved by aberration correction in an adaptive optics (AO) optical system (see

2.2.2). Otherwise, in a human eye, especially for large pupil sizes, optical imperfections of the eye do not allow for a diffraction-limited retinal image.

2.1.2 Retina and photoreceptors

The retina, thin and orderly layered neural tissue, lines the back of the eye and is responsible for converting light into neural signals. The human retina is specialized to detect visible light, comprised of electromagnetic waves with a wavelength between 360 and 850 nm (Stockman and Rider 2023). The light has to pass layers of downstream neurons before inducing phototransduction in the outer segments of the photoreceptor cells (Tomita 1970; Yau 1994). The light-evoked hyperpolarization signals are transmitted to and processed by neurons in the rest of the retina by a complex, highly organized and converging network of electrical and chemical synapses (Ramón y Cajal et al. 1995; Dowling 2011). As a result, from initially about 100 million photoreceptors, roughly 1 million ganglion cell axons exit the retina as bundles, forming the optic nerve (Oppel 1967; Rodieck 1973).

The majority of photoreceptors are rods. Those about 92 million cells (Curcio et al. 1990) are highly sensitive to low light levels, which makes them essential for scotopic and mesopic vision, at the cost of lower spatial and temporal resolution. The roughly 5 million cone photoreceptors (Curcio et al. 1990) are responsible for color vision and high acuity vision under photopic to mesopic light conditions. The three types of cones are sensitive to different wavelengths, S- (short), M- (medium) and L-cones (long) have their maximum absorbance at 420 nm, 534 nm and 563 nm, respectively (Bowmaker and Dartnall 1980). This trichromatic system allows humans to perceive a wide ranged color spectrum. S-cones do not only differ from M- and L-cones morphologically (Curcio et al. 1991; Ahnelt et al. 1987; Calkins et al. 1998) and genetically (Nathans et al. 1986), but comprise only 5 -10 % of the cone mosaic, are rather regularly distributed and present only outside the central fovea (Curcio et al. 1991; Bumsted and Hendrickson 1999). In contrast, M- and L-cones are more randomly distributed and concentrated within the central 1-degree diameter of the fovea, termed foveola. This is an outcome of a developmental process called fovealization. The cellular architecture of the cone mosaic changes during development to optimize for high acuity daytime vision (Caves et al. 2018; Tuten and Harmening 2021). During early prenatal development, cone photoreceptors originate from progenitor cells in

the retinal neuroepithelium (Reese 2011). The initially evenly distributed cones start to migrate towards the foveola during prenatal development. By mid-gestation, cones are more densely packed in the central retina compared to the periphery (Yuodelis and Hendrickson 1986). Although the fovea itself is not yet fully formed, each foveolar cone already connects to one ON and one OFF bipolar followed by one ON and OFF midget retinal ganglion cell, called "privat line", to convey each cone's spatial information to postreceptoral stages of visual processing (Zhang et al. 2020). The width of the foveola and the cone diameters reach an adult stage around 45 months of age. At this time, cone outer segment length and packing density are still only half the typical adult values (Yuodelis and Hendrickson 1986) and continue to be maximally thinned and densely packed for peak spatial sampling, which is approached at an age of 5 to 6 years (Hirsch and Curcio 1989; Rossi and Roorda 2010; Williams and Coletta 1987; Lai et al. 2011). For optimized high-acuity daytime vision, the foveola is free of glia cells and potentially shadowing blood vessles and postreceptoral neurons are displaced centrifugally (Hendrickson and Yuodelis 1984; Syrbe et al. 2018). Histological samples and, more recent, *in vivo* retinal imaging data demonstrated that the highest cone density in the central foveola is highly variable between individuals (Curcio and Allen 1990; Wang et al. 2019; Cava et al. 2020; Reiniger et al. 2021). Cone spacing increases rapidly with eccentricity (Osterberg 1935; Curcio et al. 1987; Curcio et al. 1990; Chui et al. 2008) and outside the foveola, also visual resolution and contrast sensitivity fall off rapidly (Volkmann 1846; Green 1970; Enoch and Hope 1973; Marcos and Navarro 1997). This is not only due to the lower density of cones, but also as the neuronal convergence between cones and midget retinal ganglion cells (mRGCs), strongly increases towards periphery (Curcio and Allen 1990; Dacey 1993; Kolb and Marshak 2003; Drasdo et al. 2007). The mRGCs serve as projection neurons and convey the information to the rest of the brain, therefore the organization of mRGC receptive fields is essential for the spatial resolution capacity across the retina (McMahon et al. 2000; Sincich et al. 2009; Rossi and Roorda 2010; Zhang et al. 2020).

2.1.3 Fixational eye motion

The preceding description of the visual system was missing one very important and complex factor for visual processing, fixational eye movements. They have been observed in a

wide variety of species (Martinez-Conde and Macknik 2008), including the owl (Steinbach 2004), a predator who is commonly believed to keep its eyes very still.

Even when we try to maintain stable fixation of an object or a stimulus, tiny, involuntary eye movements incessantly occur. They include microsaccades (rather straight and fast movements), drifts (slow meandering movements), and tremor (oscillations superimposed on drifts) which transport the visual image across the retinal photoreceptor mosaic (Martinez-Conde et al. 2004). These movements are rather microscopic compared to other eye motion (e.g. when scanning the environment or following a moving target of interest), but still shift the retinal image of the stimulus across several hundreds of photoreceptor cells. It is remarkable that we are usually unaware of them, as they produce motion signals at speeds that would be immediately noticeable if they came from external objects rather than from our own eyes (Kowler 2011). The role of fixational eye motion for visual perception is diverse, complex and of increasing interest to researchers from different fields.

The role of fixational eye movements for vision have been debated since their discovery in the 1950s (for reviews, see Rolfs 2009; Rucci and Poletti 2015; Rucci and Victor 2015; Poletti 2023). Fixational eye movements have long been considered to be a challenge for the visual system to overcome in order to create fine spatial representations (Burak et al. 2010; Pitkow et al. 2007) and prevent perceptual blurring of the image (Packer and Williams 1992), but a variety of parallel and subsequent research revealed that eye movements rather enhance visual perception, because they impact the structure of neural activity (Leopold and Logothetis 1998; Greschner et al. 2002; Kagan et al. 2008) and transform a static scene into a spatiotemporal input signal (Rucci and Desbordes 2003; Rucci et al. 2007; Ko et al. 2010; Poletti et al. 2013; Chen and Hafed 2013; Rucci and Victor 2015; Ratnam et al. 2017; Intoy and Rucci 2020). Most research focused on microsaccades, which have been argued to serve different functions (for a review, see Poletti and Rucci 2016). One of the early hypothesis is that they are a targeted movements, counteracting fixational errors (Engbert and Kliegl 2004; Nachmias 1959; Cornsweet 1956) by quickly bringing back the target of interest towards the spatial locus of attention (Hafed and Clark 2002; Engbert and Kliegl 2003). After it became possible to immobilize stimuli on the retina in a laboratory condition and it was observed that visual percepts tend to

progressively loose contrast until they disappear completely under this retinal stabilization (Ditchburn and Ginsborg 1952; Barlow 1952; Riggs and Ratliff 1952; Yarbus 1967), Microsaccades have been argued to prevent the image from fading (Ditchburn et al. 1959; Martinez-Conde et al. 2006; McCamy et al. 2012). However, there is evidence that image fading is no concern for the visual system (Poletti and Rucci 2010; Kowler 2011) and therefore fading prevention might just be an "incidental, if not accidental" role of fixational eye motion (from Nachmias 1961). Between microsaccades, a slow roaming motion, called ocular drift, has been shown to encode fine visual details (Ahissar and Arieli 2012; Ahissar et al. 2016) and play an important role in visual resolution (Intoy and Rucci 2020; Clark et al. 2022). Ocular drift lets the retina meander across the fixated stimulus at frequencies between 1 and 40 Hz with amplitudes between a few arcmin and a few tens of arcmin. It is associated with a low-amplitude (< 1 arcmin), high frequency (40 - 100 Hz) jitter of the eye, known as ocular tremor (Eizenman et al. 1985), which is suggested to be a by-product of the clock-like firing of oculomotor neurons. In this thesis, those two components of fixational eye motion are considered together under the term 'ocular drift' to refer to the inter-saccadic motion of the eye. Originally formulated by Hering 1899, it has been argued for more than a century, that ocular drift may be beneficial to visual acuity by not just refreshing, but structuring neural activity (Averill and Weymouth 1925; Marshall and Talbot 1942; Arend 1973; Ahissar and Arieli 2001; Ahissar and Arieli 2012). However, there is still ongoing debates about the beneficial or detrimental role of fixational eye movements for vision.

2.2 Retinal Imaging

Among all sensory systems, the eye offers a unique possibility: because of its transparent cornea and lens, the eye affords a direct and non-invasive view of the retina and its individual receptors. The ability to look inside the living human eye is central to our understanding of how signals that arise from single sensory neurons are transformed into perception. Imaging the retina also plays a crucial role in clinical diagnostics, management, and monitoring of various eye conditions. Today, there are several standard tools for retinal imaging that are routinely used in research as well as clinical settings (Furlan 2017). In parallel, a variety of imaging systems, specialized for scientific purposes, is

used for basic research and further exploring technological developments. The following two chapters will provide an overview into the evolution of retinal imaging devices with a focus on visualizing individual retinal cells.

2.2.1 Historical background of retinal imaging devices

Most of our understanding about pathologic changes in the living human eye is based on findings of the past two centuries. Before, a large number of important eye diseases were simply called 'black cataract', since it has not been possible to visualize and differentiate them. Since 1850, when Helmholtz built and published the first ophthalmoscope based on a candle as light source and a semitransparent mirror set at an angle (Helmholtz 1851), the idea behind direct ophthalmoscopy did not change. The first drawings of the human retina were published by the Dutch ophthalmologist van Trigt in 1853 (Muirhead 2020) and inspection and evaluation of the retina became routine.

The first useful photographic images that showed retinal blood vessels were obtained by the German ophthalmologist Gerloff (Gerloff 1891), before in 1910, Gullstrand developed the fundus camera (Gullstrand 1910), a concept that is still one of the primary methods of retinal imaging. Two further breakthroughs in retinal imaging were the development of confocal scanning laser ophthalmoscopy (cSLO, Webb et al. 1987) and optical coherence tomography (OCT, Huang et al. 1991). cSLO enhanced optical sectioning by using a pinhole to block out-of-focus light, resulting in higher resolution and contrast, enabling estimates of 3-D shape. However, only OCT allowed for truly 3-D optical sectioning of the retina by providing fast and high-resolution cross-sectional imaging (Velthoven et al. 2007).

In 1985 first attempts to resolve single photoreceptors in a living vertebrate eye with a conventional analoge fundus camera were made in garter snake (Thamnophis, Land and Snyder 1985) and cane toad (Bufo marinus, Jagger 1985). Even though those observations were made in animal eyes with good optics and large photoreceptor cells they suggested that imaging single photoreceptors would also be possible in the human eye. Following further technological advances, Miller et al. developed a digital fundus camera to resolve individual photoreceptors in the human eye > 0.5 deg from the foveal center (Miller et al. 1996). Shortly after, also cSLO and OCT have been shown to enable the

visualization of the retinal cone mosaic outside the foveal center in young adults with good optical quality, when carefully correcting their defocus and astigmatism (Wade and Fitzke 1998; Pircher et al. 2006; Reiniger et al. 2017). However, the lateral resolution of all these ophthalmoscopic imaging devices was still not satisfactory and limited to the individual eye's remaining ocular aberrations that were imposed on the retinal image. The need for more robust methods, which allow for an inspection of retinal degeneration etc. on a cellular level even in eyes with larger LOA or HOA led to further developments.

2.2.2 High resolution retinal imaging - Adaptive optics scanning laser ophthalmoscopy

To improve the spatial resolution of the retinal image to a cellular level, the current state-of-the-art is the use of adaptive optics (AO), a method that has its origins in astronomy. The conceptual framework of continuously measuring and correcting the dynamic optical path distortions had been laid out by Babcock 1953. As one of the main applications, AO were implemented in ground-based telescopes to overcome turbulences in the earth's atmosphere (Hardy et al. 1977). First attempts to implement an active mirror in an SLO have been made by Dreher et al. 1989, but their approach was missing a wavefront sensor and could therefore only correct previously determined LOA aberrations (defocus and astigmatism). In parallel, several approaches had been made to examine the aberrations of the eye (Tscherning 1894; Hartmann 1900; Rosenblum and Christensen 1976; Howland and Howland 1977; Walsh et al. 1984; Artal et al. 1988; Campbell et al. 1990; Howland 2000), but the objective measurement and correction of the ocular wavefront aberrations only became fast and simple enough to be routinely used after applying Hartmann-Shack wavefront sensing (Shack and Platt 1971) to the human eye (Liang et al. 1994; Liang and Williams 1997). It improved the precision to measure wavefront distortions by dividing incoming light into a grid of small sub-apertures using a lenslet array (instead of a single lens), each focusing light onto a detector. The position of the focused spots indicates the local slope of the wavefront, enabling detailed and accurate reconstruction of the wavefront's shape. Typically, a deformable mirror is used to correct the phase errors of the aberrated wavefront, although other methods, like liquid crystal spatial light modulation and custom phase-correcting plates, have been proposed (Vargas-Martin et al. 1998;

Burns et al. 2002). A deformable mirror has a flexible surface that can be dynamically adjusted by numerous small actuators to correct for optical aberrations in real time.

The integration of AO took advantage of the larger numerical aperture offered by larger pupils, resulting in the first reliable images of the human cone photoreceptor mosaic and led to improvements in visual acuity and contrast sensitivity when stimuli were projected along the same optical path (Liang et al. 1997; Roorda and Williams 1999; Roorda and Williams 2002; Yoon and Williams 2002). Significant improvements in retinal image resolution could be made in flood-illumination (Liang et al. 1997; Rha et al. 2006), cSLO (Roorda et al. 2002; Merino and Loza-Alvarez 2016) as well as OCT (Miller et al. 2003; Hermann et al. 2004; Jonnal et al. 2016). However, flood-based systems were not able to compensate for the continuous fixational eye movements or to correct for the effects of chromatic dispersion and were therefore unable to target specific retinal loci. A huge amount of trials and statistical interference were necessary to link psychophysical performance to the retinal structure (Hofer et al. 2005; Makous et al. 2006).

SLO appeared to serve as a better alternative, as it also has the major advantage of being able to optically section the retina to target a particular retinal depth (Roorda et al. 2002). Its core principle is that a focused imaging beam is scanned across the retina in a raster pattern, with the back reflected light being continuously sensed by a photon detector to generate a pixel by pixel image at video rates (Webb et al. 1980). It was recognized to be particularly relevant for research and clinical applications, when it was shown that stimuli could be directly encoded in the SLO images by modulating the imaging raster. This allowed to generate stimulus projections at targeted retinal locations to measure visual acuity and perimetric sensitivity (Mainster et al. 1982). The combination of SLO and AO was therefore promising and after a quarter century still continues to evolve and produce new outcomes in terms of engineering advances and scientific discoveries (Williams et al. 2023). The diffraction limited imaging beam allowed for *en face* imaging with unmatched lateral and axial resolutions of 1.9 and 33 μm, respectively (Zhang and Roorda 2006; Roorda 2010). The advancements enabled by AO have sparked numerous innovative approaches to further enhance ophthalmic image quality, pushing it towards the theoretical limit. These strategies included reducing residual aberrations generated within the AO ophthalmoscope itself (Burns et al. 2007; Gómez-Vieyra et al. 2009; Kowalski et al.

2022) and refining scanning accuracy (Akondi et al. 2020). Further improvements, which enabled the resolution of the smallest photoreceptor cells, foveal cones and rods, were made by using shorter wavelength imaging and stimulation (Grieve et al. 2006; Dubra and Sulai 2011), optimizing system designs and using deformable mirrors with more actuators or higher speed (Zhang et al. 2006; Dubra et al. 2011; Merino et al. 2011). Due to those unprecedented features, AOSLO has been used to study photoreceptor structure in a variety of retinal diseases (for reviews see: Morgan et al. 2023; Britten-Jones et al. 2024). The possibility to precisely select the location of the stimulus on the retina also offered the capability to directly link retinal structure and visual function (Rossi and Roorda 2010; Tuten et al. 2012; Harmening et al. 2014; Wang et al. 2015; Kocaoglu et al. 2016).

2.3 Psychophysics

Psychophysics as a field, termed by Gustav Fechner (Fechner 1860), seeks to understand human perception in relation to the physical properties of a stimulus. Within vision science, measures such as sensitivity to light stimuli, color vision, contrast sensitivity or visual acuity are typically quantified by threshold measurements. However, psychophysics extends beyond vision science and applies to all sensory organs.

Since threshold estimation in psychophysics depends on the participant's responses, the nature of the task and questioning influences the results. In psychophysical experiments, observers are given a specific task, such as identifying the location of a gap in a black ring on a white background (Landolt ring) among eight possible directions (see publication 1, Figure 1B). Each stimulus-response combination, scored as correct or incorrect, constitutes a trial. After multiple trials, the probability of a correct response can be estimated. To quantify how performance varies with stimulus size, a psychometric function can be fit to model the proportion of correct responses (ordinate) relative to the gap size (abscissa) (see Publication 3, Figure 1e). If the observer were guessing, the chance probability would be 1/8 (0.125), while an easily visible stimulus could yield probability as high as 1. The observer's threshold is the gap size needed to achieve a predetermined proportion correct, typically halfway between chance and perfect performance.

The classical psychophysical methods for determining these thresholds by varying the presented stimulus strength or size include the method of constant stimuli, method of

limits, and method of adjustment (Treutwein 1995; Kingdom and Prins 2010). In this thesis I employed two adaptive staircase procedures: PEST (Best Parameter Estimation by Sequential Testing) and QUEST (Quick Estimate by Sequential Testing)(Lieberman and Pentland 1982; Watson and Pelli 1983), which can be categorized as a modified form of the method of adjustment.

I applied psychophysics to study perceptual performance, thereby focusing on the fundamental threshold of acuity. Various methods for defining acuity have been proposed. However, they can be summarized in four widely accepted categories:

- Minimum visible acuity (detection of a feature),
- Minimum resolvable acuity (resolution of two features),
- Minimum recognizable acuity (identification of a feature) and
- Minimum discriminable acuity (discrimination of a change in a feature, e.g. size, position or orientation) (Levi 2011; Hooke 1705; Jurin 1738).

Resolution and identification acuity differ between individuals, but share the same magnitude and are collectively referred to as visual acuity, while detection acuity remains relatively consistent across individuals (Levi 2011). To investigate individual differences in acuity thresholds relative to variations in HOA and photoreceptor densities, I utilized visual acuity and discrimination acuity (commonly known as hyperacuity) as performance measures. The following sections provide a background on the evolution of research into the limits of acuity.

2.3.1 Visual acuity

Visual acuity (VA) refers to the precision to which small visual details can be resolved or identified. Since being a reasonably fast, affordable and easy method to find visual deficiencies due to either optical or neural causes, it has been a cornerstone in ophthalmology and optometry for centuries, evolving significantly over time to meet the demands of clinical practice and scientific inquiry.

The evaluation of vision has already been of importance in ancient times. One of the earliest forms of assessing acuity was the distinction of double stars in ancient Egypt and

Persia (Wade 2007; Jong 2024). The ability to perceive e.g. the separation of the two stars Mizar and Alcor in the Big Dipper was considered good vision, and would have required a vision quality equivalent to today's 20/20 Snellen VA (60 arcsec) (Bohigian 2008).

While the general idea of relating the minimum angle of resolution to a corresponding size on the retina was already mentioned by Euclid around 300 BCE, it took two millennia until, based on Hookes experimental results of the minimum angle being 1 arcmin (60 arcsec) for most people (Hooke 1674), Porterfield, Smith and Jurin estimated the size of a "retinal fiber" to be between 0.003 and 0.005 mm (about 40 - 70 arcsec) (Porterfield 1737; Smith 1738; Jurin 1738). Those values were very similar to early measures derived from microscopy about a century later (Treviranus 1837). By combining his visual acuity measurements with microscopic examinations of the retina in other species, Treviranus was able to correlate indirect estimates of retinal cell size with direct observations. Based on later histological preparations of human retinae, which allowed for indirect comparisons of human foveolar photoreceptor density and psychometric resolution thresholds, the hypothesis that photoreceptor spacing imposes the fundamental limit for visual resolution in the center of the fovea was addressed more clearly, and put forward (Green 1970; Enoch and Hope 1973; Thibos et al. 1987; Curcio and Allen 1990; Marcos and Navarro 1997).

Still, the direct comparison of resolution threshold and cone density within the same individual *in vivo* remained to be inaccessible, as the resolution of fine retinal structures is hindered by the optical aberrations of the eye. In the vast majority of eyes, also visual acuity is limited by optical aberrations (Campbell and Green 1965). More recently, AOSLO based imaging and stimulation (see 2.2.2) allowed for simultaneous *in vivo* measurements of the photoreceptor mosaic and visual acuity outside the foveola. It could be shown that between 0.5 and 2.5 deg eccentricity visual acuity was not limited by cone density but rather by the lower midget retinal ganglion cell density (Rossi and Roorda 2010). A comparison between resolution thresholds and the size of the photoreceptors which were actually used for resolving small details still relied on estimates rather than a direct comparison. Therefore, to confirm or correct the hypothesis that visual resolution is limited by cone spacing, it is still necessary to directly measure high-resolution thresholds while visualizing the foveolar photoreceptor mosaic in the same individuals.

2.3.2 Hyperacuity

Hyperacuity refers to the ability of the visual system to discriminate differences in position, size or orientation with a precision that is considerably smaller than the size or spacing of foveolar cones (Westheimer 1975). Deviations in hyperacuity thresholds can sometimes reveal visual processing problems that are not apparent with standard visual acuity tests (Hu et al. 2021).

It was already noticed in the early 18th century that threshold estimates were influenced by different stimuli employed to assess visual resolution (Hooke 1705; Jurin 1738). Volkmann examined resolution with the aid of threads from a spider's web and measured the limit of discrimination between 2 threads to be about 5 to 8 arcsec (Volkmann 1836). Therefore, the values for resolving the separation between a pair of spider's threads was about an order of magnitude lower than typical visual acuity (being about 40 - 70 arcsec). Volkmann argued that human visual resolution could not be limited by the sizes of retinal cells, because it was finer than their dimensions (Volkmann 1846), before the term hyperacuity was coined. Later, Wülfing tested acuity as a positional offset between a pair of lines, a stimulus now know as Vernier bars (see Publication 1, Figure 1B), and also found thresholds in the range of arcsec (Wülfing 1892). By 1899 Hering had reached the conclusion that mechanisms that transcended the simple receptor mechanism were at work here (Hering 1899). He suggested that the high precision could be explained by neural averaging of the stimulated receptor signals during small eye movements (Strasburger et al. 2018). Various approaches have been made to study the perceptual characteristics of hyperacuity (Westheimer and McKee 1975; Westheimer et al. 1976; Westheimer and McKee 1977; Bradley and Skottun 1987; Whitaker and MacVeigh 1991), and physiological and computational models have been developed to shed light on the mechanisms behind hyperacuity (Findlay 1973; Geisler 1984; Jiang et al. 2017).

Today, it is known that hyperacuity depends on the ability of the neural visual system to interpret subtle differences within the spatial patterns of the optical image on the retina. This emphasizes the high precision of neural processing to identify the location of the centroid of retinal light distribution. Thus, Herings assumption still holds. It is likely that cone absorption profiles, with respect to tiny fixational eye movements, play an important role in resolving Vernier bars with a precision that is finer than the spacing of foveal cones.

2.4 Aims of the projects

Human visual performance can be limited by both optical (refractive errors or aberrations, see 2.1.1) and neural (retinal or cortical, see 2.1.2) factors. Understanding the limits of visual resolution from both perspectives is crucial for advancing vision science, medical applications, and technology. By today, the optical aberrations of the eye can be measured very accurately. Consequently, the variation in optical quality between eyes and its implications for vision have been extensively studied. While it is indisputable that LOA, which are routinely corrected by glasses or contact lenses, have a direct impact on visual resolution, it is still unclear in how far also the smaller HOA systematically impact visual acuity and hyperacuity (Villegas et al. 2008). Various additional factors, such as photoreceptor and ganglion cell density, neural adaptation, and cortical processing, may influence the measurable impact of HOA (Rossi and Roorda 2010; Artal et al. 2004; Artal 2015; Hou et al. 2017; Jiang et al. 2017; Wang et al. 2018). Thus, in the 1st study of this thesis I aimed to access whether even the small-scale differences between individual optical imperfections of the eye influence visual resolution and discrimination thresholds (see 2.3).

Since optical imperfections hamper our ability to see with sharp focus, they at the same time restrict the view into the eye and the examinability of small retinal structures *in vivo*. Therefore, the photoreceptor cells, which are the first specialized sensory neurons in visual signal processing, are difficult to visualize and quantify. Nevertheless, the fact that there must be a limiting element for human visual resolution has intrigued researchers since centuries (Wade 2007). Based on indirect comparisons of cone cell densities in histological preparations and threshold measurements that were obtained in different individuals, the hypothesis has been put forward that when optical limitations could be bypassed, the cone spacing in the center of the retina would impose the fundamental limit for visual resolution. The central ±0.5 degrees of the human retina, called foveola, are of special importance when studying visual perception, as the retinal location which is preferably used for fixation lies within the foveola and it's anatomical characteristics are tuned for peak spatial vision.

The AOSLO has demonstrated immense potential as an imaging tool, providing real-time, high-resolution *in vivo* retinal images (Williams 2011). Beyond imaging, it also serves as a platform for psychophysical experiments by enabling the targeted testing of individual

photoreceptor cells (see 2.2.2). However, due to technological limitations in resolution, previous AOSLO-based psychophysical research has focused on targeting the slightly larger cones outside the foveola (Rossi and Roorda 2010) and the hypothesis of the foveolar cone spacing being the fundamental limit for visual resolution remained unverified. Therefore, after reaching cone cell resolution within the foveola with our AOSLO, the further aims of my doctorate were to study the cellular mosaic within this most central part of the retina and it's direct relationship to visual function in a fixation and a resolution task. First, a fixation task was chosen to investigate whether the foveolar location with highest cell density is also used during targeted fixation of an object or whether another relationship between individual topography and fixation behavior exists (2nd study). Second, a visual acuity task was chosen to investigate the ultimate visual resolution limit, when optical influences are bypassed and photoreceptor arrangement can be directly linked and analyzed (3rd study).

This yet rather static description of those relationships disregards a very important and omnipresent additional factor that also gets even more crucial to be analyzed when being able to link it to the sensory neurons in the center of the foveola. Small and unconscious fixational eye movements occur incessantly (see 2.1.3) and their role for vision has been debated since decades. On the one hand, they have been considered to induce smearing and pose a challenge for the visual system to overcome in order to maintain sharp spatial representations (Pitkow et al. 2007; Burak et al. 2010). On the other hand, research revealed that eye movements enhance visual perception (Greschner et al. 2002; Kagan et al. 2008; Rucci et al. 2007; Ratnam et al. 2017; Intoy and Rucci 2020). Therefore, the last aim of my doctorate was to put a particular focus on questioning how small-scale fixational eye movements align with the cell resolved anatomy of the foveola (2nd study) and on how this interaction might help or hinder visual function in a high resolution acuity task (3rd study).

Taken together, I investigated the static and dynamic components of fine spatial vision with a focus on optical aberrations, the cone cell mosaic within the foveola, and fine-scale fixational eye movements.

2.5 Introduction references

Ahissar, E. and Arieli, A. Figuring space by time. *Neuron*. 2001; 32 (2): pp. 185–201

Ahissar, E. and Arieli, A. Seeing via Miniature Eye Movements: A Dynamic Hypothesis for Vision. *Front. Comput. Neurosci.* 2012; 6 (11): pp. 1 –27

Ahissar, E., Arieli, A., Fried, M., and Bonneh, Y. On the possible roles of microsaccades and drifts in visual perception. *Vis. Res*. 2016; 118: pp. 25–30

Ahnelt, P. K., Kolb, H, and Pflug, R. Identification of a subtype of cone photoreceptor, likely to be blue sensitive, in the human retina. *J. Comp. Neurol.* 1987; 255 (1): pp. 18–34

Akondi, V., Kowalski, B., Burns, S. A., and Dubra, A. Dynamic distortion in resonant galvanometric optical scanners. *Optica*. 2020; 7 (11): pp. 1506–1513

Arend, L. E. Spatial differential and integral operations in human vision: implications of stabilized retinal image fading. *Psychol. Rev.* 1973; 80 (5): pp. 374–395

Artal, P. Image Formation in the Living Human Eye. *Annu. Rev. Vis. Sci.* 2015; 1: pp. 1–17

Artal, P., Benito, A., and Tabernero, J. The human eye is an example of robust optical design. *J. Vis.* 2006; 6 (1): pp. 1–7

Artal, P., Chen, L., Fernández, E. J., Singer, B., Manzanera, S., and Williams, D. R. Neural compensation for the eye's optical aberrations. *J. Vis.* 2004; 4 (4): p. 4

Artal, P., Santamaría, J., and Bescós, J. Retrieval of wave aberration of human eyes from actual point-spread-function data. *J. Opt. Soc. Am. A*. 1988; 5 (8): pp. 1201–1206

Averill, H. L. and Weymouth, F. W. Visual perception and the retinal mosaic. II. The influence of eye-movements on the displacement threshold. *J. Comp. Psychol.* 1925; 5 (2): pp. 147–176

Babcock, H. W. The possibility of compensating astronomical seeing. *Publ. Astron. Soc. Pacific*. 1953; 65 (386): pp. 229–236

Barlow, H. B. Eye movements during fixation. *J. Physiol.* 1952; 116 (3): pp. 290–306

Bergeron, A., Matsuo, S., and Guitton, D. Superior colliculus encodes distance to target, not saccade amplitude, in multi-step gaze shifts. *Nat. Neurosci.* 2003; 6 (4): pp. 404–413

Bohigian, G. M. An Ancient Eye Test-Using the Stars. *Surv. Ophthalmol.* 2008; 53 (5): pp. 536–539

Born, M. and Wolf, E. The Diffraction Theory of Aberrations. In: *Princ. Opt. Electromagn. Theory Propagation, Interf. Diffr. Light*. New York: Pergamon Press, 1989: pp. 459–490

Bowmaker, J. K. and Dartnall, H. J. Visual pigments of rods and cones in a human retina. *J. Physiol.* 1980; 298: pp. 501–511

Bradley, A. and Skottun, B. C. Effects of contrast and spatial frequency on vernier acuity. *Vision Res.* 1987; 27 (10): pp. 1817–1824

Britten-Jones, A. C., Thai, L., Flanagan, J. P., Bedggood, P. A., Edwards, T. L., Metha, A. B., and Ayton, L. N. Adaptive optics imaging in inherited retinal diseases: A scoping review of the clinical literature. *Surv. Ophthalmol.* 2024; 69 (1): pp. 51–66

Bumsted, K and Hendrickson, A. Distribution and development of short-wavelength cones differ between Macaca monkey and human fovea. *J. Comp. Neurol.* 1999; 403 (4): pp. 502–516

Burak, Y., Rokni, U., Meister, M., and Sompolinsky, H. Bayesian model of dynamic image stabilization in the visual system. *Proc. Natl. Acad. Sci. U. S. A.* 2010; 107 (45): pp. 19525–19530

Burns, S. A., Marcos, S., Elsner, A. E., and Bara, S. Contrast improvement of confocal retinal imaging by use of phase-correcting plates. *Opt. Lett.* 2002; 27 (6): pp. 400–402

Burns, S. A., Tumbar, R., Elsner, A. E., Ferguson, D., and Hammer, D. X. Large-field-of-view, modular, stabilized, adaptive-optics-based scanning laser ophthalmoscope. *J. Opt. Soc. Am. A*. 2007; 24 (5): pp. 1313–1326

Calkins, D. J., Tsukamoto, Y, and Sterling, P. Microcircuitry and mosaic of a blue-yellow ganglion cell in the primate retina. *J. Neurosci.* 1998; 18 (9): pp. 3373–3385

Campbell, F. W. and Green, D. G. Optical and retinal factors affecting visual resolution. *J. Physiol.* 1965; 181 (3): pp. 576–93

Campbell, M. C., Harrison, E. M., and Simonet, P. Psychophysical measurement of the blur on the retina due to optical aberrations of the eye. *Vision Res.* 1990; 30 (11): pp. 1587–1602

Cava, J. A., Allphin, M. T., Mastey, R. R., Gaffney, M., Linderman, R. E., Cooper, R. F., and Carroll, J. Assessing Interocular Symmetry of the Foveal Cone Mosaic. *Investig. Opthalmology & Vis. Sci.* 2020; 61 (14): pp. 1–11

Caves, E. M., Brandley, N. C., and Johnsen, S. Visual Acuity and the Evolution of Signals. *Trends Ecol. & Evol.* 2018; 33 (5): pp. 1–15

Chen, C.-Y. and Hafed, Z. M. Postmicrosaccadic enhancement of slow eye movements. *J Neurosci*. 2013; 33 (12): pp. 5375–5386

Chen, C.-Y., Hoffmann, K.-P., Distler, C., and Hafed, Z. M. The Foveal Visual Representation of the Primate Superior Colliculus. *Curr. Biol.* 2019; 29 (13): pp. 2109–2119

Chui, T. Y. P., Song, H. X., and Burns, S. A. Individual variations in human cone photoreceptor packing density: Variations with refractive error. *Investig. Ophthalmol. Vis. Sci.* 2008; 49 (10): pp. 4679–4687

Clark, A. M., Intoy, J., Rucci, M., and Poletti, M. Eye drift during fixation predicts visual acuity. *Proc. Natl. Acad. Sci. U. S. A.* 2022; 119 (49): pp. 1–10

Cornsweet, T. N. Determination of the stimuli for involuntary drifts and saccadic eye movements. *J. Opt. Soc. Am.* 1956; 46 (11): pp. 987–993

Curcio, C. A., Allen, K. A., Sloan, K. R., Lerea, C. L., Hurley, J. B., Klock, I. B., and Milam, A. H. Distribution and morphology of human cone photoreceptors stained with anti-blue opsin. *J. Comp. Neurol.* 1991; 312 (4): pp. 610–624

Curcio, C. A. and Allen, K. A. Topography of ganglion cells in human retina. *J. Comp. Neurol.* 1990; 300 (1): pp. 5–25

Curcio, C. A., Packer, O., and Kalina, R. E. A whole mount method for sequential analysis of photoreceptor and ganglion cell topography in a single retina. *Vision Res.* 1987; 27 (1): pp. 9–15

Curcio, C. A., Sloan, K. R., Kalina, R. E., and Hendrickson, A. E. Human photoreceptor topography. *J. Comp. Neurol.* 1990; 292 (4): pp. 497–523

Dacey, D. M. The mosaic of midget ganglion cells in the human retina. *J. Neurosci.* 1993; 13 (12): pp. 5334–5355

Derrington, A. M. and Lennie, P. Spatial and temporal contrast sensitivities of neurones in lateral geniculate nucleus of macaque. *J. Physiol*. 1984; 357: pp. 219–240

Ditchburn, R. W., Fender, D. H., and Mayne, S. Vision with controlled movements of the retinal image. *J. Physiol.* 1959; 145 (1): pp. 98–107

Ditchburn, R. W. and Ginsborg, B. L. Vision with a stabilized retinal image. *Nature*. 1952; 170 (4314): pp. 36–37

Dowling, J. E. The retina: An approachable part of the brain: Harvard University Press, 2011

Drasdo, N., Millican, C. L., Katholi, C. R., and Curcio, C. A. The length of Henle fibers in the human retina and a model of ganglion receptive field density in the visual field. *Vision Res.* 2007; 47 (22): pp. 2901–2911

Dreher, a. W., Bille, J. F., and Weinreb, R. N. Active optical depth resolution improvement of the laser tomographic scanner. *Appl. Opt.* 1989; 28 (4): pp. 804–808

Dubra, A. and Sulai, Y. Reflective afocal broadband adaptive optics scanning ophthalmoscope. *Biomed. Opt. Express*. 2011; 2 (6): pp. 1757–1768

Dubra, A., Sulai, Y., Norris, J. L., Cooper, R. F., Dubis, A. M., Williams, D. R., and Carroll, J. Noninvasive imaging of the human rod photoreceptor mosaic using a confocal adaptive optics scanning ophthalmoscope. *Biomed. Opt. Express*. 2011; 2 (7): pp. 1864–1876

Eizenman, M, Hallett, P. E., and Frecker, R. C. Power spectra for ocular drift and tremor. *Vis. Res*. 1985; 25 (11): pp. 1635–1640

Engbert, R. and Kliegl, R. Microsaccades uncover the orientation of covert attention. *Vis. Res*. 2003; 43 (9): pp. 1035–1045

Engbert, R. and Kliegl, R. Microsaccades keep the eyes' balance during fixation. *Psychol. Sci.* 2004; 15 (6): pp. 431–436

Enoch, J. M. and Hope, G. M. Interferometric resolution determinations in the fovea and parafovea. *Doc. Ophthalmol.* 1973; 34 (1): pp. 143–156

Fechner, G. T. Elemente der Psychophysik: Breitkopf und Härtel, 1860

Findlay, J. M. Feature detectors and vernier acuity. *Nature*. 1973; 241 (5385): pp. 135–137

Furlan, W. D. Basic ophthalmic instruments. In: Artal, P., ed. *Handb. Vis. Opt. Fundam. Eye Opt. Vol. One*. Boca Raton, FL: CRC Press, Taylor & Francis Group, 2017: pp. 103–120

Geisler, W. S. Physical limits of acuity and hyperacuity. *J. Opt. Soc. Am. A.* 1984; 1 (7): pp. 775–82

Gerloff, O. Über die Photographie des Augenhintergrundes. *Zehender Klin. Monatsblätter für Augenheilkd.* 1891; 29: pp. 397 –403

Gilbert, C. D. (2013). The Constructive Nature of Visual Processing. In: *Princ. Neural Sci.* Ed. by E. R. Kandel, J. Schwartz, T. M. Jessell, S. A. Siegelbaum, and A. Hudspeth. 5th ed. New York: McGraw-Hill. Chap. 25, pp. 556–576.

Gómez-Vieyra, A., Dubra, A., Malacara-Hernández, D., and Williams, D. R. First-order design of off-axis reflective ophthalmic adaptive optics systems using afocal telescopes. *Opt. Express*. 2009; 17 (21): pp. 18906–18919

Green, D. G. Regional variations in the visual acuity for interference fringes on the retina. *J. Physiol.* 1970; 207 (2): pp. 351–356

Greschner, M., Bongard, M., Rujan, P., and Ammermüller, J. Retinal ganglion cell synchronization by fixational eye movements improves feature estimation. *Nat Neurosci*. 2002; 5 (4): pp. 341–347

Grieve, K., Tiruveedhula, P., Zhang, Y., and Roorda, A. Multi-wavelength imaging with the adaptive optics scanning laser ophthalmoscope. *Opt. Express*. 2006; 14 (25): pp. 12230–12242

Gullstrand, A. Neue methoden der reflexlosen Ophthalmoskopie. *Berichte Dtsch. Ophthalmol. Gesellschaft*. 1910;:

Hafed, Z. M., Chen, C. Y., Tian, X., Baumann, M. P., and Zhang, T. Active vision at the foveal scale in the primate superior colliculus. *J. Neurophysiol.* 2021; 125 (4): pp. 1121–1138

Hafed, Z. M. and Clark, J. J. Microsaccades as an overt measure of covert attention shifts. *Vision Res.* 2002; 42 (22): pp. 2533–2545

Hafed, Z. M., Goffart, L., and Krauzlis, R. J. A neural mechanism for microsaccade generation in the primate superior colliculus. *Science (80-.).* 2009; 323 (5916): pp. 940–943

Hardy, J. W., Lefebvre, J. E., and Koliopoulos, C. L. Real-time atmospheric compensation. *J. Opt. Soc. Am.* 1977; 67 (3): pp. 360–369

Harmening, W. M., Tuten, W. S., Roorda, A., and Sincich, L. C. Mapping the perceptual grain of the human retina. *J. Neurosci.* 2014; 34 (16): pp. 5667–5677

Hartmann, J. Bemerkungen über den Bau und die Justierung von Spektrographen. *Zeitschrift fuer Instrumentenkd.* 1900; 20: p. 47

Helmholtz, H. von. Beschreibung eines Augen-Spiegels zur Untersuchung der Netzhaut im lebenden Auge. Berlin: Förstner, 1851

Helmholtz, H. von. Handbuch der physiologischen Optik. Leipzig: Leopold Voss, 1867

Hendrickson, A. E. and Yuodelis, C. The morphological development of the human fovea. *Ophthalmology*. 1984; 91 (6): pp. 603–612

Hering, E. (1899). Ueber die Grenzen der Sehschärfe [On the limits of visual acuity]. In: *Berichte über die Verhandlungen der Königlich-Sächsischen Gesellschaft der Wissenschaften zu Leipzig. Math. Classe; Naturwissenschaftlicher Teil, 51*. Leipzig, Germany: Georg Thieme, pp. 16–24.

Hermann, B, Fernández, E. J., Unterhuber, A, Sattmann, H, Fercher, A. F., Drexler, W, Prieto, P. M., and Artal, P. Adaptive-optics ultrahigh-resolution optical coherence tomography. *Opt. Lett.* 2004; 29 (18): pp. 2142–4

Hirsch, J and Curcio, C. A. The spatial resolution capacity of human foveal retina. *Vision Res.* 1989; 29 (9): pp. 1095–1101

Hofer, H., Singer, B., and Williams, D. R. Different sensations from cones with the same photopigment. *J. Vis.* 2005; 5: pp. 444–454

Hooke, R. (1674). Animadversions on the first part of the Machina coelestis of the honourable, learned, and deservedly famous astronomer Johannes Hevelius, consul of Dantzick together with an explication of some instruments.

Hooke, R. The Posthumous Works of Robert Hooke. London: Sam. Smith and Benj. Walford, 1705

Hou, C., Kim, Y.-J., and Verghese, P. Cortical sources of Vernier acuity in the human visual system: An EEG-source imaging study. *J. Vis.* 2017; 17 (6): pp. 1–12

Howland, H. C. The history and methods of opthalmic wavefront sensing. *J. Refract. Surg.* 2000; 16 (5): pp. 552–553

Howland, H. C. and Howland, B. A subjective method for the measurement of monochromatic aberrations of the eye. *J. Opt. Soc. Am.* 1977; 67 (11): pp. 1508–1518

Hu, M. L., Ayton, L. N., and Jolly, J. K. The clinical use of Vernier acuity: Resolution of the visual cortex is more than meets the eye. *Front. Neurosci.* 2021; 15 (October): pp. 1–12

Huang, D., Swanson, E. a., Lin, C. P., Schuman, J. S., Stinson, W. G., Chang, W., Hee, M. R., Flotte, T, Gregory, K., and Puliafito, C. a. Optical coherence tomography. *Science*. 1991; 254 (5035): pp. 1178–81

Hubel, D. H. and Wiesel, T. N. Uniformity of monkey striate cortex: A parallel relationship between field size, scatter, and magnification factor. *J. Comp. Neurol.* 1974; 158 (3): pp. 295–305

Intoy, J. and Rucci, M. Finely tuned eye movements enhance visual acuity. *Nat. Commun.* 2020; 11 (1): pp. 1–11

Iskander, D. R., Collins, M. J., and Davis, B. Optimal modeling of corneal surfaces with Zernike polynomials. *IEEE Trans. Biomed. Eng.* 2001; 48 (1): pp. 87–95

Jagger, W. S. Visibility of photoreceptors in the intact living cane toad eye. *Vision Res.* 1985; 25 (5): pp. 729–31

Jayabalan, G. S. and Bille, J. F. The Development of Adaptive Optics and Its Application in Ophthalmology. In: Bille, J. F., ed. *High Resolut. Imaging Microsc. Ophthalmol.* Cham: Springer International Publishing, 2019: pp. 339–358

Jiang, H., Cottaris, N., Golden, J., Brainard, D., Farrell, J. E., and Wandell, B. A. Simulating retinal encoding: factors influencing Vernier acuity. *Electron. Imaging*. 2017; 29 (14): pp. 177–181

Jong, P. T. V. M. D. A history of visual acuity testing and optotypes. *Eye*. 2024; 38 (1): pp. 13–24

Jonnal, R. S., Kocaoglu, O. P., Zawadzki, R. J., Liu, Z., Miller, D. T., and Werner, J. S. A Review of Adaptive Optics Optical Coherence Tomography: Technical Advances, Scientific Applications, and the Future. *Investig. Ophthalmol. Vis. Sci.* 2016; 57 (9): OCT51–68

Jurin, J. An essay on distinct and indistinct vision. In: Smith, R., ed. *A Compleat Syst. Opt. Four Books*: Cambridge, 1738: pp. 115–171

Kagan, I., Gur, M., and Snodderly, D. M. Saccades and drifts differentially modulate neuronal activity in V1: effects of retinal image motion, position, and extraretinal influences. *J Vis*. 2008; 8 (14): pp. 1–25

Kiely, P. M., Smith, G., and Carney, L. G. The mean shape of the human cornea. *Opt. Acta (Lond).* 1982; 29 (8): pp. 1027–1040

Kingdom, F. A. A. and Prins, N. Psychophysics: A Practical Introduction. London: Academic Press, 2010

Ko, H. K., Poletti, M., and Rucci, M. Microsaccades precisely relocate gaze in a high visual acuity task. *Nat. Neurosci.* 2010; 13 (12): pp. 1549–1554

Kocaoglu, O. P., Liu, Z., Zhang, F., Kurokawa, K., Jonnal, R. S., and Miller, D. T. Photoreceptor disc shedding in the living human eye. *Biomed. Opt. Express*. 2016; 7 (11): pp. 4554–4568

Kolb, H. and Marshak, D. The midget pathways of the primate retina. *Doc. Ophthalmol.* 2003; 106 (1): pp. 67–81

Kowalski, B., Akondi, V., and Dubra, A. Correction of non-uniform angular velocity and sub-pixel jitter in optical scanning. *Opt. Express*. 2022; 30 (1): pp. 112–124

Kowler, E. Eye movements: The past 25years. *Vision Res.* 2011; 51 (13): pp. 1457–1483

Lai, Y. H., Wang, H. Z., and Hsu, H. T. Development of visual acuity in preschool children as measured with Landolt C and Tumbling e charts. *J. AAPOS*. 2011; 15 (3): pp. 251–255

Land, M. F. and Snyder, A. W. Cone mosaic observed directly through natural pupil of live vertebrate. *Vision Res.* 1985; 25 (10): pp. 1519–1522

Larsen, J. S. The sagittal growth of the eye. IV. Ultrasonic measurement of the axial length of the eye from birth to puberty. *Acta Ophthalmol.* 1971; 49 (6): pp. 873–886

Leopold, D. A. and Logothetis, N. K. Microsaccades differentially modulate neural activity in the striate and extrastriate visual cortex. *Exp. Brain Res.* 1998; 123 (3): pp. 341–345

Levi, D. M. Visual Acuity. In: Kaufman, P. L., Alm, A., Levin, L. A., Nilsson, S. F., Ver Hoeve, J., and Wu, S., eds. *Adler's Physiol. Eye*. Edingburg: Saunders/Elsevier, 2011: pp. 627–647

Liang, J., Grimm, B, Goelz, S, and Bille, J. F. Objective measurement of wave aberrations of the human eye with the use of a Hartmann-Shack wave-front sensor. *J. Opt. Soc. Am. A. Opt. Image Sci. Vis.* 1994; 11 (7): pp. 1949–1957

Liang, J. and Williams, D. R. Aberrations and retinal image quality of the normal human eye. *J. Opt. Soc. Am. A*. 1997; 14 (11): pp. 2873–2883

Liang, J., Williams, D., and Miller, D. Supernormal vision and high-resolution retinal imaging through adaptive optics. *J. Opt. Soc. Am. A Opt. Image Sci. Vis.* 1997; 14 (11): pp. 2884–2892

Lieberman, H. R. and Pentland, A. P. Microcomputer-based estimation of psychophysical thresholds: The Best PEST. *Behav. Res. Methods & Instrum.* 1982; 14: pp. 21–25

Mainster, M. A., Timberlake, G. T., Webb, R. H., and Hughes, G. W. Scanning Laser Ophthalmoscopy: Clinical Applications. *Ophthalmology*. 1982; 89 (7): pp. 852–857

Makous, W., Carroll, J., Wolfing, J. I., Lin, J., Christie, N., and Williams, D. R. Retinal microscotomas revealed with adaptive-optics microflashes. *Investig. Ophthalmol. Vis. Sci.* 2006; 47 (9): pp. 4160–4167

Marcos, S. and Navarro, R. Determination of the foveal cone spacing by ocular speckle interferometry: Limiting factors and acuity predictions. *J. Opt. Soc. Am. A*. 1997; 14 (4): pp. 731–740

Marshall, W. H. and Talbot, S. A. Recent evidence for neural mechanisms in vision leading to a general theory of sensory acuity.. In: Klüver, H., ed. *Vis. Mech.* Oxford, England: Jacques Cattell, 1942: pp. 117–164

Martinez-Conde, S. and Macknik, S. L. Fixational eye movements across vertebrates: Comparative dynamics, physiology, and perception. *J. Vis.* 2008; 8 (14): pp. 1–16

Martinez-Conde, S., Macknik, S. L., and Hubel, D. H. The role of fixational eye movements in visual perception. *Nat. Rev. Neurosci.* 2004; 5 (3): pp. 229–240

Martinez-Conde, S., Macknik, S. L., Troncoso, X. G., and Dyar, T. A. Microsaccades counteract visual fading during fixation. *Neuron*. 2006; 49 (2): pp. 297–305

McCamy, M. B., Otero-Millan, J., Macknik, S. L., Yang, Y., Troncoso, X. G., Baer, S. M., Crook, S. M., and Martinez-Conde, S. Microsaccadic efficacy and contribution to foveal and peripheral vision. *J. Neurosci.* 2012; 32 (27): pp. 9194–9204

McMahon, M. J., Lankheet, M. J., Lennie, P., and Williams, D. R. Fine structure of parvocellular receptive fields in the primate fovea revealed by laser interferometry. *J. Neurosci.* 2000; 20 (5): pp. 2043–2053

Merino, D., Duncan, J. L., Tiruveedhula, P., and Roorda, A. Observation of cone and rod photoreceptors in normal subjects and patients using a new generation adaptive optics scanning laser ophthalmoscope. *Biomed. Opt. Express*. 2011; 2 (8): pp. 2189–2201

Merino, D. and Loza-Alvarez, P. Adaptive optics scanning laser ophthalmoscope imaging: technology update. *Clin. Ophthalmol.* 2016; 10: pp. 743–55

Miller, D. T., Williams, D. R., Morris, G. M., and Liang, J. Images of cone photoreceptors in the living human eye. *Vis. Res*. 1996; 36 (8): pp. 1067–1079

Miller, D. T., Qu, J., Jonnal, R. S., and Thorn, K. E. Coherence gating and adaptive optics in the eye. *Proc. SPIE Coherence Domain Opt. Methods Opt. Coherence Tomogr. Biomed. VII*. 2003; 4956: p. 65

Morgan, J. I. W., Chui, T. Y. P., and Grieve, K. Twenty-five years of clinical applications using adaptive optics ophthalmoscopy [Invited]. *Biomed. Opt. Express*. 2023; 14 (1): pp. 387–428

Muirhead, F. Adrien van Trigt, and the first published ophthalmoscopic images (De Speculo Oculi, 1853). *J. Med. Biogr.* 2020; 29 (4): pp. 1 –8

Nachmias, J. Determiners of the drift of the eye during monocular fixation. *J Opt Soc Am*. 1961; 51 (7): pp. 761–766

Nachmias, J. Two-dimensional motion of the retinal image during monocular fixation. *J Opt Soc Am*. 1959; 49 (9): pp. 901–908

Nathans, J, Thomas, D, and Hogness, D. S. Molecular genetics of human color vision: the genes encoding blue, green, and red pigments. *Science (80-.).* 1986; 232 (4747): pp. 193–202

Oppel, O. Studies on the distribution and number of retinal ganglion cells in the human. *Albr. von Graefe's Arch. Clin. Exp. Ophthalmol.* 1967; 172 (1): pp. 1–22

Opstal, A. J. van. Neural encoding of instantaneous kinematics of eye-head gaze shifts in monkey superior colliculus. *Commun. Biol.* 2023; 6 (1): pp. 1–17

Osterberg, G. A. Topography of the layer of rods and cones in the human retina. *Acta Ophthalmol.* 1935; 13: pp. 1–97

Packer, O and Williams, D. R. Blurring by fixational eye movements. *Vis. Res*. 1992; 32 (10): pp. 1931–1939

Pircher, M., Baumann, B., Götzinger, E., and Hitzenberger, C. K. Retinal cone mosaic imaged with transverse scanning optical coherence tomography. *Opt. Lett.* 2006; 31 (12): pp. 1821–3

Pitkow, X., Sompolinsky, H., and Meister, M. A neural computation for visual acuity in the presence of eye movements. *PLoS Biol.* 2007; 5 (12): pp. 2898–2911

Poletti, M. An eye for detail: Eye movements and attention at the foveal scale. *Vision Res.* 2023; 211 (108277): pp. 1–12

Poletti, M., Listorti, C., and Rucci, M. Microscopic eye movements compensate for nonhomogeneous vision within the fovea. *Curr. Biol.* 2013; 23 (17): pp. 1691–1695

Poletti, M. and Rucci, M. Eye movements under various conditions of image fading. *J. Vis.* 2010; 10 (3): pp. 1–18

Poletti, M. and Rucci, M. A compact field guide to the study of microsaccades: Challenges and functions. *Vision Res.* 2016; 118: pp. 83–97

Porterfield, W. An essay concerning the motions of our eyes. Part 1. Of their external motions. Edinburgh: Med. Ess. Obs., 1737

Ramón y Cajal, S., Swanson, N., and Swanson, L. W. Histology of the Nervous System of Man and Vertebrates. New York: Oxford University Press, 1995

Ratnam, K., Domdei, N., Harmening, W. M., and Roorda, A. Benefits of retinal image motion at the limits of spatial vision. *J. Vis.* 2017; 17 (1): pp. 1–11

Reese, B. E. Development of the retina and optic pathway. *Vision Res.* 2011; 51 (7): pp. 613–632

Reiniger, J. L., Domdei, N., Holz, F. G., and Harmening, W. M. Technical principles of adaptive optics in ophthalmology. *Der Ophthalmol.* 2017; 114 (3): pp. 198–205

Reiniger, J. L., Domdei, N., Holz, F. G., and Harmening, W. M. Human gaze is systematically offset from the center of cone topography. *Curr. Biol.* 2021; 31 (18): pp. 4188–4193

Rha, J., Jonnal, R. S., Thorn, K. E., Qu, J., Zhang, Y., and Miller, D. T. Adaptive optics flood-illumination camera for high speed retinal imaging. *Opt. Express*. 2006; 14 (10): pp. 4552–4569

Riggs, L. A. and Ratliff, F. The effects of counteracting the normal movements of the eye. *J. Opt. Soc. Am.* 1952; 42: pp. 872–873

Rodieck, R. W. The Vertebrate Retina: Principles of Structure and Function. San Francisco: W.H.Freeman & Co Ltd, 1973

Rolfs, M. Microsaccades: Small steps on a long way. *Vision Res.* 2009; 49 (20): pp. 2415–2441

Roorda, A. Applications of adaptive optics scanning laser ophthalmoscopy. *Optom. Vis. Sci.* 2010; 87 (4): pp. 260–8

Roorda, A. and Glasser, A. Wave aberrations of the isolated crystalline lens. *J. Vis.* 2004; 4 (4): pp. 250–261

Roorda, A., Romero-Borja, F., Donnelly Iii, W., Queener, H., Hebert, T., and Campbell, M. Adaptive optics scanning laser ophthalmoscopy. *Opt. Express*. 2002; 10 (9): pp. 405–412

Roorda, A. and Williams, D. R. The arrangement of the three cone classes in the living human eye. *Nature*. 1999; 397 (6719): pp. 520–522

Roorda, A. and Williams, D. R. Optical fiber properties of individual human cones. *J. Vis.* 2002; 2 (5): pp. 404–412

Rosenblum, W. M. and Christensen, J. L. Objective and Subjective Spherical Aberration Measurements of the Human Eye. In: Wolf, E, ed. Amsterdam: Elsevier, 1976: pp. 69–91

Rossi, E. and Roorda, A. The relationship between visual resolution and cone spacing in the human fovea. *Nat Neurosci*. 2010; 13 (2): pp. 156–157

Rubin, M. L. Spectacles: Past, present, and future. *Surv. Ophthalmol.* 1986; 30 (5): pp. 321–327

Rucci, M. and Desbordes, G. Contributions of fixational eye movements to the discrimination of briefly presented stimuli. *J. Vis.* 2003; 3 (11): pp. 852–864

Rucci, M., Iovin, R., Poletti, M., and Santini, F. Miniature eye movements enhance fine spatial detail. *Nature*. 2007; 447 (7146): pp. 851–854

Rucci, M. and Poletti, M. Control and Functions of Fixational Eye Movements. *Annu. Rev. Vis. Sci.* 2015; 1: pp. 499–518

Rucci, M. and Victor, J. D. The unsteady eye: An information-processing stage, not a bug. *Trends Neurosci.* 2015; 38 (4): pp. 195–206

Schira, M. M., Wade, A. R., and Tyler, C. W. Two-dimensional mapping of the central and parafoveal visual field to human visual cortex. *J. Neurophysiol.* 2007; 97 (6): pp. 4284–4295

Shack, R. and Platt, B. Production and use of a lenticular Hartmann screen. *J Opt Soc Am*. 1971; 61: pp. 656–660

Sincich, L. C., Zhang, Y., Tiruveedhula, P., Horton, J. C., and Roorda, A. Resolving single cone inputs to visual receptive fields. *Nat. Neurosci.* 2009; 12 (8): pp. 967–969

Smith, R. Compleat System of Opticks in Four Books. Cambridge:, 1738

Steinbach, M. J. Owls' eyes move. *Br. J. Ophthalmol.* 2004; 88 (8): p. 1103

Stockman, A. and Rider, A. T. Formulae for generating standard and individual human cone spectral sensitivities. *Color Res. Appl.* 2023; 48 (6): pp. 818–840

Strasburger, H., Huber, J., and Rose, D. Ewald Hering's (1899) on the limits of visual acuity: A translation and commentary - With a supplement on Alfred Volkmann's (1863) Physiological Investigations in the Field of Optics. *Iperception.* 2018; 9(3) (1899): pp. 1–14

Syrbe, S., Kuhrt, H., Gärtner, U., Habermann, G., Wiedemann, P., Bringmann, A., and Reichenbach, A. Müller glial cells of the primate foveola: An electron microscopical study. *Exp. Eye Res.* 2018; 167: pp. 110–117

Thibos, L. N., Cheney, F. E., and Walsh, D. J. Retinal limits to the detection and resolution of gratings. *J. Opt. Soc. Am. A*. 1987; 4 (8): pp. 1524–1529

Tomita, T. Electrical activity of vertebrate photoreceptors. *Q. Rev. Biophys.* 1970; 3 (2): pp. 179–222

Treutwein, B. Adaptive psychophysical procedures. *Vision Res.* 1995; 35 (17): pp. 2503–2522

Treviranus, G. R. Beiträge zur Aufklärung der Erscheinungen und Gesetze des organischen Lebens: Resultate neuer Untersuchungen über die Theorie des Sehens und über den innern Bau der Netzhaut des Auges. Bremen: Heyse, 1837

Tscherning, M. Die Monochromatischen abberationen des Menschlichen Auges. *Z. Psychol. Physiol. Sinn.* 1894; 6: pp. 456–471

Tuten, W. S. and Harmening, W. M. Foveal vision. *Curr Biol*. 2021; 31 (11): R701–R703

Tuten, W. S., Tiruveedhula, P., and Roorda, A. Adaptive optics scanning laser ophthalmoscope-based microperimetry. *Optom. Vis. Sci.* 2012; 89 (5): pp. 563–74

Vargas-Martin, F., Prieto, P. M., and Artal, P. Correction of the aberrations in the human eye with a liquid-crystal spatial light modulator: limits to performance. *J. Opt. Soc. Am. A*. 1998; 15 (9): pp. 2552–2562

Velthoven, M. E. van, Faber, D. J., Verbraak, F. D., Leeuwen, T. G. van, and Smet, M. D. de. Recent developments in optical coherence tomography for imaging the retina. *Prog. Retin. Eye Res.* 2007; 26 (1): pp. 57–77

Villegas, E. A., Alcón, E., and Artal, P. Optical quality of the eye in subjects with normal and excellent visual acuity. *Investig. Ophthalmol. Vis. Sci.* 2008; 49 (10): pp. 4688–4696

Volkmann, A. Sehen. Braunschweig: Vieweg, 1846

Volkmann, A. W. Neue Beiträge zur Physiologie des Gesichtssinnes: Breitkopf und Härtel, 1836

Wade, A. and Fitzke, F. In vivo imaging of the human cone-photoreceptor mosaic using a confocal LSO. *Lasers Light Ophthalmol.* 1998; 8 (3): pp. 129–136

Wade, N. J. Image, eye and retina. *J Opt Soc Am A Opt Image Sci Vis*. 2007; 24 (5): pp. 1229–1249

Walsh, G., Charman, W. N., and Howland, H. C. Objective technique for the determination of monochromatic aberrations of the human eye. *J. Opt. Soc. Am. A*. 1984; 1 (9): pp. 987–992

Wang, Q., Tuten, W. S., Lujan, B. J., Holland, J., Bernstein, P. S., Schwartz, S. D., Duncan, J. L., and Roorda, A. Adaptive optics microperimetry and OCT images show preserved function and recovery of cone visibility in macular telangiectasia type 2 retinal lesions. *Investig. Ophthalmol. Vis. Sci.* 2015; 56 (2): pp. 778–786

Wang, Y., Bensaid, N., Tiruveedhula, P., Ma, J., Ravikumar, S., and Roorda, A. Human foveal cone photoreceptor topography and its dependence on eye length. *Elife*. 2019; 8: pp. 1–21

Wang, Y., Bensaid, N., Tiruveedhula, P., Ma, J., Roorda, A., and Ravikumar, S. (2018). The Relationship between Cone Density and Axial Length: CAL Study. In: *Annu. Meet. Assoc. Res. Vis. Ophthalmol.* Berkeley, California, United States.

Watson, A. B. and Pelli, D. G. QUEST: a Bayesian adaptive psychometric method. *Percept. & Psychophys.* 1983; 33 (2): pp. 113 –120

Webb, R. H., Hughes, G. W., and Delori, F. C. Confocal scanning laser ophthalmoscope. *Appl. Opt.* 1987; 26 (8): pp. 1492–1499

Webb, R. H., Hughes, G. W., and Pomerantzeff, O. Flying spot TV ophthalmoscope. *Appl. Opt.* 1980; 19 (17): pp. 2991–2997

Westheimer, G. Visual Acuity and Hyperacuity. *Invest. Ophthalmol.* 1975; 64 (8): pp. 570–572

Westheimer, G. Specifying and controlling the optical image on the human retina. *Prog. Retin. Eye Res.* 2006; 25 (1): pp. 19–42

Westheimer, G. and McKee, S. P. Spatial configurations for visual hyperacuity. *Vision Res.* 1977; 17 (8): pp. 941–947

Westheimer, G. and McKee, S. P. Visual acuity in the presence of retinal-image motion. *J. Opt. Soc. Am.* 1975; 65 (7): pp. 847–50

Westheimer, G., Shimamura, K, and McKee, S. P. Interference with line-orientation sensitivity. *J. Opt. Soc. Am.* 1976; 66 (4): pp. 332–8

Whitaker, D. and MacVeigh, D. Interaction of spatial frequency and separation in vernier acuity. *Vision Res.* 1991; 31 (7-8): pp. 1205–12

Williams, D. R. Imaging single cells in the living retina. *Vision Res.* 2011; 51 (13): pp. 1379–1396

Williams, D. R., Burns, S. A., Miller, D. T., and Roorda, A. Evolution of adaptive optics retinal imaging [Invited]. *Biomed. Opt. Express*. 2023; 14 (3): pp. 1307–1338

Williams, D. R. and Coletta, N. J. Cone spacing and the visual resolution limit. *J. Opt. Soc. Am. A*. 1987; 4 (8): pp. 1514–1523

Williams, D. R. and Hofer, H. Formation and acquisition of the retinal image. In: Chalupa, L. M. and Werner, J. S., eds. *Vis. Neurosci.* Cambridge, MA: The MIT Press, 2003: pp. 795–810

Wülfing, E. A. Ueber den kleinsten Gesichtswinkel. *Z. Biol.* 1892; 29: pp. 199–202

Yarbus, A. L. Eye movements and vision. New York: Plenum Press, 1967

Yau, K. W. Phototransduction mechanism in retinal rods and cones. The Friedenwald lecture. *Investig. Ophthalmol. Vis. Sci.* 1994; 35 (1): pp. 9–32

Yoon, G.-Y. and Williams, D. R. Visual performance after correcting the monochromatic and chromatic aberrations of the eye. *J. Opt. Soc. Am. A. Opt. Image Sci. Vis.* 2002; 19 (2): pp. 266–275

Young, T. The Bakerian Lecture: On the mechanism of the eye. *Philos. Trans. R. Soc. London*. 1801; 91: pp. 23–88

Yuodelis, C. and Hendrickson, A. A qualitative and quantitative analysis of the human fovea during development. *Vision Res.* 1986; 26 (6): pp. 847–855

Zhang, C., Kim, Y. J., Silverstein, A. R., Hoshino, A., Reh, T. A., Dacey, D. M., and Wong, R. O. Circuit reorganization shapes the developing human foveal midget connectome toward single-cone resolution. *Neuron*. 2020; 108 (5): pp. 905–918

Zhang, Y., Poonja, S., and Roorda, A. MEMS-based adaptive optics scanning laser ophthalmoscopy. *Opt. Lett.* 2006; 31 (9): pp. 1268–1270

Zhang, Y. and Roorda, A. Evaluating the lateral resolution of the adaptive optics scanning laser ophthalmoscope. *J. Biomed. Opt.* 2006; 11 (1): p. 014002

3 Publications

On the following pages, copies of the three first-authorship publications of this dissertation are printed in the respective journal layouts.

3.1 Habitual higher order aberrations affect Landolt but not Vernier acuity

Reiniger, J. L., Lobecke, A. C., Sabesan, R., Bach, M., Verbakel, F., Brabander, J. de, Holz, F. G., Berendschot, T. T., and Harmening, W. M. Habitual higher order aberrations affect Landolt but not Vernier acuity. J Vis. 2019; 19 (5): pp. 1–15; doi: 10.1167/19.5.11

Journal of Vision (2019) 19(5):11, 1–15

Habitual higher order aberrations affect Landolt but not Vernier acuity

Jenny L. Reiniger — Department of Ophthalmology, University of Bonn, Germany

Anne C. Lobecke — Department of Neurobiology, University of Bielefeld, Germany

Ramkumar Sabesan — Department of Ophthalmology, University of Washington, Seattle, WA, USA

Michael Bach — Eye Center, Medical Center—University of Freiburg, Faculty of Medicine, University of Freiburg, Germany

Frenne Verbakel — University Eye Clinic Maastricht, The Netherlands

John de Brabander — University Eye Clinic Maastricht, The Netherlands

Frank G. Holz — Department of Ophthalmology, University of Bonn, Germany

Tos T. J. M. Berendschot — University Eye Clinic Maastricht, The Netherlands

Wolf M. Harmening — Department of Ophthalmology, University of Bonn, Germany

To assess whether the eye's optical imperfections are relevant for hyperacute vision, we measured ocular wave aberrations, visual hyperacuity, and acuity thresholds in 31 eyes of young adults. Although there was a significant positive correlation between the subjects' performance in Vernier- and Landolt-optotype acuity tasks, we found clear differences in how far both acuity measures correlate with the eyes' optics. Landolt acuity thresholds were significantly better in eyes with low higher order aberrations and high visual Strehl ratios ($r^2 = 0.22$, $p = 0.009$), and significantly positively correlated with axial length ($r^2 = 0.15$, $p = 0.03$). A retinal image quality metric, calculated as two-dimensional correlation between perfect and actual retinal image, was also correlated with Landolt acuity thresholds ($r^2 = 0.27$, $p = 0.003$). No such correlations were found with Vernier acuity performance ($r^2 < 0.03$, $p > 0.3$). Based on these results, hyperacuity thresholds are, contrary to resolution acuity, not affected by higher order aberrations of the eye.

Introduction

The relationship between optical quality of the eye and its primary function, seeing, is a well-studied field. Typically, a special emphasis is given to measurements of visual acuity, the ability to discriminate small visual optotypes, because of the natural simplicity of how such measurements can be performed, their applicability for clinical assessment of visual function, and their profound meaning in real-life situations. On the other hand, in everyday vision tasks, seeing is comprised of more than reading letters, and it seems that our eyes and brain have evolved to make use of even the tiniest spatial information available. This is

Citation: Reiniger, J. L., Lobecke, A. C., Sabesan, R., Bach, M., Verbakel, F., de Brabander, J., Holz, F. G., Berendschot, T. T. J. M., & Harmening, W. M. (2019). Habitual higher order aberrations affect Landolt but not Vernier acuity. *Journal of Vision*, *19*(5):11, 1–15, https://doi.org/10.1167/19.5.11.

https://doi.org/10.1167/19.5.11 Received July 13, 2018; published May 17, 2019 ISSN 1534-7362

exemplified by our ability to detect the offset in a pair of lines or dots to a much finer degree than we are able to read. Psychophysical thresholds derived from Vernier and similar positional discrimination tasks are usually only a fraction of the eye's resolving power, and are well below the two-point sampling capacity of the retinal photoreceptor mosaic (Curcio, Sloan, Kalina, & Hendrickson, 1990; Hering, 1899; Hirsch & Curcio, 1989; Strasburger, Huber, & Rose, 2018). This is why the perceptual performance in these tasks was termed hyperacuity (Westheimer, 1975).

Since its first encounter (Wülfing, 1892), the interrelation between stimulus and perceptual characteristics in hyperacuity tasks have been described in diverse approaches. Besides other parameters, the dependencies of spatial configuration (Westheimer & McKee, 1977), luminance (Bradley & Skottun, 1987), contrast (Wehrhahn & Westheimer, 1990), motion (Westheimer & McKee, 1975), spatial frequency (Whitaker & MacVeigh, 1991), and orientation (Westheimer, Shimamura, & McKee, 1976) were studied before. Hyperacuity is subject to short-term task learning (Mckee & Westheimer, 1978), and has become a model paradigm for studies of long-term perceptual learning (Fahle, 1993). Consequentially, physiological and computational models of the mechanisms behind hyperacuity have been developed (Findlay, 1973; Geisler, 1984; Jiang et al., 2017), identifying Vernier acuity not being some miraculous singularity, but an intrinsic property of the neural networks underlying spatial vision (Westheimer, 2009). This is further illustrated by the fact that Vernier acuity is also a hyperacuity phenomenon in other species, such as monkeys (Kiorpes, Kiper, & Movshon, 1993), cats (Murphy & Mitchell, 1991), rats (Seymoure & Juraska, 1997), and birds (Harmening, Göbbels, & Wagner, 2007).

By artificial large-scale deterioration of the retinal image like blurring one's vision with trial lenses or semitranslucent screens, it was demonstrated that two-point acuity and Vernier acuity vary markedly as a function of blur (Bedell, Patel, & Chung, 1999; Krauskopf & Farell, 1991; Levi & Klein, 1990). However, the impairment of Vernier thresholds by retinal image degradation is highly dependent on the chosen stimulus parameters (e.g., gap size) (Williams, Enoch, & Essock, 1984). Different neurological visual disorders, like strabismic or anisometropic amblyopia, were shown to have distinct relations to visual acuity and grating resolution, differing from subjects with normal vision, thus Vernier acuity was established to research the etiology of amblyopia (Hou, Good, & Norcia, 2018; Levi & Klein, 1982). Comparably, less is known about how small-scale image degradation by the habitual optics of the eye, especially higher order aberrations—imperfections that cannot be corrected with glasses or contact lenses—interact with acuity thresholds. For conventional resolution tasks, the relationship between the habitual higher order ocular aberrations and their effect on perceptual performance cannot be readily inferred by conclusions drawn from artificially altered retinal image quality. For example, while an adaptive optics correction of the higher-order ocular aberrations can improve visual acuity to degrees that are in agreement with the eye's optical modulation transfer function (Yoon & Williams, 2002), the question of whether visual acuity in subjects with less higher-order aberrations is better than in those with more aberrations was not clearly answered for a population with normal and excellent visual acuities (Villegas, Alcon, & Artal, 2008).

We here ask how far hyperacuity thresholds depend on the eye's habitual optical quality in healthy subjects. Because of the surprisingly limited number of studies relating normal visual acuity to habitual ocular aberrations, and to address possible differences and relations across the two acuity measurements, we also assessed Landolt acuity in the same subjects.

Material and methods

Subjects

Acuity thresholds and optical measurements were assessed in both eyes of 32 young adults. Subjects were student volunteers at the RWTH Aachen chosen without prior visual screening and two of the authors (ACL, WMH). One subject was excluded from further analysis because of exceptionally high between-eyes threshold differences. The remaining 31 subjects were aged 22–36 (mean ± standard deviation: 27 ± 3 years), 12 subjects were female. Subjects participated in two separate experiments (acuity and optical measurements) carried out on two different days. During acuity assessment, ametropic participants wore their habitual correction (contact lenses, $n = 8$; spectacles, $n = 8$), emmetropic subjects wore no correction ($n = 15$). For acuity-optics correlation analyses, results from only the right eyes were used (Supplementary Table S1). Written informed consent was obtained from all participants after the experiment procedures and possible risks had been explained verbally. The study was performed in compliance with the tenets of the Declaration of Helsinki.

Acuity measurements

Acuity thresholds (Landolt-optotype acuity and Vernier acuity, respectively) were obtained in a

psychophysical experiment. Subjects were seated 13 m in front of an LCD panel (Belinea, Germany; angular pixel pitch ~4.5 arcsec), which delivered visual stimuli generated by the "Freiburg Visual Acuity and Contrast Test" (FrACT, version 3.5, https://michaelbach.de/fract/), a customizable acuity testing software. Acuity thresholds were obtained both binocularly and monocularly, with the fellow eye occluded by a translucent sheet in monocular runs (Figure 1A). Visual stimuli were high-contrast, dark optotypes presented on a bright background (background luminance: 300 cd/m^2, Michelson contrast: 0.99). Optotypes were either Landolt Cs of variable size or a pair of horizontally displaced lines with a Gaussian luminance profile of fixed size (physical dimensions in degree of visual angle, total stimulus height: 0.5°, line sigma: 0.5 arcmin, gap height: 0.2 arcmin). Psychophysical procedures employed by the FrACT have been described in detail elsewhere (Bach, 1996, 2007). Briefly, a forced-choice, adaptive staircase with self-paced trial progress was used. The subject's task was to discriminate between eight possible directions of gap openings in the Landolt C, or between one of two offset directions in the Vernier lines, respectively. Following the applied best parameter estimation by sequential testing procedure (Lieberman & Pentland, 1982), stimulus intensities at each trial equaled the current threshold estimate (Figure 1B). A motivating high intensity trial was introduced every sixth trial. The staircase terminated after 24 trials in Landolt acuity tests and after 42 trials in Vernier acuity tests, and the next estimate after recording the last response was taken as the threshold outcome. Subjects indicated their response by pressing the corresponding key on a computer keyboard. Calculated as the mean of 6–8 consecutive runs, acuity thresholds are expressed in logMAR, the logarithmic minimum angle of resolution in minutes of arc of visual angle. Pupil size was measured concurrently during all behavioral experimental trials by video pupillometry. The mean value of a stable sequence of pupil diameter across 5 s at the end of each behavioral run is reported here and was used for further analysis (Supplementary Table S1).

Optical measurements and data analysis

Optical quality of the subjects' eyes was assessed by measuring the ocular wavefront aberrations using a near-infrared (785 nm) thin beam principle of optical ray tracing across a 5-mm pupil (iTrace, Tracey Technologies, Houston, TX). Measurements were carried out at natural viewing conditions, i.e., subjects did not wear their habitual correction, and no accommodative block, pupil dilation, or corneal lubrication was administered. The experimental room

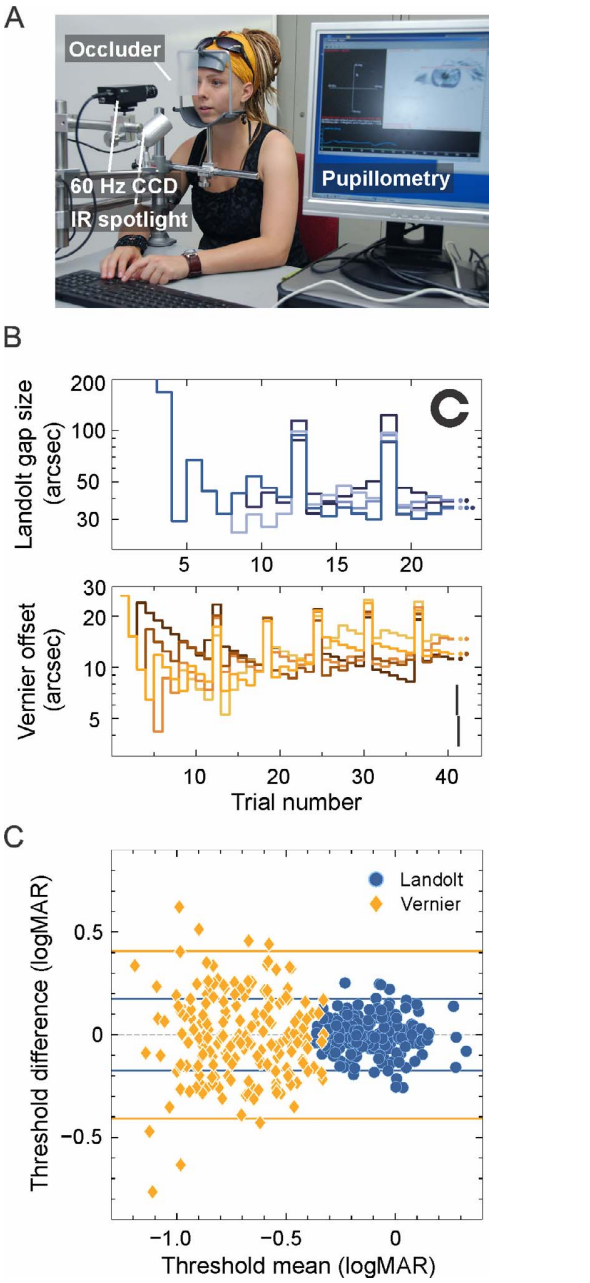

Figure 1. Behavioral testing. (A) The observer's viewing stage during psychophysical measurements. A head and chin rest provided constant viewing distance (13 m), and stable eye positioning for custom video pupillometry. (B) Example staircases for Landolt (top) and Vernier (bottom) acuity estimation. Five repeated runs are shown; the final threshold estimation is given by the filled circles. Note the motivating "bonus" trials every sixth trial. Example stimuli for Landolt/Vernier acuity testing are shown in the upper and lower right corner, respectively. (C) Bland-Altman analysis, plotting the difference between each pair of two consecutive monocular threshold measurements against their mean value in logMAR. Horizontal lines mark the 95% interval of threshold differences. Blue circles are results from Landolt acuity measurements, yellow diamonds are Vernier acuity results.

was darkened to allow maximum natural pupil sizes. Subjects were prompted to blink their eyes normally. The mean of three consecutive measurements was used to express wavefront errors as the Zernike polynomial expansion up to the eighth order (Supplementary Table S1). Axial length (AL) was determined by optical low coherence reflectometry with a Lenstar LS 900 (Haag-Streit, Koeniz, Switzerland). To report optical quality of the subjects' eyes during behavioral testing, wavefront errors that were recorded at 5 mm pupil diameter had to be recalculated and scaled to the actual pupil diameter present during behavioral testing. A set of recursive conversion equations was used for the rescaling of individual Zernike terms (calculations based on equations presented in Schwiegerling, 2002, using a correction term shown in Visser et al., 2011). The point-spread function (PSF) of each eye was calculated (Maeda, 2008) and further used to calculate theoretical retinal image quality by convolution of computer generated vector graphics. Because accommodation was not controlled for during acuity and optical measurements and the exact refractive state was unknown during behavioral testing, a through-focus analysis was carried out: for each eye, a combined defocus/astigmatism term was computationally found that optimized retinal image quality (defined as image correlation maximum between measured and ideal PSF-convoluted images; see next paragraph). Because lower order aberrations (LOA) in half of the subjects were corrected by their individual habitual correction (contact or spectacle lenses), we also calculated the theoretical residual lower order aberrations as the difference between the power vectors (Thibos, Wheeler, & Horner, 1997) of measured and corrected LOA (defocus and astigmatism). Spectacle prescriptions were corrected for a standard cornea vertex distance of 12 mm.

To report wavefront aberrations independent of the individual pupil diameter during acuity experiments, root mean square error was normalized by the pupil area and converted to an ophthalmic prescription, expressed as the equivalent defocus in diopters (Thibos, Hong, Bradley, & Cheng, 2002). To quantify retinal image quality, three different metrics were calculated for each eye. The Strehl ratio of an optical system is defined as the ratio between the peak intensity of the PSFs in the actual system versus one from a diffraction-limited system. The visual Strehl ratio (VSX) additionally incorporates a standardized neural weighting function (Thibos, Hong, Bradley, & Applegate, 2004) and has been shown to have a stronger correlation with visual performance (Marsack, Thibos, & Applegate, 2004). Finally, an image convolution-based method described by Watson and Ahumada (2008) and modified by Zheleznyak, Sabesan, Oh, MacRae, and Yoon (2013) was used. Briefly, the individual PSF's were calculated for polychromatic white light (405–695 nm wavelength, weighted by the photopic spectral sensitivity function V_λ) (Ravikumar, Thibos, & Bradley, 2008). Computer-generated bitmaps of the retinal stimulus at threshold (size = mean threshold of all eyes) were then convolved with both, a diffraction limited PSF and the actual PSF of the individual eye. The two-dimensional image correlation coefficient (MATLAB, MathWorks, Natick, MA; 2-D correlation coefficient *corr2*) calculated between both images is then used as the retinal image quality metric. The metric's values range between 0 and 1, where 1 would imply that the individual PSF's retinal stimulus image is identical to the diffraction limited one (Watson & Ahumada, 2008; Zheleznyak et al., 2013).

Because many of the optical parameters and image quality metrics found here were not normally distributed, we used Spearman's rank correlation for evaluating those data. For comparing the normally distributed acuity threshold of Landolt and Vernier measurements, Pearson's correlation was calculated.

Results

Landolt and Vernier acuity thresholds

We measured Vernier and visual acuity with the "Freiburg visual acuity and contrast test" (FrACT; see Acuity measurements), a test software that has so far been applied to measure normal acuity and contrast sensitivity (Bühren, Terzi, Bach, Wesemann, & Kohnen, 2006; Rocha, Vabre, Chateau, & Krueger, 2010), but not hyperacuity thresholds. Thus, we first wished to confirm the validity of the methods applied here and procedures to correctly identify the subjects' Vernier acuity, by comparing our results with the literature on Vernier acuity thresholds in healthy subjects.

Across all tested eyes, we found thresholds to be normally distributed ranging from −1.06 to −0.36 logMAR (equaling 5.2 to 25.9 seconds of arc), with an overall mean threshold of −0.7 ± 0.2 logMAR (11.5 ± 3.5 arcsec) (Figure 2A). Landolt acuity values were normally distributed as well. With a mean Landolt acuity of −0.1 ± 0.1 logMAR (45.1 ± 7.0 arcsec) in our experiments, the mean hyperacuity ratio (Landolt acuity/Vernier acuity threshold) was 4.1, although the individual per eye ratios differed substantially (range: 1.4–10.6). These findings match reports where Vernier acuity tests were performed with untrained subjects (Abbud & Cruz, 2002). By combining two individual consecutive measurements to form a test/retest pair, a Bland-Altman plot was constructed (Figure 1C). Note that 95% of all test/retest differences lay within a range of about ±0.41 logMAR for Vernier thresholds, whereas the differences between Landolt acuity

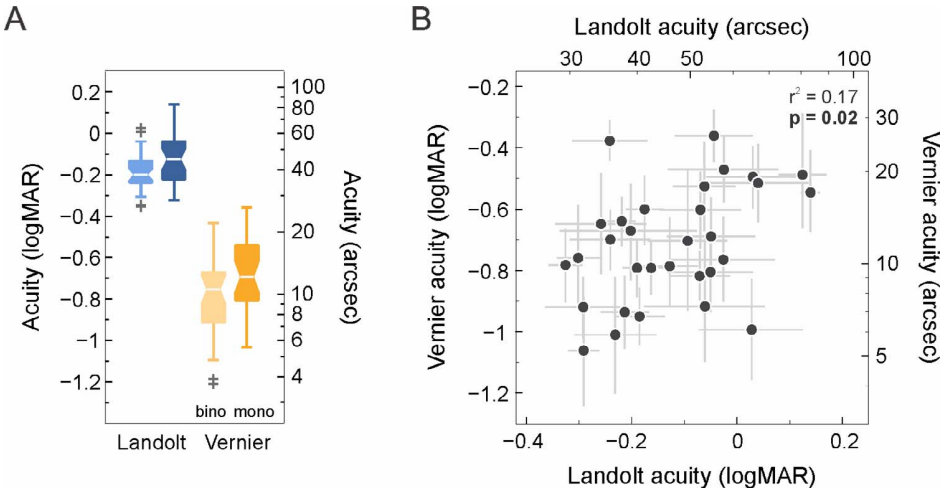

Figure 2. Psychophysical acuity thresholds. (A) Binocular ("bino," light) and monocular ("mono," dark) thresholds for Landolt and Vernier acuity for all 31 subjects are shown as boxplots. Landolt and Vernier acuity values are plotted in blue and yellow, respectively. Horizontal lines signify medians, the edges of the box are the first and third quartile [interquartile range (IQR)], notches display the 95% confidence interval of the median and whiskers extend to the most extreme data points without outliers (>1.5 IQR), which are shown with individual cross markers. Monocular and binocular thresholds for Landolt and Vernier acuity differ significantly (*t* test, $p \ll 0.001$). (B) Vernier acuity thresholds plotted against Landolt acuity thresholds of all right eyes. The gray error bars represent the standard deviations of threshold estimates between the consecutive measurements. The two metrics are significantly positively correlated ($r^2 = 0.17$, $p = 0.02$).

thresholds were in the range of about ±0.18 logMAR. The mean coefficients of variance (CVs; i.e., standard deviation divided by mean) of our Vernier measurements were 0.30 and 0.29 (binocular and monocular, respectively). This is contrasted by mean CVs of 0.1 and 0.15 in Landolt acuity thresholds. Expressed differently, the mean standard error for Vernier thresholds was between 0.53 and 0.67 arcsec, and 0.73–1.3 arcsec in Landolt tests. These findings match earlier results (Lindblom & Westheimer, 1989), and confirm that measures of Vernier acuity are prone to relatively large intertest variability (Abbud & Cruz, 2002). Vernier acuity is subject to binocular summation, i.e., thresholds measured with two eyes are usually lower (better) than those measured with one eye alone. We find a mean summation ratio of 1.35 (range: 0.6–3.6). These results are in agreement with earlier findings performed at similar stimulus configuration and contrast (Banton & Levi, 1991; Lindblom & Westheimer, 1989). In conclusion, our behavioral results generally paralleled earlier results, and we were therefore confident that the here applied stimuli and methods provide sufficient fidelity to measure Vernier acuity with the FrACT in untrained subjects.

The correlation between Landolt and Vernier acuity thresholds across eyes (Figure 2B) was significantly positive ($p = 0.02$). That is, subjects that had good performance in the Landolt test tended to have lower thresholds in the Vernier task as well. As one example, the subject with the lowest mean Vernier acuity threshold (−1.06 logMAR) had a mean Landolt acuity threshold of −0.29, among the lowest within the study. Equally, the subject with one of the highest mean Landolt acuity thresholds (0.12 logMAR) also had one of the highest Vernier acuity thresholds (−0.49 logMAR). However, overall predictive power of the correlation was relatively weak ($r^2 = 0.17$). The linear fit to the threshold data expressed in logMAR had a slope of 0.68, indicating an exponential relation between Landolt and Vernier acuity thresholds on a linear scale.

Ocular biometry and optical quality

Ocular biometry of all eyes was assessed by pupil diameter measurement during psychophysical testing and by axial length measurements during optical testing. The pupil size varied between 3.1 and 4.8 mm (mean ± SD: 3.8 ± 0.46 mm) during Landolt and 3.1–4.9 mm (mean ± SD: 3.8 ± 0.45 mm) during Vernier acuity testing (Figure 3A). Pupil sizes during both acuity experiments were highly correlated ($r^2 = 0.86$, $p \ll 0.001$), with an average deviation between pupil diameters of 0.14 mm (±0.11 mm). During aberration measurements, all pupil diameters were under natural conditions, but larger than 5 mm, a prerequisite for wavefront aberration measurements. Axial lengths were between 22.3 mm and 27.2 mm (mean ± SD: 24.3 ± 1.2 mm; Figure 3B) and were strongly correlated with the individual eyes' lower order aberrations ($r^2 = 0.56$, $p \ll 0.001$).

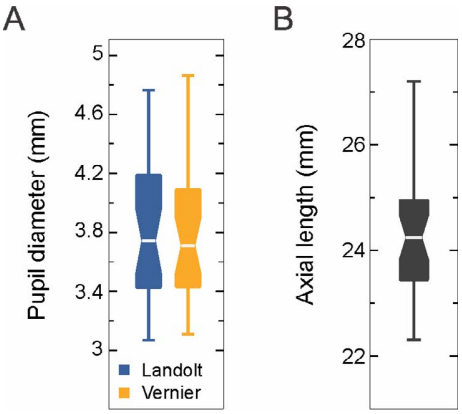

Figure 3. Ocular biometry. (A) Pupil diameter for Landolt (blue) and Vernier (yellow) acuity measurements determined by video pupillometry during behavioral testing. Wavefront aberrations were measured for a 5 mm pupil size and Zernike coefficients were recalculated for analysis according to the pupil sizes measured during vision testing. (B) Axial length determined by low coherence reflectometry. Boxplot conventions as in Figure 2.

Optical quality was assessed by measuring the ocular wave aberrations under natural viewing conditions and with natural pupils. Reported wavefront errors are given for a 5 mm pupil diameter. Wave aberrations of all eyes were expressed as a set of Zernike coefficients up to the eighth order (Figure 4A and B). Since we aimed to measure visual performance under natural viewing conditions, ametropic subjects wore their habitual correction devices (spectacles or contact lenses) during acuity tests. For these subjects, refractive defocus correction was between 0 and −8.0 D; however, 75% of the eyes had a prescribed defocus of −3.0 D or less and three-fourths of the remaining subjects with higher myopia wore contact lenses for correction. Prescribed astigmatic correction was −0.75 D or less in 90% of all eyes, with three of the subjects needing higher astigmatic corrections of −1.5, −1.75, and −2.25 D, respectively. The resulting residual defocus values (difference between objectively measured and corrected LOA) were on average −0.12 D (between −1.63 and 2.35 D). The calculated mean residual absolute astigmatism was 0.44 D (between 0.02 and 1.5 D), with 66% of all eyes having a residual astigmatism below 0.5 D (Figure 4A; habitual correction).

Higher order aberrations (HOA) had an average root mean square (RMS) of 0.2 ± 0.06 μm and ranged between 0.07 and 0.34 μm. Individual Zernike coefficients of coma, trefoil (averaged horizontal and vertical) and spherical aberration ranged from 0.02 μm to 0.26 μm, 0.02–0.19 μm, and 0.07–0.19 μm, respectively. Due to the smaller pupil sizes measured during behavioral testing, the impact of ocular aberrations was lower in those conditions. Zernike coefficients were thus recalculated to scale to the individual pupil sizes present during behavioral tests. As a metric of optical quality which factors out the different pupil sizes, we calculated the HOA equivalent defocus (Figure 4C). The mean equivalent defocus for HOA measured at 5 mm pupils was 0.23 D ± 0.07 D (range: 0.07–0.38 D). Average HOA equivalent defocus was similar during Vernier and Landolt acuity measurement (because of

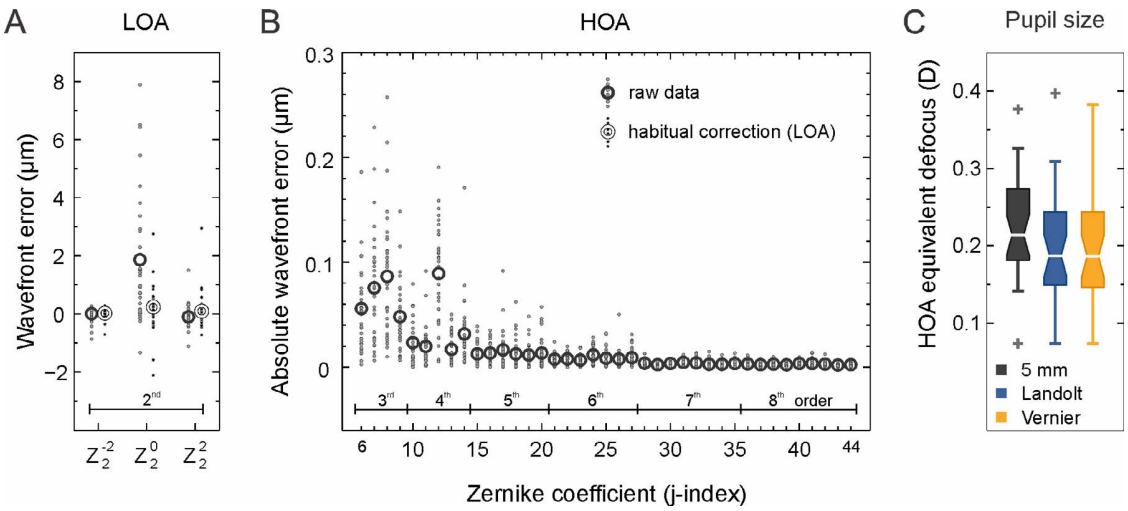

Figure 4. Ocular wavefront errors. (A) Lower order wavefront aberrations (LOA) of all eyes (5 mm pupil size). Small dots are individual eyes, circle markers are average values across eyes. Dark circles are raw data; bright circles are residual errors after correcting for habitual correction devices, worn by some subjects. (B) Absolute higher order aberrations (HOA) expressed in μm of all eyes (5 mm pupil size). Small dots are individual eyes; circle markers are average values across eyes. (C) Equivalent defocus values for HOA (Zernike order 3–8), calculated by normalizing the HOA by the individual pupil area during Landolt/Vernier acuity experiments, (n = 31). Boxplot conventions as in Figure 2.

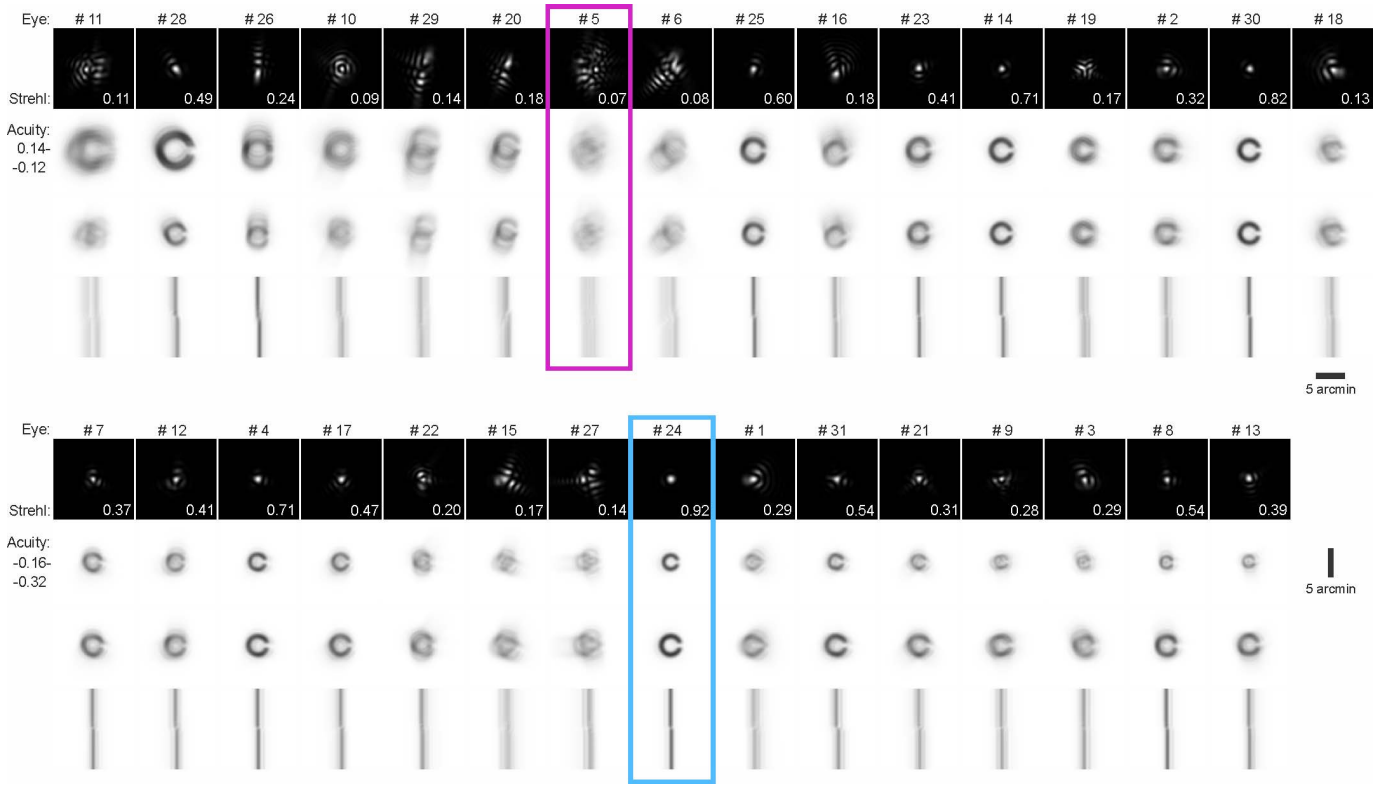

Figure 5. Retinal image quality. Qualitative representation of individual wavefront aberrations and their impact on the retinal image. The data of 31 tested eyes are shown in two rows, consisting of four different analyses ordered by the individual Landolt acuity thresholds (in logMAR), from worst (top left) to best (bottom right). Point spread functions (PSF) are shown in the first row (theoretical distribution of monochromatic light, 555 nm, normalized to span 0 to 1 for better visibility). Strehl ratio values are shown in the lower right corner of the PSF images. Rows two to four show a convolution of the individual PSF with: Landolt stimuli scaled to individual threshold size (row 2), Landolt stimuli at a fixed size (row 3), and the center part of the Vernier stimulus scaled to individual threshold size (row 4). The two subjects with highest and the lowest Strehl ratio are highlighted in light blue and magenta, respectively (compare Figure 6, 7). The edge length of PSF images is 10 arcmin, the scale bar for all stimulus images is 5 arcmin.

the similar pupil sizes, compare Figure 3A), with mean values of 0.20 D ± 0.07 D and 0.19 D ± 0.07 D during Landolt and Vernier acuity testing, respectively. The range of HOA equivalent defocus values was also similar for Landolt (0.07–0.40 D) and Vernier (0.07–0.38 D) acuity measurements.

Retinal image quality metrics and correlations

To assess retinal image quality, the polychromatic PSF was calculated for each eye and convolved with computer generated bitmaps of the optotypes used in the acuity experiments. Figure 5 arranges the PSFs of all 31 eyes ordered by their visual acuity (Landolt C), suggesting qualitatively that eyes with "better" PSF's have higher visual acuities. Accordingly, the Strehl ratio values (first row in Figure 5), were negatively correlated with Landolt acuity thresholds ($r^2 = 0.18$, $p = 0.016$), implying that eyes with higher Strehl ratios tended to have better visual acuity thresholds. When the eye's individual PSF was convolved with a computer-generated stimulus image at a fixed size (–0.12 logMAR, average threshold), retinal image quality seemed to qualitatively improve with increasing visual acuity (third row in Figure 5). This is similar for Vernier acuity stimuli, although Strehl ratios were not significantly correlated with Vernier thresholds ($r^2 = 0.02$, $p = 0.51$). In general, we observe a broad distribution of visual acuity thresholds for similar amounts of aberration.

Since the optics of an individual eye are an essential factor for the formation of the retinal image, we analyzed optical quality as well as optical biometry as factors potentially influencing acuity thresholds. We find a weak positive correlation between axial length (AL) and Landolt acuity ($r^2 = 0.15$, $p = 0.03$) but no significant correlation between AL and Vernier acuity thresholds ($r^2 = 0.01$, $p = 0.62$) (Figure 6). There was no significant correlation between the amount of HOA RMS (μm) at a 5 mm pupil and AL ($r^2 = 0.01$, $p = 0.55$). However, there was a weak positive correlation

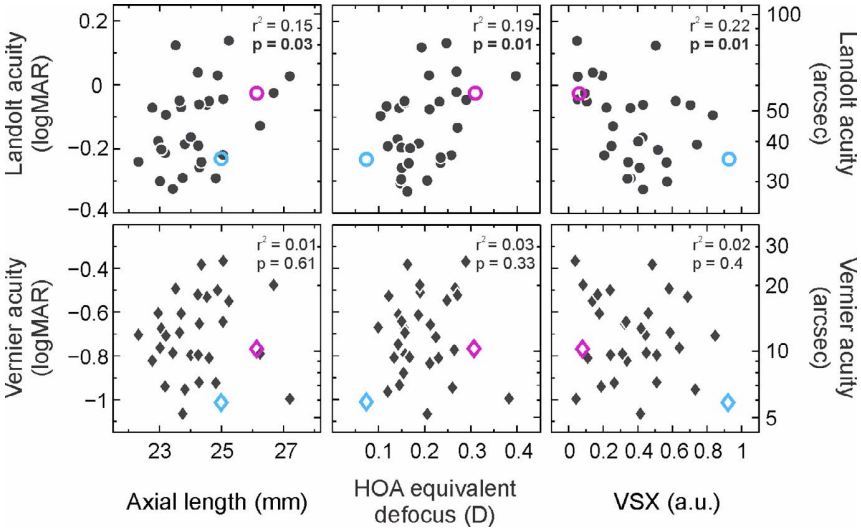

Figure 6. Correlation of behavioral and optical parameters. Landolt and Vernier acuity thresholds are plotted against optical parameters: axial length, HOA equivalent defocus and visual Strehl ratio (VSX) ($n = 31$). Coefficients of determination r^2 and probability values p (Spearman's rank correlation) are shown in the upper right corner of each plot. Data points of the two subjects with the highest and lowest Strehl ratio are plotted in light blue and magenta, respectively (compare Figure 5).

between HOA RMS and Landolt acuity thresholds ($r^2 = 0.15$, $p = 0.03$), whereas no correlation was found between HOA RMS and Vernier acuity thresholds ($r^2 = 0.02$, $p = 0.46$). Zernike coefficients of second (residual LOA) and third order (spherical aberration, coma, and trefoil) were examined separately. Neither Landolt nor Vernier acuity correlated with the total residual LOA. Coma was positively correlated with Landolt acuity ($r^2 = 0.22$, $p = 0.008$), but not significantly correlated with Vernier acuity ($r^2 = 0.002$, $p = 0.81$). No correlation with either of the acuities could be found for spherical aberration or trefoil. We also calculated the HOA equivalent defocus for factoring out the individual pupil sizes during experiments (Figure 6). Landolt acuity thresholds showed a significantly positive correlation with the HOA equivalent defocus ($r^2 = 0.19$, $p = 0.014$), but no correlation was found for Vernier acuity thresholds ($r^2 = 0.03$, $p = 0.33$).

It has to be noted that metrics of optical quality in the pupil plane, such as HOA equivalent defocus, may be limited to describe subjective image quality and visibility, because further downstream retinal and neural factors play a key role in image processing steps and the final perceptual decision. We included VSX and a two-dimensional image correlation coefficient in our analysis as two additional metrics to meet this concern. Landolt acuity thresholds were negatively correlated with VSX ($r^2 = 0.22$, $p = 0.009$), i.e., eyes with higher VSX values also had better visual acuity thresholds. Vernier acuity thresholds were not significantly correlated with VSX ($r^2 = 0.02$, $p = 0.4$). The image correlation metric (Figure 7A) also revealed a difference in how the retinal images correlate with Landolt and Vernier acuity thresholds, respectively. Similar to most of the other analyzed metrics, Landolt acuity was significantly correlated with the image correlation coefficients ($r^2 = 0.27$, $p = 0.003$). Vernier acuity thresholds, on the other hand, did not correlate with the image correlation coefficients ($r^2 = 0.002$, $p = 0.8$). As an example, the two subjects with the highest and the lowest Strehl ratio (plotted in light blue and magenta, respectively) populate different parts of the spectrum of exhibited acuity thresholds. Landolt acuity thresholds of those subjects were in the upper versus lower half of the spectrum and for Vernier acuity, both thresholds were in the upper half of the acuity spectrum (Figure 7B).

Discussion

Ocular optics measurements from eyes of 31 healthy subjects who performed Vernier acuity and Landolt acuity threshold experiments were presented. Our main findings were:

1. Vernier acuity and Landolt acuity thresholds were significantly correlated across subjects, i.e., subjects who were good at discriminating Landolt optotypes were also good at detecting the offset in a pair of Vernier lines, and vice versa. Our data is among the largest singular sets on the relationship between these two acuity measurements in healthy subjects.
2. We found that subjects' Landolt acuity thresholds were significantly but weakly correlated with some

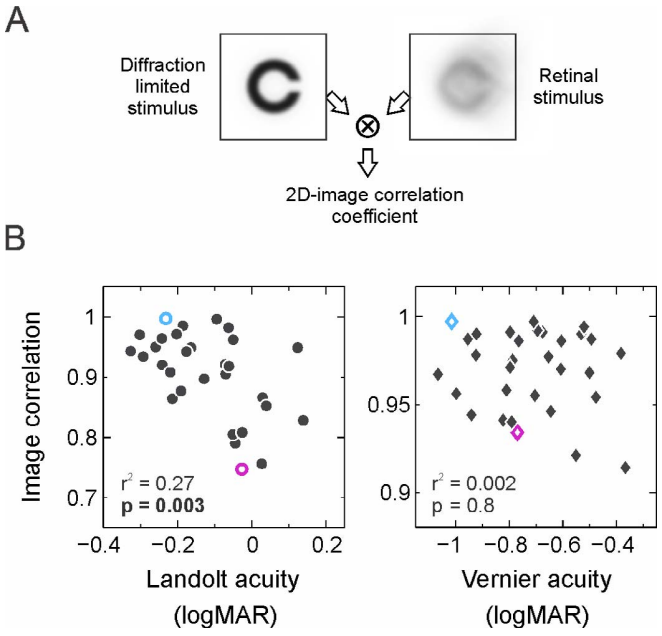

Figure 7. Stimulus-image correlation. (A) Schematic representation of the calculation of image correlation coefficients as a metric for retinal image quality. The two-dimensional image correlation coefficient is obtained by computing the cross-correlation for two stimuli, one convolved with the diffraction limited PSF, the other one convolved with the eye's individual PSF. (B) Stimulus image correlation coefficients are plotted as a function of Landolt (left)/Vernier (right) acuity thresholds ($n = 31$). Data points of the two subjects with the highest and lowest Strehl ratio are plotted in light blue and magenta, respectively (compare Figure 5). Only Landolt acuity correlates significantly with the image correlation coefficients, shown in the lower left corner of each plot.

higher order ocular optics metrics, both regarding the quality of the wavefront in the pupil plane, and regarding the quality of the retinal image. Subjects with more higher order ocular aberrations tended to have lower visual acuity. Albeit perhaps intuitive, this finding is not entirely trivial and is only partially supported by earlier studies.

3. Vernier acuity thresholds did not show a correlation with any of the optical quality metrics we tested. At the most extreme, some subjects exhibiting similar retinal images were both among the very best and the worst at discriminating the offset in the Vernier stimulus. Generally, no predictions about Vernier acuity could be drawn from optics measurements alone. To the best of our knowledge, this is the first report of Vernier acuity thresholds and their (missing) relationship to habitual optical quality.

There are only a few studies that directly compare perceptual performance in both hyperacuity and normal visual acuity tasks. Most of them investigate the relation between both types of acuity in visually deprived subjects. Significant correlations between Vernier and visual acuity were shown in amblyopic subjects with different etiologies of amblyopia and subjects with cataract. In the latter case, the slope of a linear fit to logarithmic Snellen and Vernier acuity was reported as 0.74 under optimal stimulus conditions (Enoch, Essock, & Williams, 1984). In amblyopia, slopes of subjects with strabismic and anisometropic etiology differed from the whole amblyopic population (slope = 1.15, $n = 427$). For anisometropes, the slope was 1.44, while for the strabismic subjects it was 0.79 (McKee, Levi, & Movshon, 2003). In an earlier study, the slopes in these groups were reversed, most likely explained by a much smaller sample size ($n = 12$) (Levi & Klein, 1982). In a group of normal controls ($n = 68$), significantly positive correlations were found between Vernier and visual acuity (McKee et al., 2003). A separate study analyzing differences between bisection discrimination and Vernier discrimination with and without visual backward masking did not find any correlation between visual acuity and Vernier acuity, and neither with other hyperacuity tasks (Cappe, Clarke, Mohr, & Herzog, 2014).

In our study, we find a significant but weak correlation between Landolt and Vernier acuity thresholds with a linear fit slope of 0.62 (Figure 2). Among obvious differences in methodology, one explanation of variation between our and earlier results might be eye selection. Throughout our analysis, we present data from the right eyes of all subjects only (to avoid bias), but we tested binocular and left eye performance as well. Although correlation coefficients and significance levels differ, left eye data ($n = 30$) show the same trends for the relation between acuity thresholds and the later discussed optical quality. Thus, our population possibly included preferred as well as nonpreferred eyes, a factor that might contribute to acuity correlations. For instance, data from McKee et al. (2003), which we reanalyzed by grouping into preferred and non-preferred eyes, showed differences among both groups: Landolt and Vernier acuity were only significantly correlated in preferred eyes (preferred: $r^2 = 0.14$, $p = 0.002$; nonpreferred: $r^2 = 0.03$, $p = 0.14$) (McKee et al., 2003). If we grouped our data into preferred (better Landolt acuity thresholds) and non-preferred eyes, we remain to find similar correlation trends in the preferred eye group, and no significant correlations for the non-preferred eyes, matching results from McKee et al. According to this grouping, our right eye data contained 61% preferred eyes (in which thresholds differed on average about 19% from the left eye), which supports the hypothesis that next to optical factors, neural mechanisms are playing a key role in the processing of acuity targets.

As a first summary, there seem to be factors in the visual pathway affecting both types of acuity and also factors that primarily influence only one of them. It may seem parsimonious to assume that external physical factors limiting acuity are also at play in hyperacuity tasks. It is clear that the eyes' optics influence retinal image formation, but the relationship between the ocular aberrations present in an individual eye and its performance in acuity tasks is more complex. By employing computationally aberrated letter charts it was shown that various optical metrics were significantly correlated with the decrease in acuity compared to nonaberrated letters (Marsack et al., 2004). Correspondingly, visual acuity of aberrated letters could be predicted from wavefront aberrations using different optically and physiologically informed models of spatial vision (Watson & Ahumada, 2008). Acuity was shown to be increasingly better in eyes with less aberrations when contrast and/or luminance is decreased (Applegate, Marsack, & Thibos, 2006). On the other hand, in subjects with normal and excellent visual acuity, no clear correlations between optical aberrations and low contrast tumbling E acuity could be found (Villegas et al., 2008). At high stimulus contrasts and short stimulus presentation times (to avoid potential temporal summation effects) the same study found weak correlations with single HOA components, i.e., coma, trefoil, and logarithmic Strehl ratio.

In our study, using more natural viewing conditions, we find a significant, if weak, correlation between Landolt acuity and the eye's individual HOA. We suggest that our study design, testing at smaller pupil sizes and in a subject group with more relaxed inclusion criteria, e.g., allowing for a wider range of visual acuities, might explain these differences. In any case, we also observe a wide distribution of visual acuity thresholds for similar amounts of aberrations, and this distribution of optical performance was even larger for Vernier acuity. Various factors may influence these variations in addition to the here investigated optical aberrations, such as cone photoreceptor density, ganglion cell density, intraocular scatter, neural adaptation, and cortical processing (Artal, 2015; Artal et al., 2004; Hou, Kim, & Verghese, 2017; Jiang et al., 2017; Rossi & Roorda, 2010; Wang et al., 2018).

Eye biometry data recorded here may act as an indirect measure of retinal sampling capacity. We found that axial length (AL) was positively correlated with Landolt acuity, but not with Vernier acuity. Axial elongation of the myopic eye, due to stretching of the retina, was found to be a primary cause for reduced sampling density of cone photoreceptors in the perifoveal region (Chui, Yap, Chan, & Thibos, 2005). Axial length (AL) was generally found to be highly negatively correlated to the sampling limit and packing density of the human cone mosaic (cones/mm^2) (Lombardo, Serrao, Ducoli, & Lombardo, 2012). A recent foveal cone density analysis obtained by adaptive optics scanning laser ophthalmoscopy in 28 healthy subjects confirmed a significant decrease in linear cone density (cones/mm^2) with increasing AL. However, considering that the foveal photoreceptor density might not decrease proportionally to the eye growth during myopic progression, the more appropriate unit for comparing AL and acuity would be the angular cone density (cones/deg^2). This analysis showed a significant increase of cones/deg^2 in longer eyes (Wang et al., 2018), suggesting a possible increase in visual acuity with increasing AL. However, another study, investigating the relationship between axial length and best corrected visual acuity, shows a significant decline in visual acuity for longer eyes (Lü et al., 2011), similarly to our results. In light of a possible increase in cone recruitment in myopic eyes, other factors might outweigh increased sampling. For habitual viewing, one factor might be a demagnified retinal image by spectacle correction. Additionally, eyeball elongation, which is highly correlated with increasing spherical equivalent, might introduce more HOA, which in turn decreases retinal image quality. This hypothesis is well studied and yet remains controversial. Various studies report significantly higher values for some of the HOA (Buehren, Collins, & Carney, 2005; Karimian, Feizi, & Doozande, 2010; Kasahara et al., 2017; Wei, Lim, Chan, & Tan, 2006) or total RMS (He et al., 2002; Marcos, Sawides, Gambra, & Dorronsoro, 2008; Paquin, Hamam, & Simonet, 2002) in higher myopic subjects. In contrast, Kwan et al. showed significantly smaller RMS values of fourth-order aberrations and spherical aberration in highly myopic than in nonmyopic eyes (Kwan, Yip, & Yap, 2009). Other studies reported that HOA were unrelated to refractive error (Cheng, Bradley, Hong, & Thibos, 2003) as well as AL (Lombardo et al., 2012), which can also be seen in our data (HOA vs AL, $r^2 = 0.01$, $p = 0.55$). Even if the relation between HOA and AL is still a matter of debate, both seem to be factors influencing visual acuity thresholds.

On a general note, a methodological limitation to our assessment of acuity was that subjects wore their habitual refractive correction during testing. This may have had an impact on data interpretation in different ways. First, optically, allowing for different correction devices resulted in retinal image size differences between eyes that were corrected with glasses and those corrected with contact lenses, due to additional demagnification in the case of glasses. However, since only three of the subjects with myopia higher than 1 D were wearing glasses for refractive correction, we do not expect a strong influence on the overall results. Second, we did not correct lower order aberrations

(LOA) beyond spectacle prescription during acuity testing. Therefore, any residual LOA could have affected performance during threshold measurements. However, residual LOA and acuity thresholds were not significantly correlated (Landolt: $r^2 = 0.24$, $p = 0.14$; Vernier: $r^2 = 0.04$, $p = 0.81$). Generally, a subjective refraction is highly fluctuating between different points in time, and the "best correction" was shown to vary about 0.25 to 0.5 D over a day (Chakraborty, Read, & Collins, 2014). LOA are therefore to be treated as a somewhat variable parameter. To account for this, we used optimized individual defocus values for each subject by letting them vary to maximize retinal image quality, as our visual system does naturally.

With regard to possible uncertainty of optics measurements in general, there are a few additional sources of variability to expect. For one, the iTrace aberrometer itself showed relatively good measurement repeatability for all Zernike coefficients (highest repeatability for corneal aberrations), but there is still some variation in the absolute amounts of individual Zernike coefficients, even for consecutive measured data (Visser et al., 2011). Also, there are small differences in measured aberrations across points in time (Srivannaboon, Reinstein, & Archer, 2007; Visser et al., 2011). HOA RMS fluctuations within one week or one year were shown to be on average 0.021 (week) and 0.031 (year) μm, respectively (Cheng, Himebaugh, Kollbaum, Thibos, & Bradley, 2004). Our mean HOA RMS across eyes was 0.22 μm. Thus, fluctuations of about 10% of our aberration values could be expected. Fluctuations of such amounts, however, are likely to not contribute much to image quality metrics, as they were shown to have almost no impact on the radial-averaged MTF, for instance (Cheng et al., 2004). We thus expect that the introduced variability of measurements of optical quality would not change our main finding. For following studies, it would be interesting to further investigate visual performance under the correction of individual lower and higher order aberrations, such as is provided in an adaptive optics stimulation system.

Because one of the goals of this study was to analyze the influence of aberrations under habitual viewing conditions, the procedure allowed for similar viewing conditions as the subjects had in everyday life, and thus visual degradation introduced by departure from aberrations that subjects were adapted to is minimized. It was shown that the neural visual system adapts to blur (Webster, Georgeson, & Webster, 2002) and to the eye's own aberrations (Artal et al., 2004). If subjects adapt to their specific aberration patterns, it may be reasonable to assume that the actual amount of aberrations would have a smaller effect on vision, a view that is supported by our general outcome that correlations between optics and acuity are significant but carry only a weak predictive power (all below 30% variability explained). Although the effect of neural adaptation is probably not too large, it may contribute to the robustness of the visual system, leading to similar performance for a large range of ocular optics quality in different subjects.

As a summary, we found clear differences between acuity and hyperacuity threshold in relation to the eye's optics, and it remains yet unclear which factors determine the distribution of Vernier thresholds in our subjects the most. That these individual differences might have real-world consequences can be derived from recent results looking at higher level perceptual tasks, such as reading. Vernier acuity potentially contributes to an early stage of hierarchical letter and word processing, as psychophysical thresholds in these tasks showed a correlation with the processing of Chinese characters (but not with other visual stimuli) (Tan et al., 2018). Moreover, visually evoked potentials (VEP) measured with Vernier targets allow for the characterization of the magnitude of acuity in amblyopic eyes better than VEP grating acuity (Hou et al., 2018).

Studies investigating the cortical sources of acuity go along with our findings. Functional testing of the visual cortex by electroencephalography showed that detection thresholds for grating acuity were similar in all four examined stages of cortical hierarchy [striate visual cortex (V1), hV4, lateral occipital cortex (LOC), middle temporal cortex], whereas only V1 and LOC were sensitive to Vernier displacements. This supports the hypothesis that grating acuity is limited by retinal sampling factors and that the striate cortex passes the information on to extrastriate cortices without further filtering. This may be different for Vernier acuity thresholds, as they show up in only two of the four examined cortical stages. The meaning of LOC for spatial perception processing is not completely understood yet, and it is discussed whether the activation of LOC might be related to a general sensitivity to the relative position of features (Hou et al., 2017). Conceptually, and supported by ideal-observer analysis, the retinal entry point to the visual path should also affect an observer's performance in hyperacuity tasks. The spatial information used to judge relative position in a foveal Vernier acuity task must be present in the spatial-temporal distribution of cone photoreceptor absorptions, because subsequent processing cannot add to this information. A biologically inspired simulation of the factors that potentially influence Vernier thresholds indicates eye movements, luminance level, defocus and bar length of the target as important factors (Jiang et al., 2017). Analyzing the exact spatiotemporal retinal sampling pattern during foveal inspection of a Vernier target and linking this directly to behavioral performance via photoreceptor-targeted

microstimulation (Harmening, Tuten, Roorda, & Sincich, 2014; Ratnam, Domdei, Harmening, & Roorda, 2017) could lend further insights into how far low-level retinal sampling behavior plays a role in hyperacute perception.

Keywords: Vernier acuity, Landolt acuity, image blur, retinal sampling, psychophysics, aberrometry, spatial vision

Acknowledgments

The authors thank Frank Schaeffel for providing the pupillometry software. We thank all subjects for their patient participation in the experiments.

Supported by the National Institutes of Health (P30-EY001730), unrestricted grant from Research to Prevent Blindness (RS), and Emmy Noether Program of the German Research Foundation (DFG) Ha5323-5/1 (WMH). RS holds a career award at the Scientific Interfaces from the Burroughs Wellcome Fund and a career development award from the Research to Prevent Blindness.

At the time of data collection, ACL and WMH were affiliated with Institute of Zoology and Animal Physiology, RWTH Aachen, Germany.

Commercial relationships: none.
Corresponding author: Wolf M. Harmening.
Email: wolf.harmening@ukbonn.de.
Address: Department of Ophthalmology, University of Bonn, Germany.

References

Abbud, C. M. M., & Cruz, A. A. V. (2002). Variability of Vernier acuity measurements in untrained subjects of different ages. *Brazilian Journal of Medical and Biological Research*, *35*(2), 223–227. retrieved from http://www.ncbi.nlm.nih.gov/pubmed/11847526

Applegate, R. A., Marsack, J. D., & Thibos, L. N. (2006). Metrics of retinal image quality predict visual performance in eyes with 20/17 or better visual acuity. *Optometry and Vision Science*, *83*(9), 635–640. https://doi.org/10.1097/01.opx.0000232842.60932.af

Artal, P. (2015). Image Formation in the Living Human Eye. *Annual Review of Vision Science*, *1*, 1–17. https://doi.org/10.1146/annurev-vision-082114-035905

Artal, P., Chen, L., Fernández, E. J., Singer, B., Manzanera, S., & Williams, D. R. (2004). Neural compensation for the eye's optical aberrations. *Journal of Vision*, *4*(4):4, 281–287, https://doi.org/10.1167/4.4.4. [PubMed] [Article]

Bach, M. (1996). The Freiburg Visual Acuity test–automatic measurement of visual acuity. *Optometry and Vision Science*, *73*(1), 49–53. Retrieved from http://www.ncbi.nlm.nih.gov/pubmed/8867682

Bach, M. (2007). The Freiburg Visual Acuity Test-variability unchanged by post-hoc re-analysis. *Graefe's Archive for Clinical and Experimental Ophthalmology*, *245*(7), 965–971. https://doi.org/10.1007/s00417-006-0474-4

Banton, T., & Levi, D. M. (1991). Binocular summation in vernier acuity. *Journal of the Optical Society of America A*, *8*(4), 673–680.

Bedell, H. E., Patel, S., & Chung, S. T. (1999). Comparison of letter and Vernier acuities with dioptric and diffusive blur. *Optometry and Vision Science*, *76*(2), 115–120. Retrieved from http://www.ncbi.nlm.nih.gov/pubmed/10082058

Bradley, A., & Skottun, B. C. (1987). Effects of contrast and spatial frequency on vernier acuity. *Vision Research*, *27*(10), 1817–1824.

Buehren, T., Collins, M. J., & Carney, L. G. (2005). Near work induced wavefront aberrations in myopia. *Vision Research*, *45*(10), 1297–1312. https://doi.org/10.1016/j.visres.2004.10.026

Bühren, J., Terzi, E., Bach, M., Wesemann, W., & Kohnen, T. (2006). Measuring contrast sensitivity under different lighting conditions: Comparison of three tests. *Optometry and Vision Science*, *83*(5), 290–298. https://doi.org/10.1097/01.opx.0000216100.93302.2d

Cappe, C., Clarke, A., Mohr, C., & Herzog, M. H. (2014). Is there a common factor for vision? *Journal of Vision*, *14*(8):4, 1–11, https://doi.org/10.1167/14.8.4. [PubMed] [Article]

Chakraborty, R., Read, S. A., & Collins, M. J. (2014). Diurnal variations in ocular aberrations of human eyes. *Current Eye Research*, *39*(3), 271–281. https://doi.org/10.3109/02713683.2013.841257

Cheng, X., Bradley, A., Hong, X., & Thibos, L. N. (2003). Relationship between refractive error and monochromatic aberrations of the eye. *Optometry and Vision Science*, *80*(1), 43–49. Retrieved from https://journals.lww.com/optvissci/Fulltext/2003/01000/Relationship_between_Refractive_Error_and.7.aspx

Cheng, X., Himebaugh, N. L., Kollbaum, P. S., Thibos, L. N., & Bradley, A. (2004). Test-retest reliability of clinical Shack-Hartmann measurements. *Investigative Ophthalmology and Visual Science*, *45*(1), 351–360. https://doi.org/10.1167/iovs.03-0265

Chui, T. Y. P., Yap, M. K. H., Chan, H. H. L., & Thibos, L. N. (2005). Retinal stretching limits peripheral visual acuity in myopia. *Vision Research*, *45*(5), 593–605. https://doi.org/10.1016/j.visres.2004.09.016

Curcio, C. A., Sloan, K. R., Kalina, R. E., & Hendrickson, A. E. (1990). Human photoreceptor topography. *The Journal of Comparative Neurology*, *292*(4), 497–523. https://doi.org/10.1002/cne.902920402

Enoch, J. M., Essock, E. A., & Williams, R. A. (1984). Relating vernier acuity and Snellen acuity in specific clinical populations. *Documenta Ophthalmologica*, *58*(1), 71–77.

Fahle, M. (1993). Visual learning in the hyperacuity range in adults. *German Journal of Ophthalmology*, *2*(2), 83–86.

Findlay, J. M. (1973, January 12). Feature detectors and vernier acuity. *Nature*, *241*(5385), 135–137.

Geisler, W. S. (1984). Physical limits of acuity and hyperacuity. *Journal of the Optical Society of America. A, Optics and Image Science*, *1*(7), 775–782. Retrieved from http://www.ncbi.nlm.nih.gov/pubmed/6747742

Harmening, W. M., Göbbels, K., & Wagner, H. (2007). Vernier acuity in barn owls. *Vision Research*, *47*(7), 1020–1026. https://doi.org/10.1016/j.visres.2007.01.005

Harmening, W. M., Tuten, W. S., Roorda, A., & Sincich, L. C. (2014). Mapping the perceptual grain of the human retina. *The Journal of Neuroscience*, *34*(16), 5667–5677. https://doi.org/10.1523/JNEUROSCI.5191-13.2014

He, J. C., Sun, P., Held, R., Thorn, F., Sun, X., & Gwiazda, J. E. (2002). Wavefront aberrations in eyes of emmetropic and moderately myopic school children and young adults. *Vision Research*, *42*(8), 1063–1070. https://doi.org/10.1016/S0042-6989(02)00035-4

Hering, E. (1899). Ueber die Grenzen der Sehschärfe [On the limits of visual acuity]. In *Berichte über die Verhandlungen der Königlich-Sächsischen Gesellschaft der Wissenschaften zu Leipzig. Mathematisch-Physische Classe; Naturwissenschaftlicher Teil*, *51* (pp. 16–24). Leipzig, Germany: Georg Thieme.

Hirsch, J., & Curcio, C. A. (1989). The spatial resolution capacity of human foveal retina. *Vision Research*, *29*(9), 1095–1101.

Hou, C., Good, W. V., & Norcia, A. M. (2018). Detection of amblyopia using sweep VEP Vernier and grating acuity. *Investigative Ophthalmology & Visual Science*, *59*(3), 1435–1442. https://doi.org/10.1167/iovs.17-23021

Hou, C., Kim, Y.-J., & Verghese, P. (2017). Cortical sources of Vernier acuity in the human visual system: An EEG-source imaging study. *Journal of Vision*, *17*(6):2, 1–12, https://doi.org/10.1167/17.6.2. [PubMed] [Article]

Jiang, H., Cottaris, N., Golden, J., Brainard, D., Farrell, J. E., & Wandell, B. A. (2017). Simulating retinal encoding: Factors influencing Vernier acuity. *Electronic Imaging: Human Vision and Electronic Imaging*, *5*, 177–181.

Karimian, F., Feizi, S., & Doozande, A. (2010). Higher-order aberrations in myopic eyes. *Journal of Ophthalmic and Vision Research*, *5*(1), 3–9.

Kasahara, K., Maeda, N., Fujikado, T., Tomita, M., Moriyama, M., Fuchihata, M., & Ohno-Matsui, K. (2017). Characteristics of higher-order aberrations and anterior segment tomography in patients with pathologic myopia. *International Ophthalmology*, *37*(6), 1279–1288. https://doi.org/10.1007/s10792-016-0356-7

Kiorpes, L., Kiper, D. C., & Movshon, J. A. (1993). Contrast sensitivity and vernier acuity in amblyopic monkeys. *Vision Research*, *33*(16), 2301–2311. Retrieved from http://www.ncbi.nlm.nih.gov/pubmed/8273294

Krauskopf, J., & Farell, B. (1991). Vernier acuity: effects of chromatic content, blur and contrast. *Vision Research*, *31*(4), 735–749. Retrieved from http://www.ncbi.nlm.nih.gov/pubmed/1843773

Kwan, W. C. K., Yip, S. P., & Yap, M. K. H. (2009). Monochromatic aberrations of the human eye and myopia. *Clinical and Experimental Optometry*, *92*(3), 304–312. https://doi.org/10.1111/j.1444-0938.2009.00378.x

Levi, D. M., & Klein, S. A. (1982, July 15). Hyperacuity and amblyopia. *Nature*, *298*(5871), 268–270.

Levi, D. M., & Klein, S. A. (1990). Equivalent intrinsic blur in spatial vision. *Vision Research*, *30*(12), 1971–93. Retrieved from http://pesquisa.bvsalud.org/portal/resource/pt/mdl-2288101

Lieberman, H. R., & Pentland, A. P. (1982). Microcomputer-based estimation of psychophysical thresholds: The Best PEST. *Behavior Research Methods & Instrumentation*, *14*, 21–25.

Lindblom, B., & Westheimer, G. (1989). Binocular summation of hyperacuity tasks. *Journal of the Optical Society of America A*, *6*(4),585. https://doi.org/10.1364/JOSAA.6.000585

Lombardo, M., Serrao, S., Ducoli, P., & Lombardo, G. (2012). Variations in image optical quality of the eye and the sampling limit of resolution of the cone mosaic with axial length in young adults. *Journal of Cataract and Refractive Surgery*, *38*(7), 1147–1155. https://doi.org/10.1016/j.jcrs.2012.02.033

Lü, Y., Xia, W., Chu, R., Zhou, X., Dai, J., & Zhou, H. (2011). [Relationship between best corrected visual acuity and refraction parameters in myopia]. [In Chinese.] *Fa Yi Xue Za Zhi*, *27*(2), 94–97. Retrieved from http://www.ncbi.nlm.nih.gov/pubmed/21604445

Maeda, P. (2008). Zernike polynomials to generate non-spherical wavefront, diffraction, namely, transfer function. Retrieved from http://www.pudn.com/Download/item/id/472325.html

Marcos, S., Sawides, L., Gambra, E., & Dorronsoro, C. (2008). Influence of adaptive-optics ocular aberration correction on visual acuity at different luminances and contrast polarities. *Journal of Vision*, *8*(3):1, 1–12, https://doi.org/10.1167/8.13.1. [PubMed] [Article]

Marsack, J. D., Thibos, L. N., & Applegate, R. A. (2004). Metrics of optical quality derived from wave aberrations predict visual performance. *Journal of Vision*, *4*(4):8, 322–328, https://doi.org/10.1167/4.4.8. [PubMed] [Article]

McKee, S. P., Levi, D. M., & Movshon, J. A. (2003). The pattern of visual deficits in amblyopia. *Journal of Vision*, *3*(5),5. https://doi.org/10.1167/3.5.5

Mckee, S. P., & Westheimer, G. (1978). Improvement in vernier acuity with practice. *Perception & Psychophysics*, *24*, 258–262.

Murphy, K. M., & Mitchell, D. E. (1991). Vernier acuity of normal and visually deprived cats. *Vision Research*, *31*(2), 253–266.

Paquin, M., Hamam, H., & Simonet, P. (2002). Objective measurement of optical aberrations in myopic eyes. *Optometry and Vision Science*, *79*(5), 285–291. Retrieved from http://www.ncbi.nlm.nih.gov/pubmed/12035985

Ratnam, K., Domdei, N., Harmening, W. M., & Roorda, A. (2017). Benefits of retinal image motion at the limits of spatial vision. *Journal of Vision*, *17*(1):30, 1–11, https://doi.org/10.1167/17.1.30. [PubMed] [Article]

Ravikumar, S., Thibos, L. N., & Bradley, A. (2008). Calculation of retinal image quality for polychromatic light. *Journal of the Optical Society of America. A*, *25*(10), 2395–2407. https://doi.org/10.1364/JOSAA.25.002395

Rocha, K. M., Vabre, L., Chateau, N., & Krueger, R. R. (2010). Enhanced visual acuity and image perception following correction of highly aberrated eyes using an adaptive optics visual simulator. *Journal of Refractive Surgery*, *26*(1), 52–56. https://doi.org/10.3928/1081597X-20101215-08

Rossi, E. A., & Roorda, A. (2010). The relationship between visual resolution and cone spacing in the human fovea. *Nat Neurosci*, *13*(2), 156–157. https://doi.org/10.1038/nn.2465

Schwiegerling, J. (2002). Scaling Zernike expansion coefficients to different pupil sizes. *Journal of the Optical Society of America A: Optics, Image Science, and Vision*, *19*(10), 1937–1945.

Seymoure, P., & Juraska, J. M. (1997). Vernier and grating acuity in adult hooded rats: The influence of sex. *Behavioral Neuroscience*, *111*(4), 792–800. Retrieved from http://www.ncbi.nlm.nih.gov/pubmed/9267656

Srivannaboon, S., Reinstein, D. Z., & Archer, T. J. (2007). Diurnal variation of higher order aberrations in human eyes. *Journal of Refractive Surgery*, *23*(5), 442–446. https://doi.org/10.1016/j.jalz.2013.05.1020

Strasburger, H., Huber, J., & Rose, D. (2018). Ewald Hering's (1899) on the limits of visual acuity: A translation and commentary - With a supplement on Alfred Volkmann's (1863) Physiological Investigations in the Field of Optics. *I-Perception*, *9*(3) (1899), 1–14. https://doi.org/10.1177/2041669518763675

Tan, Y., Tong, X., Chen, W., Weng, X., He, S., & Zhao, J. (2018). Vernier but not grating acuity contributes to an early stage of visual word processing. *Neuroscience Bulletin*, *34*(3), 517–526. https://doi.org/10.1007/s12264-018-0220-z

Thibos, L. N., Hong, X., Bradley, A., & Applegate, R. A. (2004). Accuracy and precision of objective refraction from wavefront aberrations. *Journal of Vision*, *4*(4):9, 329–351, https://doi.org/10.1167/4.4.9. [PubMed] [Article]

Thibos, L. N., Hong, X., Bradley, A., & Cheng, X. (2002). Statistical variation of aberration structure and image quality in a normal population of healthy eyes. *Journal of the Optical Society of America. A, Optics, Image Science, and Vision*, *19*(12), 2329–2348. https://doi.org/10.1364/JOSAA.19.002329

Thibos, L. N., Wheeler, W., & Horner, D. (1997). Power vectors: An application of Fourier analysis to the description and statistical analysis of

refractive error. *Optometry and Vision Science*, *74*(6), 367–375. Retrieved from http://www.ncbi.nlm.nih.gov/pubmed/9255814

Villegas, E. A., Alcon, E., & Artal, P. (2008). Optical quality of the eye in subjects with normal and excellent visual acuity. *Investigative Ophthalmology and Visual Science*, *49*(10), 4688–4696. https://doi.org/10.1167/iovs.08-2316

Visser, N., Berendschot, T. T. J. M., Verbakel, F., Tan, A. N., de Brabander, J., & Nuijts, R. M. M. A. (2011). Evaluation of the comparability and repeatability of four wavefront aberrometers. *Investigative Ophthalmology and Visual Science*, *52*(3), 1302–1311. https://doi.org/10.1167/iovs.10-5841

Wang, Y., Bensaid, N., Tiruveedhula, P., Ma, J., Roorda, A., & Ravikumar, S. (2018). The relationship between cone density and axial length: CAL study. In *Annual Meeting of the Association for Research in Vision and Ophthalmology (ARVO)*. Berkeley, California, United States.

Watson, A. B., & Ahumada, A. J. (2008). Predicting visual acuity from wavefront aberrations. *Journal of Vision*, *8*(4):17, 1–19, https://doi.org/10.1167/8.4.17. [PubMed] [Article]

Webster, M. A., Georgeson, M. A., & Webster, S. M. (2002). Neural adjustments to image blur. *Nature Neuroscience*, *5*(9), 839–840. https://doi.org/10.1038/nn906

Wehrhahn, C., & Westheimer, G. (1990). How vernier acuity depends on contrast. *Experimental Brain Research*, *80*(3), 618–620. Retrieved from http://www.ncbi.nlm.nih.gov/pubmed/2387359

Wei, R. H., Lim, L., Chan, W. K., & Tan, D. T. H. (2006). Higher order ocular aberrations in eyes with myopia in a Chinese population. *Journal of Refractive Surgery*, *22*(7), 695–702. Retrieved from http://www.ncbi.nlm.nih.gov/pubmed/16995552

Westheimer, G. (1975). Visual acuity and hyperacuity. *Investigative Ophthalmology*, *64*(8), 570–572. https://doi.org/10.1097/00006324-198708000-00002

Westheimer, G. (2009). Visual acuity: Information theory, retinal image structure and resolution thresholds. *Progress in Retinal and Eye Research*, *28*(3), 178–186. https://doi.org/10.1016/j.preteyeres.2009.04.001

Westheimer, G., & McKee, S. P. (1975). Visual acuity in the presence of retinal-image motion. *Journal of the Optical Society of America*, *65*(7), 847–850. Retrieved from http://www.ncbi.nlm.nih.gov/pubmed/1142031

Westheimer, G., & McKee, S. P. (1977). Spatial configurations for visual hyperacuity. *Vision Research*, *17*(8), 941–947. Retrieved from http://www.ncbi.nlm.nih.gov/pubmed/595400

Westheimer, G., Shimamura, K., & McKee, S. P. (1976). Interference with line-orientation sensitivity. *Journal of the Optical Society of America*, *66*(4), 332–338. Retrieved from http://www.ncbi.nlm.nih.gov/pubmed/1262981

Whitaker, D., & MacVeigh, D. (1991). Interaction of spatial frequency and separation in vernier acuity. *Vision Research*, *31*(7–8), 1205–1212.

Williams, R. A., Enoch, J. M., & Essock, E. A. (1984). The resistance of selected hyperacuity configurations to retinal image degradation. *Investigative Ophthalmology & Visual Science*, *25*(4), 389–399.

Wülfing, E. A. (1892). Ueber den kleinsten Gesichtswinkel. *Zeitschrift Für Biologie*, *29*, 199–202.

Yoon, G., & Williams, D. R. (2002). Visual performance after correcting the monochromatic and chromatic aberrations of the eye. *Journal of the Optical Society of America A*, *19*(2), 266–275.

Zheleznyak, L., Sabesan, R., Oh, J. S., MacRae, S., & Yoon, G. (2013). Modified monovision with spherical aberration to improve presbyopic through-focus visual performance. *Investigative Ophthalmology and Visual Science*, *54*(5), 3157–3165. https://doi.org/10.1167/iovs.12-11050

3.2 Human gaze is systematically offset from the center of cone topography

Reiniger, J. L., Domdei, N., Holz, F. G., and Harmening, W. M. Human gaze is systematically offset from the center of cone topography. Curr Biol. 2021; 31 (18): pp. 4188– 4193; doi: 10.1016/j.cub.2021.07.005

Report

Current Biology

Human gaze is systematically offset from the center of cone topography

Graphical abstract

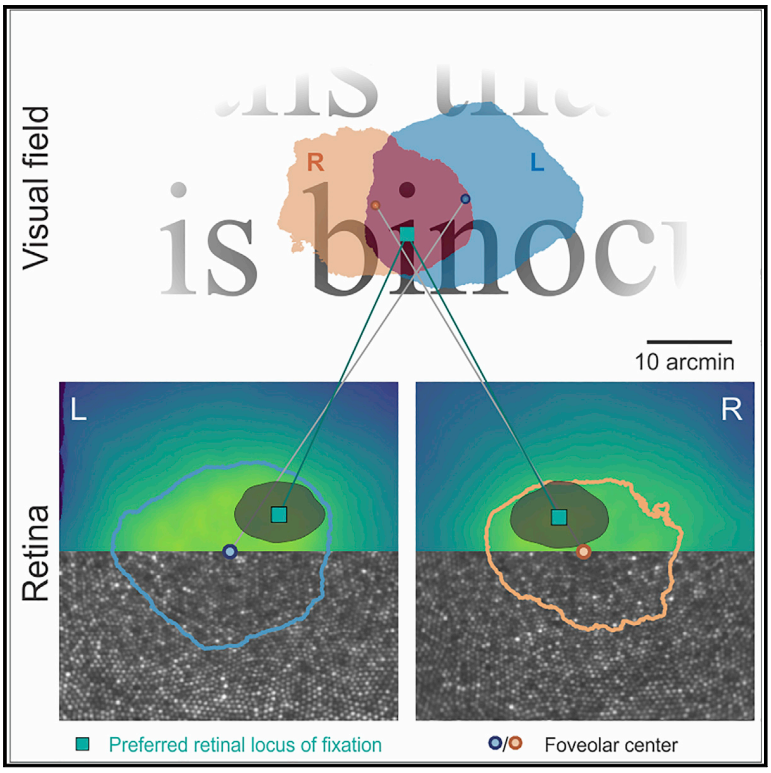

Authors

Jenny L. Reiniger, Niklas Domdei, Frank G. Holz, Wolf M. Harmening

Correspondence

wolf.harmening@ukbonn.de

In brief

Reiniger et al. show that the preferred retinal locus of fixation is systematically and reproducibly displaced from the topographical center of the human fovea. In the binocular visual field, the area of high cone density sampling is thus horizontally enlarged and offset toward an area usually containing smaller details in the natural environment.

Highlights

- Foveal cone topography is mirror symmetric between fellow eyes
- The preferred retinal locus of fixation (PRL) is reproducible over multiple years
- The PRL is offset naso-superiorly on the retina, correlated between fellow eyes
- The binocular area of high cone densities is horizontally enlarged, on average

Reiniger et al., 2021, Current Biology *31*, 4188–4193
September 27, 2021
https://doi.org/10.1016/j.cub.2021.07.005

CellPress

CellPress

Current Biology

Report

Human gaze is systematically offset from the center of cone topography

Jenny L. Reiniger,[1] Niklas Domdei,[1] Frank G. Holz,[1] and Wolf M. Harmening[1,2,*]
[1]Rheinische Friedrich-Wilhelms-Universität Bonn, Department of Ophthalmology, Ernst-Abbe-Str. 2, Bonn 53127, Germany
[2]Lead contact
*Correspondence: wolf.harmening@ukbonn.de
https://doi.org/10.1016/j.cub.2021.07.005

SUMMARY

The small physical depression of the human retina, the fovea, is the retinal locus of prime visual resolution, achieved by a peaking topography of the light-sensitive cone photoreceptor outer segments[1–3] and a post-receptor wiring scheme preserving high-density sampling.[4,5] Humans dynamically direct their gaze such that the retinal images of objects of interest fall onto the foveola, the central one-degree diameter of the fovea,[6–8] but it is yet unclear whether a relationship between the individual photoreceptor topography at this location and visual fixation behavior exists.[9,10] By employing adaptive optics *in vivo* imaging and micro-stimulation,[11–13] we created topographical maps of the complete foveolar cone mosaics in both eyes of 20 healthy participants while simultaneously recording the retinal location of a fixated visual object in a psychophysical experiment with cellular resolution. We found that the locus of fixation was systematically shifted away from the topographical center toward a naso-superior quadrant on the retina, about 5 min of arc of visual angle on average, with a mirror symmetrical trend between fellow eyes. In cyclopean view, the topographical centers were superior to the fixated target, corresponding to areas in the visual field usually more distant[14,15] and thus containing higher spatial frequencies. Given the large variability in foveal topography between individuals, and the surprising precision with which fixation is repeatedly directed to just a small bouquet of cones in the foveola, these findings demonstrate a finely tuned, functionally relevant link between the development of the cellular mosaic of photoreceptors and visual behavior.

RESULTS AND DISCUSSION

Foveolar cone topography

By high-resolution adaptive optics scanning laser ophthalmoscopy (AOSLO), cone photoreceptor topography at the very center of the fovea was analyzed in 41 eyes of 21 healthy human participants (twenty binocular and one monocular). In each retinal image, about 6,800 to 9,100 cones were marked and their location used to compute continuous two-dimensional maps of cone density (STAR Methods; Figures 1A–1F). Peak cone density (PCD) varied widely across participants (range: 10,823–18,023; average: 14,067 cones/deg^2; see also Table S1), similar to previous reports.[1,2,9,10,16–19] In alignment with histology[3] and *in vivo* imaging,[2,17] we found a steeper drop in cone density along the vertical compared to the horizontal meridian (Figures 1G and 1H), an anisotropy also found in retinas of other mammals.[20,21]

Cone density, interocular symmetry, and fixation behavior (see below) of the three children in our study (aged 10, 12, and 14 years; participants P3, P10, and P16, respectively) did not differ from the adult population. This extends cone density reports at higher eccentricites[22,23] into the foveal center. Histological studies point to an earlier cessation of centripetal cone photoreceptor migration, with a doubling of cone density between gestational week 22 and postnatal day 5, and a tripling between 5 days and 45 months postnatal.[24] Visual acuity in children was shown to approach adult performance between the ages of 5 and 6 years.[25] Thus, the children examined here are assumed to be in a comparable stage of visual development as adults.

We introduce a novel, spatially more robust metric to anchor the fovea's topographical center: the cone density centroid (CDC) was computed as the weighted center of cone densities within the 20th percentile contour (Figure 1F). In 8 participants (16 eyes), foveolar cone mosaics were imaged and analyzed on two different days. After careful alignment of high signal-to-noise ratio images, the advantage of using the CDC over PCD location as anchor became apparent. While the PCDs as well as CDC densities were highly correlated between fellow eyes ($r^2 = 0.95$, $p << 0.001$ and $r^2 = 0.89$, $p << 0.001$, respectively; Figure 1I), on average, PCD locations varied by more than 3-fold (mean ± SD: 3.0 ± 2.3 arcmin; range: 0.1–7.9 arcmin), compared to CDC locations (mean ± SD: 0.9 ± 0.7 arcmin; range: 0.1–2.6 arcmin; $p = 0.002$; paired t test). In all following analyses, the CDC was used as the singular spatial reference location of the foveolar center.

The fact that more and more optical and analytical limitations are lifted with novel imaging techniques, like lateral resolution exceeding the diffraction limit offered by AOSLO,[26] and the good agreement between *in vivo* studies are likely to lead toward

Current Biology
Report

CellPress

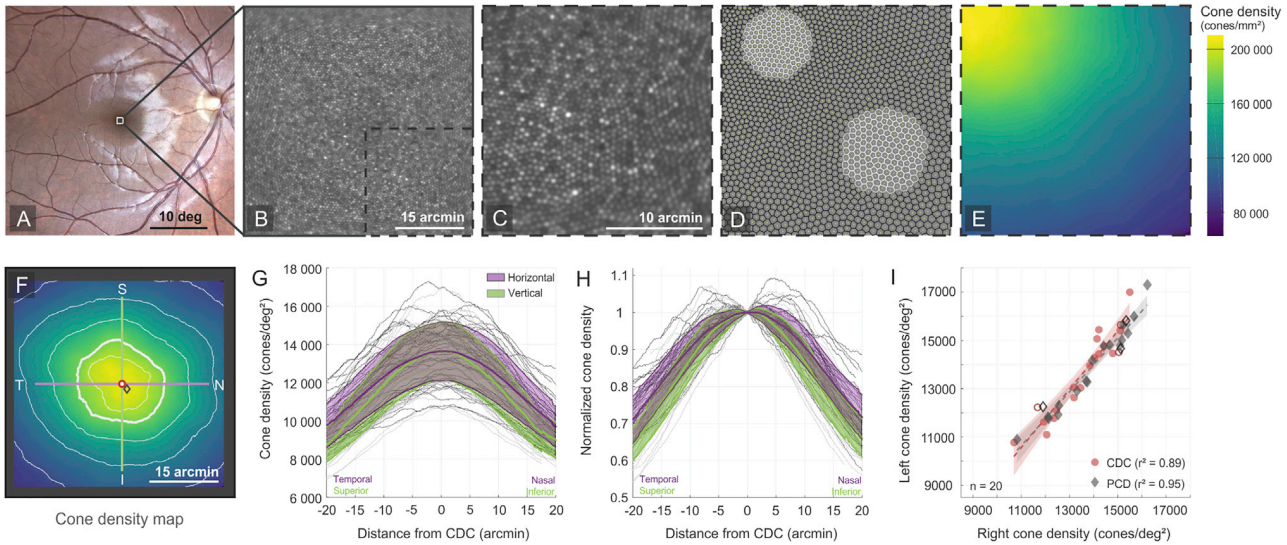

Figure 1. Cellular topography of the foveola

(A) Fundus photograph of a participant's right eye.

(B and C) AOSLO image of the foveal center (B), dashed outline enlarged in (C).

(D) Cone density was computed by the encircled area of the nearest 150 Voronoi tiles around each image pixel (two examples shown).

(E) Cone density color coded as cones/mm^2.

(F) In the full map, iso-contour lines are 10th, 20th (bold), 40th, 60th, and 80th percentiles. Diamond, peak cone density (PCD); red circle, cone density centroid (CDC). See Figure S1 for maps of all eyes. Green and purple lines are cardinal meridians shown in (G) and (H) for all eyes.

(G) Individual (thin) and average (bold) profiles of absolute cone density.

(H) Same as (G), normalized to the cone density at the CDC.

(I) Cone densities at the CDC (circles) and PCDs (diamond) were highly correlated between fellow eyes. Open markers indicate children. Regression lines and 95% confidence intervals are represented by dotted lines and shaded areas, respectively.

See Figure S2 for extended symmetry analysis.

a replacement of the gold standard for quantitative cone mosaic analysis, from histology of dissected tissue preparations[3] toward high-resolution *in vivo* imaging.

Interocular symmetry of foveolar topography

Symmetry is an extensively studied characteristic in various organs. Previous observations in the field of ophthalmic optics showed ocular symmetries between fellow eyes, such as corneal topography and ocular wavefront aberrations.[27] For cone density, high interocular correlation was shown at larger retinal eccentricities (250, 420, 760, and 1,300 μm)[28] as well as for PCD.[17] In the foveal center, similar as shown in our data, Cava et al.[1] found that, in addition to the PCD, Voronoi cell area regularity and certain iso-density contour areas are also highly symmetrical between fellow eyes. Here, we observed high topographical symmetry between fellow eyes, readily perceivable by eye (Figure S1). When the pointwise difference in density was computed between fellow eyes, the median root-mean-square (RMS) (3.8%) was only slightly larger than the difference between two maps of the same eye analyzed from different days (median RMS: 2.9%; Figure S2). Small local image distortions are likely to occur due to the scanning nature of the AOSLO, pixelwise image acquisition, and sequential stabilization processes. With a conservative estimation of such local distortions of up to 3 pixels (equaling 0.3 minutes of arc of visual angle), they remain relatively small compared to the magnitude of measured offsets between retinal locations of interest. By manually selecting a reference frame with low distortions (STAR Methods), we further minimized this confound. PCDs in fellow eyes were strongly correlated and not different between right and left eyes (paired t test; $p = 0.6$), as is also observed by Cava et al.[1] There was also no significant difference of PCDs between dominant and non-dominant eyes in our population (paired t test; $p = 0.4$). Preliminary data from an acuity study of our group, including pilot data of five participants from the present study, showed that resolution acuity was better in the dominant eyes of all five examined participants, while acuity thresholds were highly correlated with the density of the foveolar cone mosaic.[29] This suggests that better performance in the dominant eye might be related to other factors than PCD, e.g., the particular retinal locations used during the task as well as retinal motion. To test this hypothesis, resolution acuity and ocular dominance need to be investigated in a larger population. Additionally, a spatially resolved analysis of retinal image quality might help to better understand how optical limits during development influence the formation of the optimal retinal locus, as they affect the sampling limit in resolution tasks.[30]

Preferred retinal locus of fixation

In the natural environment, fixation, discrimination, or resolution requirements are often closely related. For a long time, it was common view that the anatomical center of the fovea also represents the center of fixation,[31] a view supported by the rough alignment between these retinal loci. With current imaging techniques, however, opening the door to the exact cellular makeup

CellPress

Current Biology
Report

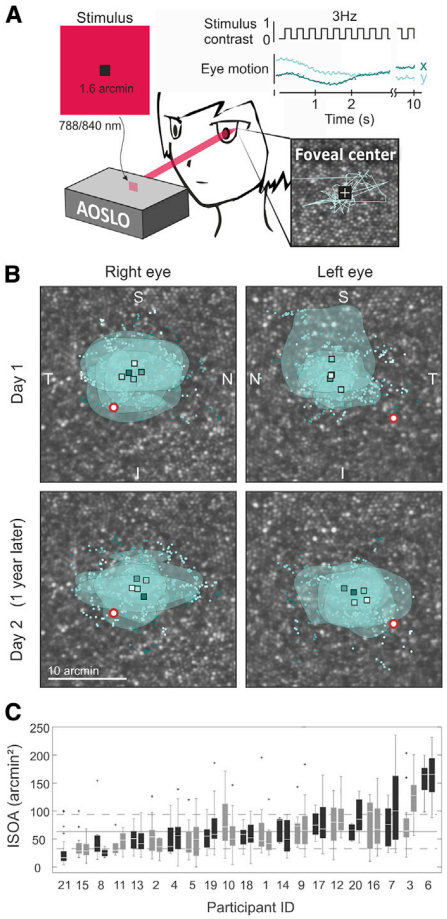

Figure 2. Measuring fixation behavior

(A) Unambiguous retinal landing points of a small flashing target were derived from multiple AOSLO videos.

(B) The PRLs (squares) of consecutive videos in right and left eyes of P5 on two different days (~1 year between measurements; see Figure S3 for fixation stability across multiple years). Small dots are all stimulus locations; marker brightness represents consecutive videos. Contours are the area containing one standard deviation of the data (isoline area [ISOA]). Red circle, CDC.

(C) ISOAs in all fellow eyes, participants ordered by average magnitude. The left bars represent left and right bars right eyes, respectively. Horizontal lines represent the average (solid) ± one standard deviation (dotted). Box whisker extends to the most extreme data values, and plus markers represent outliers (distance >1.5 × range between 25th and 75th percentiles).

of an individual eye, it was revealed that the preferred retinal locus of fixation (PRL) is offset from the location of PCD as well as from the center of the foveal avascular zone and foveal pit.[2,9,10,16,32] The PRL is also not the retinal location that provides highest sensitivity to small spot stimuli, which was recently shown to be rather plateau-like within the central 0.1 degree of the foveola.[33] However, a possible systematic relationship between the PRL and the retinal cone mosaic was yet missing.

In the majority of eyes in our population (33/41), fixation behavior was examined on 2 or more days (Table S1). PRLs could be found accurately, with a median distance of 2.3 arcmin between consecutive measurements (range: 1.0–5.6 arcmin; Figures 2B and S3B). When stimulus locations were pooled across a single day, median locations differed by only 1.5 arcmin (range: 1.0–4.2 arcmin; Figures S3A and S3B). The observed fixation stability, given by the isoline areas (ISOAs), ranged between 23 and 153 arcmin^2 in right eyes and between 29 and 154 arcmin^2 in left eyes (Table S1). The participants who had a larger median ISOA also had higher PRL variability between single measurements ($\rho = 0.39$; $p = 0.01$; Figure 2C). PRLs as well as ISOAs were highly reproducible in individuals, even across a period of up to 3.5 years (Figure S3A). This confirms and extends the finding of Kilpeläinen et al.,[32] showing PRL reproducibility over a period of 2 days, on average.

In addition to the previously described structural symmetry between fellow eyes, we also observed functional symmetries. Albeit recorded under monocular viewing, fixation stability across fellow eyes was highly correlated ($r^2 = 0.66$; $p << 0.001$; Figure 2C), supporting the hypothesis of an underlying coupling of both eyes during fixation.[34] When eyes were grouped according to ocular dominance, there was no difference between median ISOAs of dominant and non-dominant eyes ($p = 0.062$; Wilcoxon signed rank test; $n = 20$). Previous studies found functional interocular correlation in microsaccade rates and amplitudes under monocular viewing conditions[35] and bivariate contour ellipse areas[36] and suggest improved fixation stability under binocular viewing conditions.[34,35]

The relationship of cone topography and fixation

By measuring fixation behavior in a cone-resolved experiment (Figures 2A and 2B) and by careful alignment with the cone density maps of both eyes, we reveal a fine and very reproducible systematic offset between cone topography and fixation behavior. In retinal coordinates, the PRL was displaced naso-superiorly from the CDC by an average amount of 4.7 arcmin (Figure 3A), corresponding to about 10 cone diameters, in accordance with a recent monocular study comparing PRL and PCD locations.[32] Offset distances were correlated between fellow eyes in our study ($r^2 = 0.45$; $p = 0.001$; Figure S4B), with high correlation in the vertical ($r^2 = 0.72$; $p << 0.001$; Figure 3B), but not horizontal component ($r^2 = 0.09$; $p = 0.19$). The offset's angular component was thus not significantly correlated ($r^2 = 0.07$; $p = 0.28$), albeit with a mirror symmetrical trend along a vertical axis (Figure S4C). Other studies, with a lower number of subjects or a less accurate method of measuring the PRL, found larger offsets with median values of 9.8 and 11.5 arcmin.[9,10] However, a trend toward PRL formation superior to the PCD is visible also in those data. Similar PRL offsets (mean: 5.3 arcmin) could be found when re-analyzing data from Wang et al.[2] with our analysis methods (Figure S4A).

Projection of cone topography into the visual field

In the following, we assume that monocular and binocular PRLs are identical and that PRLs are retinal coordinates of corresponding points in the visual environment and thus independent of viewing distance.[37] In a cyclopean view, where both PRLs are the common center, CDCs and high cone density areas were slightly superior to the fixated point (Figures 4A and 4B), firmly linked between the two eyes. In a natural environment, the visual field above a fixated point is often farther away (e.g., horizontal surfaces, such as grounds and table tops),[14,15] creating a bottom-to-top gradient of spatial frequencies with higher frequencies above the point of fixation. A displacement of the CDC superior to fixation might allow for a better estimation of

Current Biology
Report

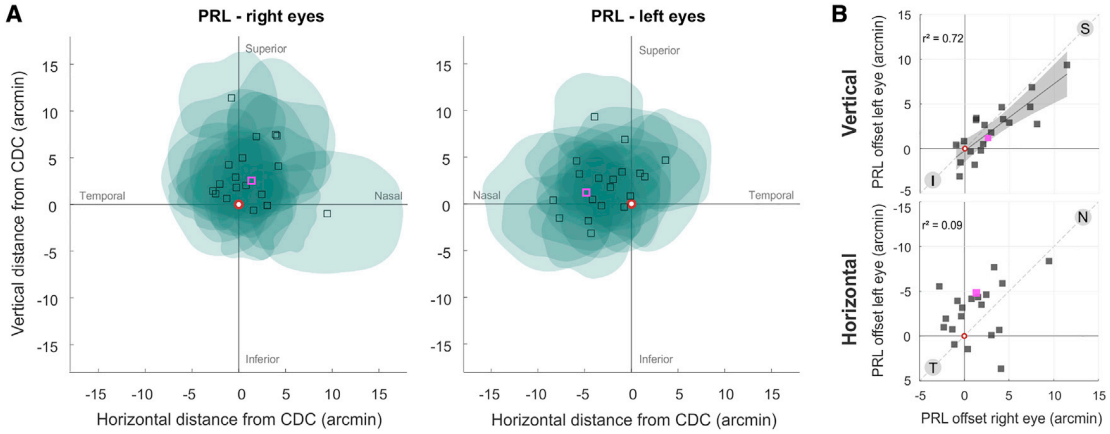

Figure 3. Relationship between cone topography and PRL in retinal coordinates

(A) Right and left eyes' median PRL and 1 SD ISOAs plotted relative to the CDC (see also Figure S4). Exemplary data pair most similar to average (P13) is highlighted in purple.

(B) Vertical offsets were strongly correlated between fellow eyes (r^2 = 0.72; p << 0.001). The linear regression and 95% confidence interval (shaded area) are shown. Horizontal offsets were not correlated (r^2 = 0.09; p = 0.19). I, inferior; N, nasal; S, superior; T, temporal retinal orientations.

See Figure S4 for distance and angular relationships.

3D structure of textured surfaces or objects. Due to the strong correlation of the vertical position in the visual field, the offset between both eyes' CDCs was more pronounced horizontally in our data (Figures 4C and 4D). Also, CDCs of most right eyes landed leftward from the left eye's CDCs, resulting in crossed disparity. Uncrossed disparities were observed in five participants only, who also had minimal horizontal offsets. Figure 4D further illustrates the geometry and magnitude of the offsets projected into the binocular field of view.

The highly ordered and systematic functional and topographical architecture we observe between fellow eyes could be the result of a developmental process creating appropriate location information for binocular spatial sampling. From such point of view, a nasal displacement might emerge as an "overshoot" during PRL formation, ensuring overlap between the high spatial frequency sampling capacity areas in both eyes. We found incomplete overlaps that essentially enlarge the visual field sampled by high-density cones in all participants (Figures 4B and 4C). By the rules of binocular combination, the eye that sees higher contrast and sharper details gets more weight in the cyclopean percept.[38] Thus, by imperfect horizontal alignment of cone topographies, the visual system might create a larger field of sharp perception with individual sharpness gradients of the two retinal images.[39]

One of the factors driving the enrichment of visual capacities during development is the demand of resolving fine structures in the visual environment, and fixation behavior seems to contribute to such strategies. In adults, fixational eye motion was shown to enhance visual resolution, for instance.[40–42] Post-receptorally, the connectivity between individual cones and midget bipolar and ganglion cells was recently shown to develop and establish a private line for the central photoreceptors already during gestation.[4] The centripetal migration of cone photoreceptors starts in parallel but takes place mainly after birth.[24] The nasal superior offset direction aligns with the closest connectivity to the optic nerve head, which could facilitate the slightly offset PRL development, even if conduction velocity of retinal ganglion cells was shown to minimize possible time differences across the retina.[43] At larger retinal eccentricities, midget ganglion cells have smaller dendritic field diameters in the nasal quadrant of human retinae,[44] which may be an outcome of the same underlying mechanisms as the biased PRL formation.

Conclusions

Taken together, participants without known retinal disease or abnormalities showed a small but systematic offset between their PRL and the center of cone density distribution, formed in a way to vertically offset high cone densities toward the superior part of the visual field and to ensure a horizontal overlap of those areas in the binocular visual field. This functional symmetry was associated with high interocular symmetry of foveolar cone topography. Binocular, foveated display systems that seek to mimic human vision with high precision could be tuned to reflect this spatial relationship.[45] Binocular *in vivo* foveal topography data may provide a basis for detecting changes in the central photoreceptor topography during retinal disease[46] and, more generally, could contribute to replace histology as gold standard for normative human photoreceptor evaluations in a healthy population.

STAR★METHODS

Detailed methods are provided in the online version of this paper and include the following:

- KEY RESOURCES TABLE
- RESOURCE AVAILABILITY
  - Lead contact
  - Materials availability
  - Data and code availability
- EXPERIMENTAL MODEL AND SUBJECT DETAILS
  - Human participants

CellPress

Current Biology
Report

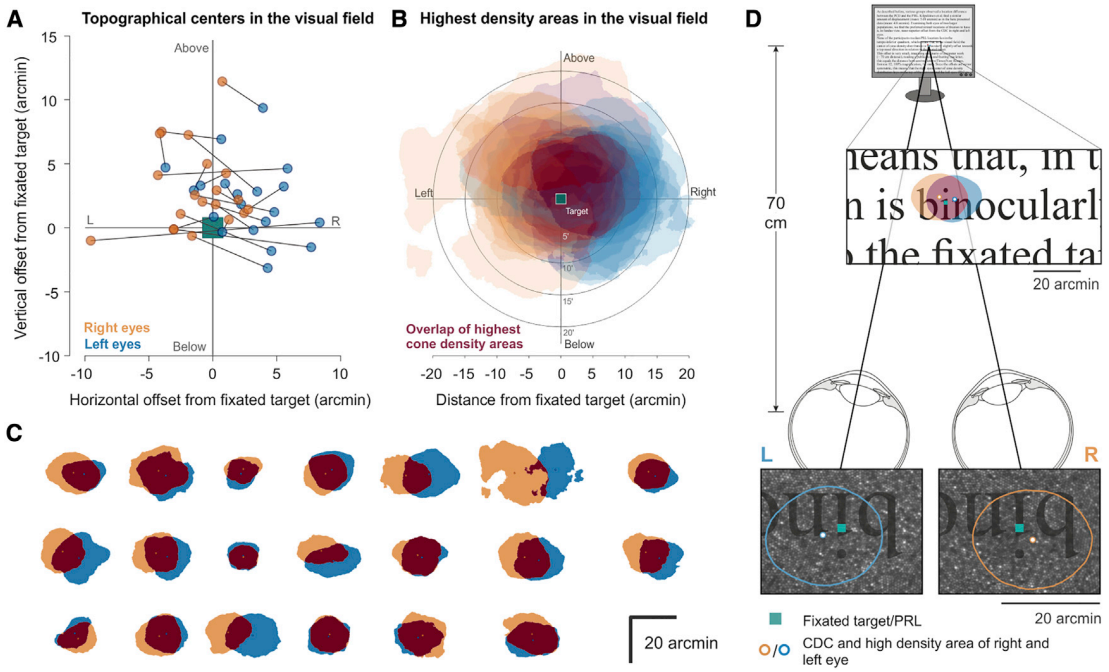

Figure 4. Projection of cone topography into the binocular visual field

(A) CDC of both eyes (right, orange; left, blue) plotted with their PRL as common center in the visual field. Lines connect fellow eyes.

(B) Similar as in (A), including retinal areas encompassing the highest 20% cone densities (within the central 50 arcmin of the fovea). Overlap is shown in dark red.

(C) Projections of high-density cone areas of all participants.

(D) The average displacement between fellow eyes, in a static reading situation, roughly equals the distance between two letters at reading distance (~1 mm). Orientation of cone mosaics is as seen from behind the observer.

SUPPLEMENTAL INFORMATION

Supplemental information can be found online at https://doi.org/10.1016/j.cub.2021.07.005.

ACKNOWLEDGMENTS

We thank Austin Roorda and the members of his lab for kindly providing image and PRL data for re-analysis. We are grateful for insightful comments by the reviewers of an earlier version of this manuscript. This work was supported by the Carl Zeiss Foundation (HC-AOSLO) and the Emmy Noether Program of the German Research Foundation (DFG) (Ha 5323/5-1).

AUTHOR CONTRIBUTIONS

J.L.R. and W.M.H. conceived the research idea. J.L.R., N.D., and W.M.H. developed the data analysis pipeline. J.L.R. performed the data analysis and convolutional neural network training. J.L.R. and W.M.H. wrote the manuscript. All authors discussed the results and edited the manuscript.

DECLARATION OF INTERESTS

The authors declare no competing interests.

Received: April 1, 2021
Revised: May 28, 2021
Accepted: July 2, 2021
Published: August 2, 2021

REFERENCES

1. Cava, J.A., Allphin, M.T., Mastey, R.R., Gaffney, M., Linderman, R.E., Cooper, R.F., and Carroll, J. (2020). Assessing interocular symmetry of the foveal cone mosaic. Invest. Ophthalmol. Vis. Sci. *61*, 23.
2. Wang, Y., Bensaid, N., Tiruveedhula, P., Ma, J., Ravikumar, S., and Roorda, A. (2019). Human foveal cone photoreceptor topography and its dependence on eye length. eLife *8*, e47148.
3. Curcio, C.A., Sloan, K.R., Kalina, R.E., and Hendrickson, A.E. (1990). Human photoreceptor topography. J. Comp. Neurol. *292*, 497–523.
4. Zhang, C., Kim, Y.J., Silverstein, A.R., Hoshino, A., Reh, T.A., Dacey, D.M., and Wong, R.O. (2020). Circuit reorganization shapes the developing human foveal midget connectome toward single-cone resolution. Neuron *108*, 905–918.e3.
5. Bryman, G.S., Liu, A., and Do, M.T.H. (2020). Optimized signal flow through photoreceptors supports the high-acuity vision of primates. Neuron *108*, 335–348.e7.
6. Poletti, M., Listorti, C., and Rucci, M. (2013). Microscopic eye movements compensate for nonhomogeneous vision within the fovea. Curr. Biol. *23*, 1691–1695.
7. Poletti, M., Rucci, M., and Carrasco, M. (2017). Selective attention within the foveola. Nat. Neurosci. *20*, 1413–1417.
8. Ko, H.K., Poletti, M., and Rucci, M. (2010). Microsaccades precisely relocate gaze in a high visual acuity task. Nat. Neurosci. *13*, 1549–1553.

9. Putnam, N.M., Hofer, H.J., Doble, N., Chen, L., Carroll, J., and Williams, D.R. (2005). The locus of fixation and the foveal cone mosaic. J. Vis. *5*, 632–639.
10. Wilk, M.A., Dubis, A.M., Cooper, R.F., Summerfelt, P., Dubra, A., and Carroll, J. (2017). Assessing the spatial relationship between fixation and foveal specializations. Vision Res. *132*, 53–61.
11. Harmening, W.M., Tuten, W.S., Roorda, A., and Sincich, L.C. (2014). Mapping the perceptual grain of the human retina. J. Neurosci. *34*, 5667–5677.
12. Rossi, E.A., and Roorda, A. (2010). The relationship between visual resolution and cone spacing in the human fovea. Nat. Neurosci. *13*, 156–157.
13. Sincich, L.C., Zhang, Y., Tiruveedhula, P., Horton, J.C., and Roorda, A. (2009). Resolving single cone inputs to visual receptive fields. Nat. Neurosci. *12*, 967–969.
14. Sprague, W.W., Cooper, E.A., Tošić, I., and Banks, M.S. (2015). Stereopsis is adaptive for the natural environment. Sci. Adv. *1*, e1400254.
15. Gibaldi, A., and Banks, M.S. (2019). Binocular eye movements are adapted to the natural environment. J. Neurosci. *39*, 2877–2888.
16. Li, K.Y., Tiruveedhula, P., and Roorda, A. (2010). Intersubject variability of foveal cone photoreceptor density in relation to eye length. Invest. Ophthalmol. Vis. Sci. *51*, 6858–6867.
17. Zhang, T., Godara, P., Blanco, E.R., Griffin, R.L., Wang, X., Curcio, C.A., and Zhang, Y. (2015). Variability in human cone topography assessed by adaptive optics scanning laser ophthalmoscopy. Am. J. Ophthalmol. *160*, 290–300.e1.
18. Cooper, R.F., Wilk, M.A., Tarima, S., and Carroll, J. (2016). Evaluating descriptive metrics of the human cone mosaic. Invest. Ophthalmol. Vis. Sci. *57*, 2992–3001.
19. Wells-Gray, E.M., Choi, S.S., Bries, A., and Doble, N. (2016). Variation in rod and cone density from the fovea to the mid-periphery in healthy human retinas using adaptive optics scanning laser ophthalmoscopy. Eye (Lond.) *30*, 1135–1143.
20. Packer, O., Hendrickson, A.E., and Curcio, C.A. (1989). Photoreceptor topography of the retina in the adult pigtail macaque (Macaca nemestrina). J. Comp. Neurol. *288*, 165–183.
21. Wikler, K.C., Williams, R.W., and Rakic, P. (1990). Photoreceptor mosaic: number and distribution of rods and cones in the rhesus monkey retina. J. Comp. Neurol. *297*, 499–508.
22. Park, S.P., Chung, J.K., Greenstein, V., Tsang, S.H., and Chang, S. (2013). A study of factors affecting the human cone photoreceptor density measured by adaptive optics scanning laser ophthalmoscope. Exp. Eye Res. *108*, 1–9.
23. Mirhajianmoghadam, H., Jnawali, A., Musial, G., Queener, H.M., Patel, N.B., Ostrin, L.A., and Porter, J. (2020). In vivo assessment of foveal geometry and cone photoreceptor density and spacing in children. Sci. Rep. *10*, 8942.
24. Yuodelis, C., and Hendrickson, A. (1986). A qualitative and quantitative analysis of the human fovea during development. Vision Res. *26*, 847–855.
25. Lai, Y.H., Wang, H.Z., and Hsu, H.T. (2011). Development of visual acuity in preschool children as measured with Landolt C and Tumbling E charts. J. AAPOS *15*, 251–255.
26. Lu, R., Aguilera, N., Liu, T., Liu, J., Giannini, J.P., Li, J., Bower, A.J., Dubra, A., and Tam, J. (2021). *In-vivo* sub-diffraction adaptive optics imaging of photoreceptors in the human eye with annular pupil illumination and sub-Airy detection. Optica *8*, 333–343.
27. Castejón-Mochón, J.F., López-Gil, N., Benito, A., and Artal, P. (2002). Ocular wave-front aberration statistics in a normal young population. Vision Res. *42*, 1611–1617.
28. Lombardo, M., Lombardo, G., Schiano Lomoriello, D., Ducoli, P., Stirpe, M., and Serrao, S. (2013). Interocular symmetry of parafoveal photoreceptor cone density distribution. Retina *33*, 1640–1649.
29. Reiniger, J.L., Domdei, N., Linden, M., Holz, F.G., and Harmening, W.M. (2019). Relationship between the foveal photoreceptor mosaic and adaptive optics corrected visual acuity. Invest. Opthalmol. Vis. Sci. *60*, 1777.
30. Reiniger, J.L., Lobecke, A.C., Sabesan, R., Bach, M., Verbakel, F., de Brabander, J., Holz, F.G., Berendschot, T.T.J.M., and Harmening, W.M. (2019). Habitual higher order aberrations affect Landolt but not Vernier acuity. J. Vis. *19*, 11.
31. Polyak, S., and Willmer, E.N. (1949). Retinal structure and colour vision. Doc. Ophthalmol. *3*, 24–56.
32. Kilpeläinen, M., Putnam, N.M., Ratnam, K., and Roorda, A. (2020). The anatomical, functional and perceived location of the fovea in the human visual system. Curr. Biol. Published online October 9, 2020. https://doi.org/10.2139/ssrn.3699785.
33. Domdei, N., Reiniger, J.L., Holz, F.G., and Harmening, W.M. (2021). The relationship between visual sensitivity and eccentricity, cone density and outer segment length in the human foveola. Invest. Ophthalmol. Vis. Sci. *62*, 31.
34. Krauskopf, J., Cornsweet, T.N., and Riggs, L.A. (1960). Analysis of eye movements during monocular and binocular fixation. J. Opt. Soc. Am. *50*, 572–578.
35. González, E.G., Wong, A.M.F., Niechwiej-Szwedo, E., Tarita-Nistor, L., and Steinbach, M.J. (2012). Eye position stability in amblyopia and in normal binocular vision. Invest. Ophthalmol. Vis. Sci. *53*, 5386–5394.
36. Zhu, X., He, W., Du, Y., Zhang, K., and Lu, Y. (2019). Interocular symmetry of fixation, optic disc, and corneal astigmatism in bilateral high myopia: the Shanghai high myopia study. Transl. Vis. Sci. Technol. *8*, 22.
37. Hillis, J.M., and Banks, M.S. (2001). Are corresponding points fixed? Vision Res. *41*, 2457–2473.
38. Home, R. (1978). Binocular summation: a study of contrast sensitivity, visual acuity and recognition. Vision Res. *18*, 579–585.
39. Gibaldi, A., Labhishetty, V., Thibos, L.N., and Banks, M.S. (2021). The blur horopter: retinal conjugate surface in binocular viewing. J. Vis. *21*, 8.
40. Rucci, M., Iovin, R., Poletti, M., and Santini, F. (2007). Miniature eye movements enhance fine spatial detail. Nature *447*, 851–854.
41. Ratnam, K., Domdei, N., Harmening, W.M., and Roorda, A. (2017). Benefits of retinal image motion at the limits of spatial vision. J. Vis. *17*, 30.
42. Rucci, M., Ahissar, E., and Burr, D. (2018). Temporal coding of visual space. Trends Cogn. Sci. *22*, 883–895.
43. Stanford, L.R. (1987). Conduction velocity variations minimize conduction time differences among retinal ganglion cell axons. Science *238*, 358–360.
44. Dacey, D.M. (1993). The mosaic of midget ganglion cells in the human retina. J. Neurosci. *13*, 5334–5355.
45. Tan, G., Lee, Y.-H., Zhan, T., Yang, J., Liu, S., Zhao, D., and Wu, S.-T. (2018). Foveated imaging for near-eye displays. Opt. Express *26*, 25076–25085.
46. Song, H., Rossi, E.A., and Williams, D.R. (2021). Reduced foveal cone density in early idiopathic macular telangiectasia. BMJ Open Ophthalmol. *6*, e000603.
47. Cunefare, D., Fang, L., Cooper, R.F., Dubra, A., Carroll, J., and Farsiu, S. (2017). Open source software for automatic detection of cone photoreceptors in adaptive optics ophthalmoscopy using convolutional neural networks. Sci. Rep. *7*, 6620.
48. Roorda, A., Romero-Borja, F., Donnelly Iii, W., Queener, H., Hebert, T., and Campbell, M. (2002). Adaptive optics scanning laser ophthalmoscopy. Opt. Express *10*, 405–412.
49. Domdei, N., Domdei, L., Reiniger, J.L., Linden, M., Holz, F.G., Roorda, A., and Harmening, W.M. (2017). Ultra-high contrast retinal display system for single photoreceptor psychophysics. Biomed. Opt. Express *9*, 157–172.
50. Poonja, S., Patel, S., Henry, L., and Roorda, A. (2005). Dynamic visual stimulus presentation in an adaptive optics scanning laser ophthalmoscope. J. Refract. Surg. *21*, S575–S580.
51. Arathorn, D.W., Yang, Q., Vogel, C.R., Zhang, Y., Tiruveedhula, P., and Roorda, A. (2007). Retinally stabilized cone-targeted stimulus delivery. Opt. Express *15*, 13731–13744.
52. Bruce, K.S., Harmening, W.M., Langston, B.R., Tuten, W.S., Roorda, A., and Sincich, L.C. (2015). Normal perceptual sensitivity arising from weakly reflective cone photoreceptors. Invest. Ophthalmol. Vis. Sci. *56*, 4431–4438.

STAR★METHODS

KEY RESOURCES TABLE

REAGENT or RESOURCE	SOURCE	IDENTIFIER
Deposited data		
Raw and analyzed data	This paper	https://doi.org/10.17632/9gkpxsmz23.1
Software and algorithms		
MATLAB R2016a (Data analysis)	MathWorks	https://www.mathworks.com
CNN-Cone-Detection	Cunefare et al.[47]	https://github.com/DavidCunefare/CNN-Cone-Detection
Other		
Re-analyzed data	Wang et al.[2]	https://doi.org/10.5061/dryad.nh0fp1b

RESOURCE AVAILABILITY

Lead contact

Further information and requests for resources should be directed to and will be fulfilled by the Lead Contact, Wolf M. Harmening (wolf.harmening@ukbonn.de).

Materials availability

This study did not generate new unique reagents.

Data and code availability

Cone mosaic images, cone coordinates and retinal locations (PCD, CDC and PRL) have been deposited at Mendeley Data and are publicly available as of the date of publication. A MATLAB code that can be used for plotting the data on the original image is provided. This paper analyzes existing, publicly available data. The access links and DOIs for the datasets and code are listed in the Key resources table.

EXPERIMENTAL MODEL AND SUBJECT DETAILS

Human participants

Forty-one eyes of twenty-one participants (7 male, 14 female, 18 adults [age: 18 – 42], 3 children [age: 10, 12 and 14]) with no known ocular conditions and only mild refractive errors (SE: ± 2.5 diopters) were studied. Participants are referred to throughout the manuscript with a singular ID, selected based on a descending order of peak cone densities for the left eye. For one of the participants (P21), data from the right eye were included as the only monocular dataset in the study, because the left eye's cone mosaic could not be resolved completely. Therefore, this eye's data were only used for PRL reproducibility analysis, as image and functional data were collected over multiple years. Most of the participants were examined on multiple days (compare Table S1). Participants P4, P13 and P21 were trained AOSLO observers and members of the lab. Mydriasis was established by two drops of 1% Tropicamide, instilled into the eyelid about 15 and 10 minutes prior to the imaging session. A third drop was administered in case imaging and experimentation continued for more than 30 minutes. A customized dental impression mold (bite bar) was used to immobilize and adjust the head position and thus to align the participants eye in front of the imaging system. Written informed consent was obtained from each participant and all experimental procedures adhered to the tenets of the Declaration of Helsinki, in accordance with the guidelines of the independent ethics committee of the medical faculty at the Rheinische Friedrich-Wilhelms-Universität of Bonn.

METHOD DETAILS

Adaptive optics retinal imaging

In vivo images of the complete foveolar cone mosaic were recorded using a custom-built adaptive optics scanning laser ophthalmoscope (AOSLO). The general setup of the AOSLO has been described previously,[48,49] pertinent differences are described here. Briefly, the AOSLO front-end featured three f = 500 mm afocal telescopes, designed to point-scan an adaptive optics corrected focal spot of light across the retina to achieve diffraction limited resolution performance in both the incident and reflected beams. A magnetic actuator-driven deformable mirror with continuous membrane surface (DM97-07, 7.2 mm pupil diameter, ALPAO, Montbonnot-Saint-Martin, France) was placed in a retinal conjugate plane and driven by the error signals of a 25x25 lenslet Shack Hartmann

Current Biology
Report

CellPress

sensor (SHSCam AR-S-150-GE, Optocraft GmbH, Erlangen, Germany). Imaging and wavefront correction wavelength was either 840 nm (±12 nm) or 788 nm (±12 nm) light, obtained by serial dichroic and bandpass filtering of a supercontinuum source (SuperK Extreme EXR-15, NKT Photonics, Birkerød, Denmark). The imaging field of view was 0.85 × 0.85 degree of visual angle. The light reflected from the retina was captured in a photomultiplier tube (PMT, H7422-50, Hamamatsu Photonics, Hamamatsu, Japan), placed behind a confocal pinhole (Pinhole diameter = 20 μm, equaling 0.47 (840nm) and 0.5 (788nm) Airy disk diameters). The PMT signal was sampled continuously in a field programmable gate array (FPGA), rendering a 512 × 512 pixel video at 30 Hz (600 pixel per degree of visual angle). With fast acousto-optic modulation of the imaging wavelengths, the square imaging field becomes a retinal display in which psychophysical visual stimulation was possible.[11,50] The best images during PRL recordings (see below) were used to create spatially registered, high signal to noise ratio images of the foveal center in which all cones could be resolved.

Image processing and cone density analysis

Acquired AOSLO video frames were spatially stabilized by real-time, strip-wise image registration in custom written software.[51] These online-stabilized videos contained frames displaying incomplete stabilization that could be due to poor image quality, eye blinks, drying tear film, etc. Such frames were identified and deleted manually. The remaining frames were averaged to obtain a single high-quality image of each retina per video. The single best of at least five such images was selected to be used for further analysis and serve as high signal-to-noise anchor image for spatial alignment with functional data recordings. All cone center locations were labeled in a semi-manual process by a single trained image grader: first, a convolutional neural network,[47] CNN, was trained to locate cone center locations with a smaller subset of only manually graded images in our pilot study. Then, all retinal images were annotated by the newly trained CNN, and manually corrected using custom software. Such corrections were especially necessary in the foveal center, and wherever cones appeared completely dark.[52] The manual correction prioritized mosaic regularity in cases of ambiguity.[3] Based on the labeled cone center locations, a Voronoi tessellation was computed (MATLAB functions: *delaunayTriangulation*, *voronoiDiagram* and *voronoin*). Each cone was regarded as occupying the space of each corresponding Voronoi cell. Angular cone density (cones/deg^2) was computed at each image pixel by averaging the Voronoi area of the nearest 150 encircled cones around that pixel (Figure 1D). This method ensured smooth cone density maps and prevented sampling artifacts as they often occur using defined shapes of masks (e.g., circular or square masks) for selection of cones in a particular area (Figure 1E). Linear cone densities were computed with respect to the individual retinal magnification factors of each eye, considering axial length, anterior chamber depth and corneal curvature,[16] based on swept source biometry (IOLMaster 700, Carl Zeiss Meditech, Jena, Germany). Finally, the cone density centroid (CDC) was determined as the weighted centroid (MATLAB function: *regionprops(region_logical, image, "WeightedCentroid")*) of the highest 20% of cone density values. The CDC is indicated by circular marker throughout the manuscript. The 20th percentile was chosen arbitrarily because the entire contour was evaluable in all eyes. CDC locations did only marginally change at other contours. At the 20% contour, cone densities equaled the highest ~13% of densities across the entire retina, considering previously reported cone densities at larger retinal eccentricities.[3,19] Therefore, the theoretical limit of cone sampling within those areas was < 35 arcsec (range: 9600 to 14900 cones/deg^2), equaling 20/13 vision or better under correction of ocular aberrations. Under natural viewing conditions, expected performance would be slightly less due to higher order aberrations and crucially depends on post-receptor circuitry, midget bipolar and ganglion cells (see Discussion).

To quantify overall symmetry between density maps, three different analyses were performed:

(1) Spatial two-dimensional differences (or reproducibility) of cone density maps of the same eye were recorded and analyzed independently on different days (columns in Figures S2A and S2B), based on a careful alignment of the cone mosaic images.
(2) The differences between density maps of fellow eyes which were recorded on the same day (rows in Figures S2A and S2B) were obtained by comparing flipping the left eyes map along the vertical axis and aligning it with the CDC of the right eyes map.
(3) The difference between individual density maps of all right eyes and a randomly selected left eye, which was flipped and aligned with the CDC of the right eye as described in analysis (2).

To quantify the two-dimensional differences, the root-mean-square (RMS) of the point-by-point difference maps was used for the comparison between absolute and normalized density maps (Figure S2C, respectively, compare with Figure 1G and 1H).

Determination of the preferred retinal location of fixation (PRL)

Using the AOSLO as stimulation platform, a small (nominal 1.6 arcmin), flashing (3 Hz) square with negative contrast polarity (light turned off) was presented as visual target at the center of the AOSLO imaging raster during image acquisition, and participants were asked to fixate the target as accurately and relaxed as possible. At least five 10 s AOSLO videos were recorded in each eye during such fixation epochs. In AOSLO videos, the visual stimulus was directly visible with respect to the retina (Figures 2A and 3B). Thus, fixation behavior can be directly and unambiguously observed in such videos. The PRL was calculated as the median fixation target location across all videos. To bring fixation behavior into spatial correspondence with the topographical analysis, averaged retinal images derived from both analyses independently were carefully aligned with each other. In 33 of the 41 eyes, PRL measurements were conducted multiple times (e.g., if participants also took part in other experiments). In three eyes (P13, P4 and P21), data were obtained in 8, 12 and 17 measurement sessions, respectively, over a period of 3.5 years. For eight participants (16 eyes)

sessions were repeated after 1 year. For quantification of fixation stability, the isoline area (ISOA) which contains one standard deviation (STD) of the data was fitted to the scatterplot of all stimulus positions (Figure 2B).

QUANTIFICATION AND STATISTICAL ANALYSIS

All statistical analyses were performed using MATLAB v2016.

Current Biology, Volume *31*

Supplemental Information

Human gaze is systematically offset from the center of cone topography

Jenny L. Reiniger, Niklas Domdei, Frank G. Holz, and Wolf M. Harmening

1

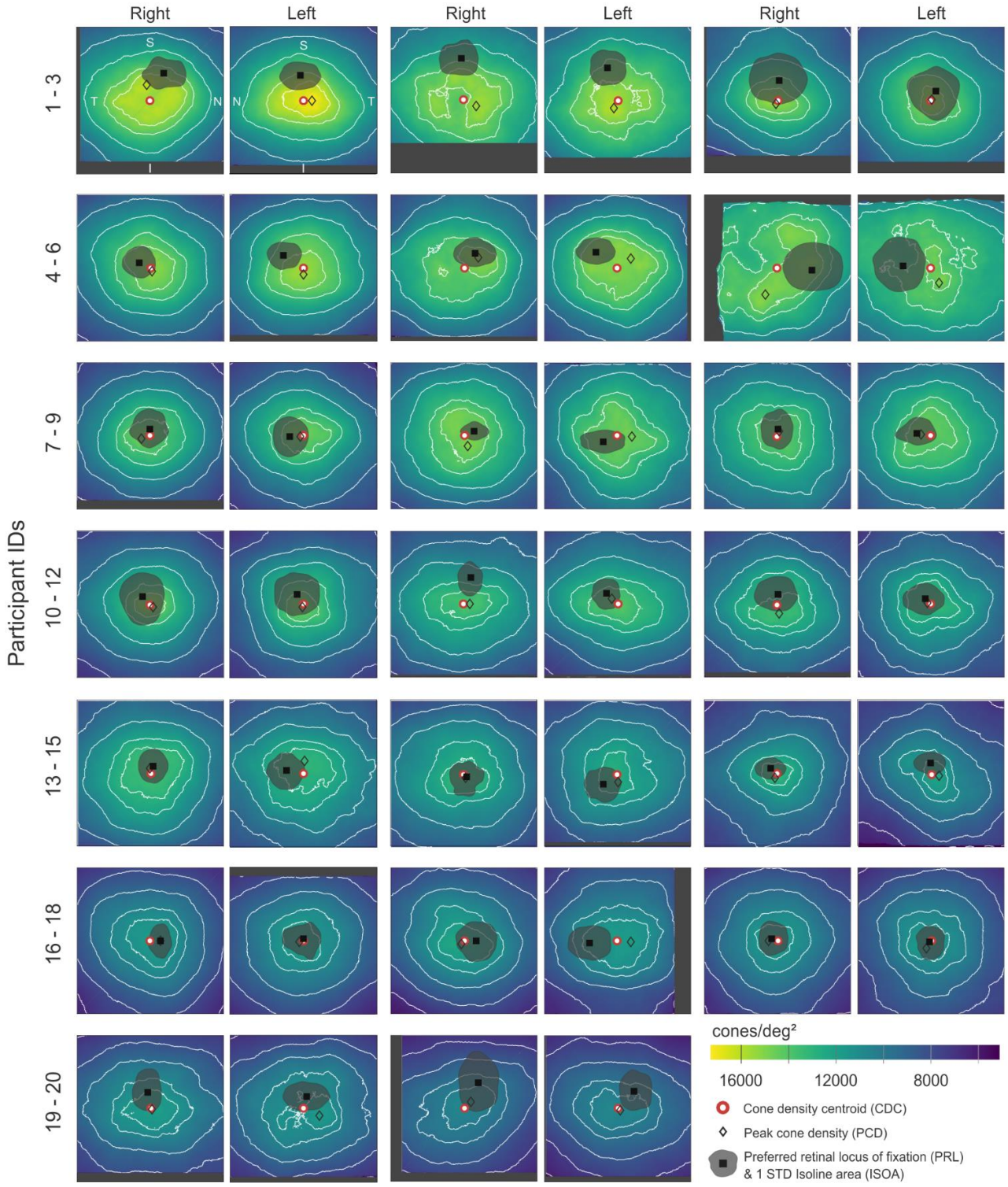

Figure S1. Binocular cone density contour maps of all participants. Related to Figure 1.

The central 40 x 40 arcmin density maps of right and left eyes are presented in fundus orientation for all participants (Superior retina is up, nasal is right for right eyes, and left in left eyes). Participants IDs (P1-P20) were ordered by PCD value exhibited, from top left to bottom right in this representation. Iso-contour lines represent the 10th, 20th, 40th, 60th and 80th percentile of density values. The cone density centroid (CDC) is indicated by a red circle. PCD = diamond, PRL = square, shown in the center of the individual fixation isoline areas (1 STD). Dark gray streaks reflect parts of the image that were cropped because of borders or poor quality.

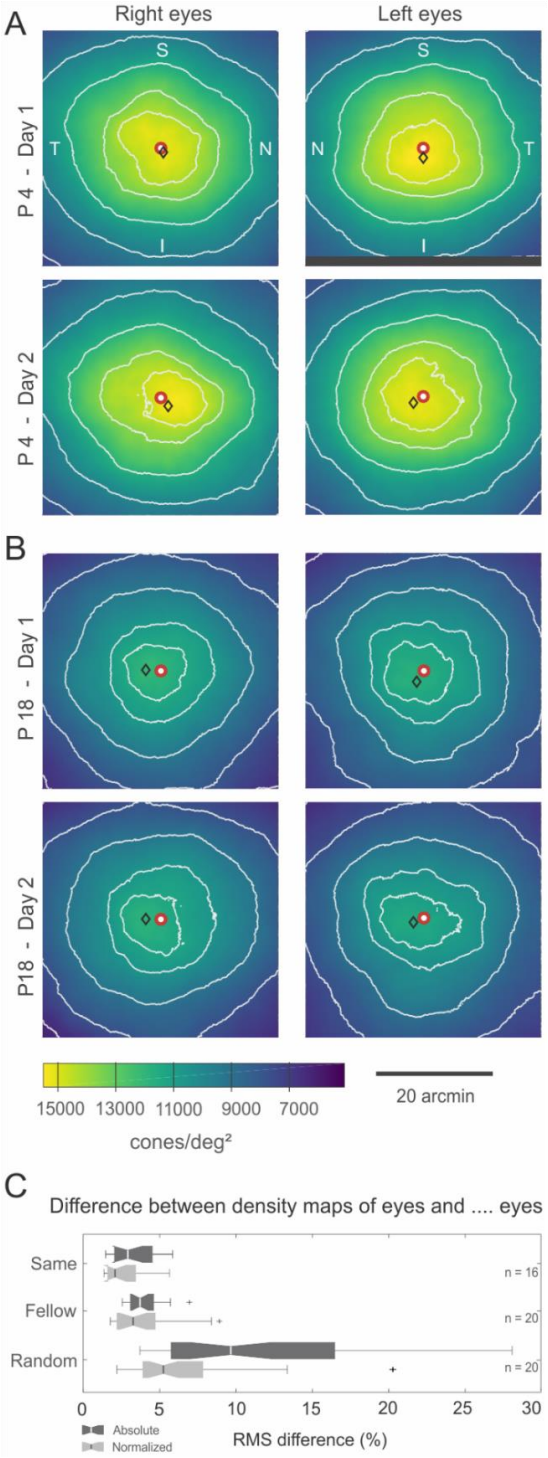

Figure S2. Symmetry of foveolar cone density maps. Related to Figure 1.

(A+B) Cone density maps of both eyes of two participants (P4 and P18) are shown in fundus orientation. Rows represent imaging sessions on different days. Contour line definition and marker (CDC and PCD) as in Figure 1. (C) The root mean square (RMS) of differences in absolute cone density values (dark fill) was evaluated for: (1) same eyes on 2 different days (median: 2.9 %, range: 1.5 – 5.9 %), (2) fellow eyes on the same day (median: 3.8 %, range: 2.6 – 6.9 %) and (3) the comparison between individual eyes and random fellow eyes showed the greatest differences (median: 9.6 %, range: 3.7 – 28.1 %), that can be explained to a large extend by the variation in absolute density

values among participants. To focus more on the two-dimensional shape of the maps, the normalized density maps were compared in the same way: (1) reproducibility showed a median value of 2.1 % (range: 1.4 – 5.6 %), (2) symmetry differences between fellow eyes were slightly greater (median: 3.3 %, range: 1.8 – 8.9 %) and the normalized differences between random partner eyes were highest (median: 5.3 %, range: 2.2 – 13.4 %). The notch represents the 95% confidence interval of the median, box whiskers extend to the most extreme data values and plus markers represent outliers (distance from box > 1.5 x range between 25th and 75th percentile).

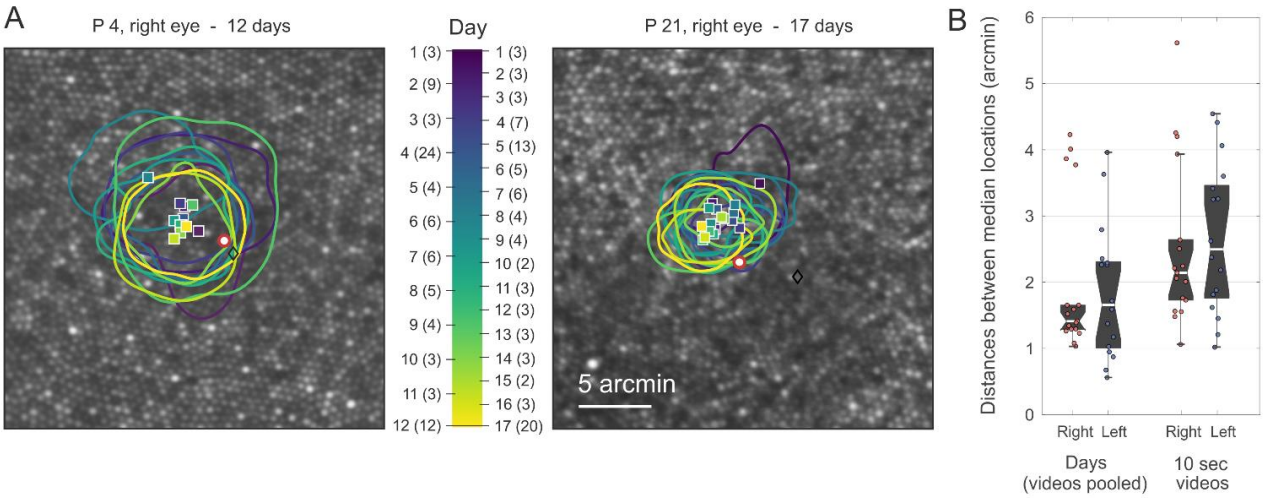

Figure S3. Fixation stability across multiple years. Related to Figure 2.

(A) PRL measurements in two participants (P4 and P21) were recorded over a period of 3.5 years on 12 and 17 different days, respectively. Color represents measurement sessions and thus time between first and last examination (2017-2020). Small dots are individual stimulus locations, squares are PRLs shown inside their 1 STD isoline areas. (B) The effect of data pooling compared between data taken from individual 10 sec videos and when pooled across multiple of such 10 sec videos recorded at the same day in all studied eyes.

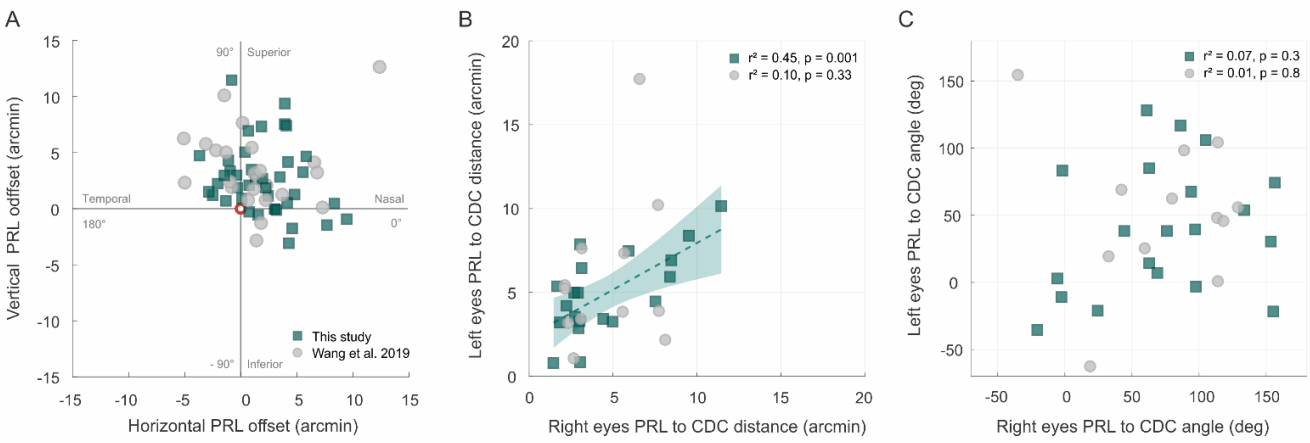

Figure S4. PRL offsets in this study and re-analyzed data from Wang et al. (2019)[S1]. Related to Figure 3.

(A) The right and left eyes' PRL relative to the CDC in retinal coordinates, combined for both eyes (this study = squares, Wang et al. = circles). The PRLs were displaced naso-superiorly from the CDC by average amounts of R: 4.5, L: 5.0 arcmin and R: 4.7, L: 5.9 arcmin for this study and Wang et al., respectively. Only in one participant (P19) both eye's PRLs were offset towards the temporal direction (see also Figure S1). (B) Offset distance was significantly correlated between fellow eyes in our study ($r^2 = 0.41$, $p = 0.002$), but not in the data provided by Wang et al. ($r^2 = 0.1$, $p = 0.33$). (C) While demonstrating a similar trend, offset direction did not show a significant correlation between fellow eyes in either population (this study: $r^2 = 0.05$, $p = 0.36$; Wang et al.: $r^2 = 0.01$, $p = 0.76$).

Participant ID	Gender	Age	Eye	Dominance	Cone mosaic				Fixation behavior					
					PCD cones/deg²	PCD cones/mm²	Density @CDC cones/deg²	Density @CDC cones/mm²	Total # of videos	# Measure-ment days	PRL variability across single runs (arcmin)	PRL variability across days (arcmin)	Median ISOA (arcmin²)	Median ISOA across days (arcmin²)
1	M	22	L	0	17309	210145	16997	206354	8	2	3.6	3.6	70.8	68.8
			R	1	16217	196477	15488	187643	8	2	5.6	3.9	50.3	128.8
2	F	21	L	0	16003	214584	15454	207225	10	2	3.3	4.0	54.9	45.7
			R	1	15667	210212	14217	190754	10	2	4.2	1.3	33.8	97.9
3	M	10	L	1	15814	217811	15650	215550	12	2	4.5	1.4	63.5	153.9
			R	0	15350	212760	15124	209632	12	2	3.9	4.2	126.4	183.0
4	F	29	L	0	15657	193441	15429	190622	15	3	1.9	2.3	36.6	46.9
			R	1	15230	190708	15101	189087	82	12	2.2	1.2	52.4	56.7
5	M	30	L	1	15301	207076	15058	203793	15	3	1.8	2.4	32.0	46.8
			R	0	15428	205507	14137	188313	15	3	1.5	1.6	66.1	61.0
6	F	28	L	1	15018	172925	14282	164448	10	2	3.3	1.6	154.4	157.3
			R	0	15157	170318	14030	157655	11	2	2.6	1.1	152.6	166.8
7	F	23	L	1	14828	198349	14774	197625	15	3	2.6	0.9	88.0	101.0
			R	0	14662	196147	14453	193346	15	3	2.2	1.3	93.0	114.0
8	F	30	L	0	14792	190964	14474	186860	10	2	2.4	2.3	38.1	53.8
			R	1	15102	188851	14789	184940	10	2	1.8	1.3	25.1	27.2
9	F	26	L	1	14763	207763	14433	203125	10	2	1.5	0.6	73.2	61.2
			R	0	14426	205894	14215	202877	9	2	2.5	1.4	66.9	86.6
10	M	12	L	0	14657	201831	14514	199867	13	2	3.4	1.2	70.9	107.5
			R	1	15126	207682	15035	206433	10	2	4.2	3.8	47.0	112.3
11	F	26	L	1	14175	187061	13971	184364	5	1	1.6	-	30.0	49.9
			R	0	13938	182418	13836	181085	6	1	2.1	-	48.3	47.5
12	F	26	L	0	13315	150790	13069	148002	10	2	1.0	1.0	64.3	70.0
			R	1	13697	153715	13191	148042	10	2	2.2	1.0	76.4	86.0
13	M	32	L	0	13286	145870	13046	143232	16	3	4.1	2.8	44.7	53.6
			R	1	13733	148503	13470	145658	37	8	2.0	1.6	40.7	49.1
14	F	20	L	0	12897	176732	12640	173207	5	1	1.1	-	83.8	72.2
			R	1	13302	183331	13175	181574	5	1	2.8	-	49.5	64.1

15	F	29	L	0	12304	158973	12108	156444	15	3	1.6	0.7	29.0	39.4
			R	1	13381	169702	12449	157885	24	5	1.1	1.4	23.3	32.2
16	M	14	L	0	12259	162728	12233	162376	5	1	2.8	-	98.9	71.6
			R	1	11904	158460	11682	155512	5	1	2.4	-	67.2	43.5
17	F	23	L	1	11927	171912	11772	169675	15	3	2.2	2.3	75.0	92.4
			R	0	12524	179022	12363	176715	36	6	2.3	1.6	65.3	85.5
18	F	31	L	0	11818	163501	11617	160723	15	3	1.2	1.0	62.1	53.3
			R	1	12105	165061	11939	162803	15	3	1.6	1.3	55.9	57.6
19	F	24	L	0	11789	161489	11089	151900	10	2	4.4	1.7	53.3	73.2
			R	1	12131	168226	12053	167150	10	2	2.1	4.0	62.5	64.5
20	F	18	L	0	10894	159556	10761	157603	5	1	3.2	-	66.0	78.9
			R	1	10823	157559	10692	155656	5	1	4.4	-	85.4	141.9
21	M	42	R	1	18023	221889	16601	204383	87	17	1.6	1.5	16.7	22.8
Median		26			14426	183331	14030	181574	10	2	2.3	1.5	62.5	68.8

Table S1. Participant statistics, ocular dominance, foveal cone mosaic metrics and PRL details. Related to STAR Methods.

Ocular dominance was measured prior to PRL measurements. PCD and CDC densities are given in angular and linear units (retinal magnification was computed based on axial length, anterior chamber depth and retinal curvature for each eye [S2]). The PRL was measured on different days and PRL variability is the retinal distance between single repeated PRL measurements (runs), or pooled data across days. Note that in participant 21, the complete cone mosaic could only be resolved in the right eye.

Supplemental References

S1. Wang, Y., Bensaid, N., Tiruveedhula, P., Ma, J., Ravikumar, S., and Roorda, A. (2019). Human foveal cone photoreceptor topography and its dependence on eye length. Elife *8*, 1–21.

S2. Li, K.Y., Tiruveedhula, P., and Roorda, A. (2010). Intersubject variability of foveal cone photoreceptor density in relation to eye length. Invest. Ophthalmol. Vis. Sci. *51*, 6858–6867.

3.3 Sub-cone visual resolution by active, adaptive sampling in the human foveola

Witten, J. L., Lukyanova, V., and Harmening, W. M. Sub-cone visual resolution by active, adaptive sampling in the human foveola. Elife. 2024; 13: pp. 1–19; doi: 10.7554/eLife.98648

RESEARCH ARTICLE

Sub-cone visual resolution by active, adaptive sampling in the human foveola

Jenny L Witten*, Veronika Lukyanova, Wolf M Harmening

Department of Ophthalmology, Rheinische Friedrich-Wilhelms-Universität Bonn, Bonn, Germany

eLife Assessment

This **important** work uses in vivo foveal cone-resolved imaging and simultaneous microscopic photostimulation to investigate the relationship between ocular drift - eye movements long thought to be random - and visual acuity. The surprising result is that ocular drift is systematic - causing the object to move to the center of the cone mosaic over the course of each perceptual trial. The tools used to reach this conclusion are state-of-the-art and the evidence presented is **convincing**. This work advances our understanding of the visuomotor system and the interplay of anatomy, oculomotor behavior, and visual acuity.

Abstract The foveated architecture of the human retina and the eye's mobility enables prime spatial vision, yet the interplay between photoreceptor cell topography and the constant motion of the eye during fixation remains unexplored. With in vivo foveal cone-resolved imaging and simultaneous microscopic photo stimulation, we examined visual acuity in both eyes of 16 participants while precisely recording the stimulus path on the retina. We find that resolution thresholds were correlated with the individual retina's sampling capacity, and exceeded what static sampling limits would predict by 18%, on average. The length and direction of fixational drift motion, previously thought to be primarily random, played a key role in achieving this sub-cone diameter resolution. The oculomotor system finely adjusts drift behavior towards retinal areas with higher cone densities within only a few hundred milliseconds to enhance retinal sampling.

***For correspondence:** jennylwitten@gmail.com

Competing interest: The authors declare that no competing interests exist.

Funding: See page 15

Preprint posted
26 March 2024
Sent for Review
15 April 2024
Reviewed preprint posted
28 June 2024
Reviewed preprint revised
08 October 2024
Version of Record published
29 October 2024

Reviewing Editor: Fred Rieke, University of Washington, United States

Introduction

Assessing visual abilities was already important in historic times (***Bohigian, 2008***), and the precise measurement of visual acuity, our ability to resolve fine spatial detail by eye, has great importance for many real-life scenarios and is up to this day the primary diagnostic tool to determine visual function in a clinical and optometric setting. Quite surprisingly, the widely-believed assumption that the packing density and arrangement of retinal photoreceptors at the foveal center set the limit to this ability has never been experimentally confirmed.

Fovealization, the morphological and functional specialization of the cellular architecture of the light-sensitive retina optimizes the human eye for high-acuity daytime vision (***Caves et al., 2018***; ***Tuten and Harmening, 2021***). Within the central one-degree diameter of the fovea, termed foveola, postreceptoral neurons are displaced centrifugally and the area is free of potentially shadowing blood vessels and glia cells (***Hendrickson and Yuodelis, 1984***; ***Syrbe et al., 2018***). The outer segments of foveolar cone photoreceptors are maximally thinned and densely packed for peak spatial sampling (***Hirsch and Curcio, 1989***; ***Rossi and Roorda, 2010***; ***Williams and Coletta, 1987***), which at the same time makes these cells the most difficult to study ex vivo (***Curcio et al., 1987***) as well as in vivo (***Rossi et al., 2011***). Each foveolar cone synapses to one ON- and one OFF-midget bipolar cell, which in turn

synapse exclusively upon single ON- and OFF-midget ganglion cells, a circuit that is adult-like before birth (**Zhang et al., 2020**). This establishes an undisturbed *private line* from individual foveal receptors to central processing stages.

Based on indirect comparisons between histological and psychophysical data, the hypothesis that cone spacing imposes the fundamental limit for visual resolution has been put forward (**Curcio et al., 1990**; **Rossi and Roorda, 2010**). It is well established that cone spacing, especially in the central fovea, is highly variable between individuals (**Cava et al., 2020**; **Curcio et al., 1990**; **Reiniger et al., 2021**; **Wang et al., 2019**), making general comparisons between acuity measurements and foveolar density estimated from histological samples susceptible to error. One of the main reasons why the hypothesis lacks direct experimental proof is that because, under natural viewing conditions, both visual resolution and experimental access to foveal photoreceptors are blurred by the imperfect optics of the human eye (**Campbell and Green, 1965**; **Marcos et al., 2008**). Here, we have overcome the optical barrier of the human eye by employing adaptive optics cell-resolved in vivo retinal imaging in conjunction with micro-psychophysics to study directly whether the individual's mosaic of foveolar cones determines visual performance in a high-acuity resolution task.

While acuity is assumed to be mainly limited by the resolving capacity of the eye's optics and retinal mosaic, it is well established that, for different visual tasks, performance thresholds can be substantially lower than the sampling grain of photoreceptors. This phenomenon has been termed hyperacuity (**Westheimer, 1975**) and depends on the neural visual system's ability to extract subtle differences within the spatial patterns of the optical image on the retina (**Westheimer, 2012**). Thus, the visual system already incorporates mechanisms to detect relative spatial offsets an order of magnitude smaller than the spatial granularity of the retina. To make use of those fine distinctions in a resolution task, the neuronal system needs to go beyond purely spatial coding of incoming signals.

Unlike a camera, the visual system depends on temporal transients arising in the receptor's cellular signals. Neurons in the retina, thalamus, and later stages of the visual pathways respond strongly to temporal changes (**Kaplan and Benardete, 2001**; **Nagano, 1980**). Thus, the fovealized retinal architecture in humans is accompanied by a dynamic sampling behavior that, by quick and precise movements of the eye, brings retinal images of objects of interest to land in the foveola (**Ko et al., 2010**). Even during steady fixation, for example of a distant face or a single letter of this text, incessant fixational eye movements slide tens to hundreds of foveolar photoreceptors across the retinal image, thereby introducing temporal modulations that translate spatial activation patterns into the temporal domain (**Kuang et al., 2012**). Small and rapid gaze shifts known as microsaccades relocate the gaze within the foveola during periods of fixation (**Ko et al., 2010**), and between microsaccades, the eyes perform a more continuous, seemingly random motion termed fixational drift (**Intoy and Rucci, 2020**; **Krauskopf et al., 1960**). Computational work suggested that fixational eye motion would introduce noise and thus impair visual acuity (**Burak et al., 2010**; **Pitkow et al., 2007**). Contrarily, recent studies on human psychophysics demonstrated fixational eye motion to be beneficial for fine spatial vision (**Intoy and Rucci, 2020**; **Rolfs, 2009**; **Rucci et al., 2007**). Especially drift motion has been increasingly argued to not just be randomly refreshing neural activity, but rather structuring it (**Clark et al., 2022**; **Hafed et al., 2021**; **Intoy and Rucci, 2020**) and being under central control (**Herrmann et al., 2017**).

The incessant motion of the eye conveys fine spatiotemporal detail that requires deciphering of continuously changing photoreceptor signals, which are linked by the geometry of the photoreceptor array and by how the eye moves. For instance, luminance modulation in individual cones will scale with drift length. Larger luminance variations on single receptors also yields more neuronal activity within the range of temporal frequencies parvocellular ganglion cells are sensitive to. Selective spatial frequencies can thus be amplified by varying drift lengths (**Intoy and Rucci, 2020**). While the neuronal mechanisms that generate fixational drift are still not fully understood (**Ben-Shushan et al., 2022**), its consequence to visual perception has been demonstrated. Drift was shown to improve visual performance in resolution tasks (**Intoy and Rucci, 2020**; **Ratnam et al., 2017**; **Rucci et al., 2007**). Indeed, considerable differences in ocular drift between individuals exist (**Cherici et al., 2012**; **Clark et al., 2022**), and subjects exhibiting less drift were shown to have better acuity (**Clark et al., 2022**). If such differences are a consequence of an active, adaptive mechanism, however, and how drift behavior is related to the photoreceptors that sample the retinal image is unknown.

The direct experimental access to the foveolar center, when other limiting factors like image blur or retinal motion are taken out of the equation or can be precisely measured, will allow to confirm or

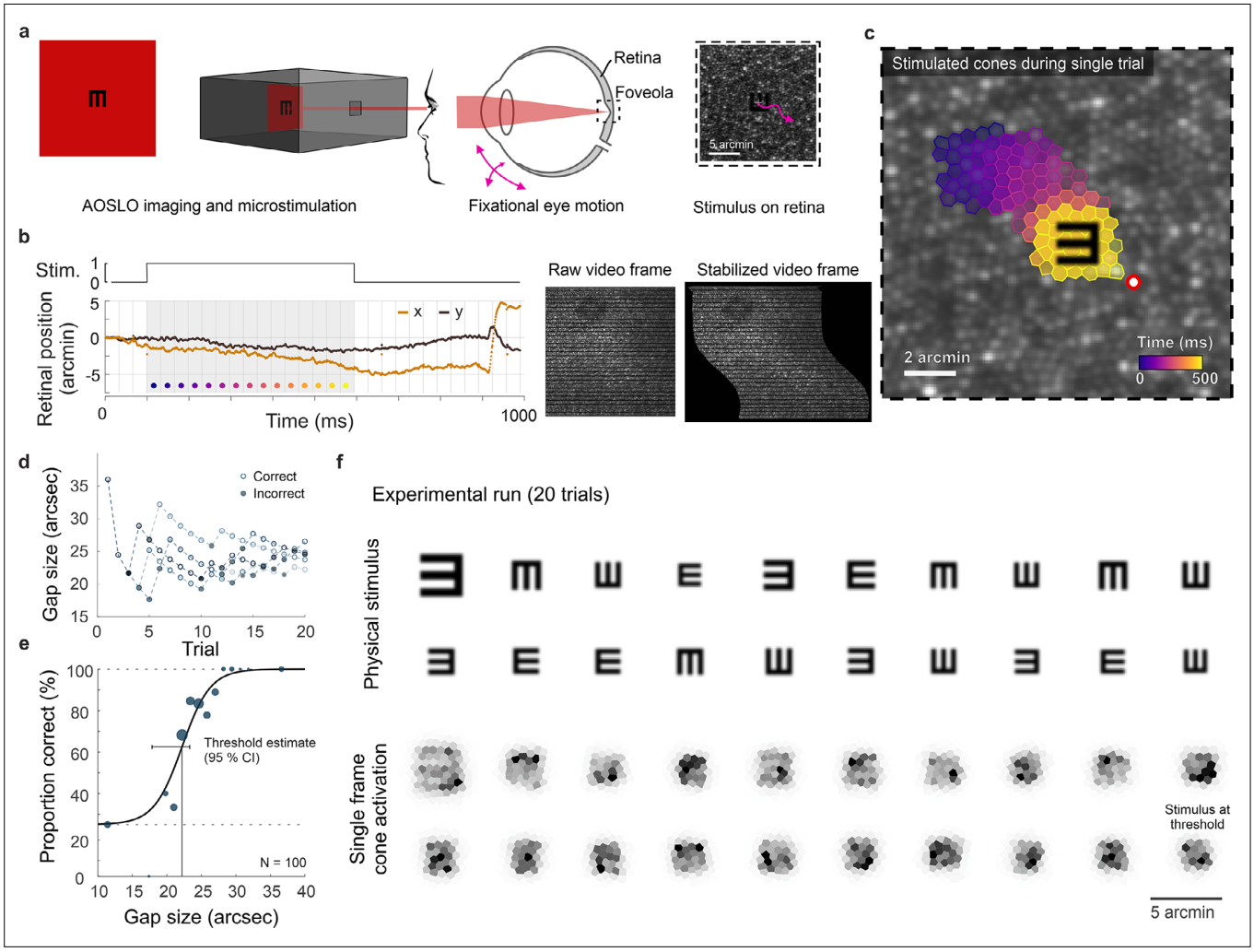

Figure 1. Cone-resolved adaptive optics micro-psychophysics. (**a**) Schematic of cell-resolved visual acuity testing in the human foveola with an adaptive optics scanning laser ophthalmoscope (AOSLO). Stimuli were dark Snellen-E optotypes presented at variable sizes and four orientations in the center of the 788 nm AOSLO imaging raster. Participants responded by indicating stimulus orientation during natural viewing, i.e., unrestricted eye motion. (**b**) Exemplary single trial retinal motion trace and strip-wise image stabilization of a single AOSLO frame (shown here during a microsaccade for better visibility). Trials containing microsaccades or blinks during the 500 ms stimulus presentation (gray shaded area) were excluded. The x-axis grid represents individual video frames (33 ms). (**c**) Foveolar retinal cone mosaic with a exemplary single trial retinal motion across the stimulus. Time is represented by color from stimulus onset to offset (purple to yellow). The cone density centroid (CDC) is shown as a red circle with white fill. (**d**) Typical psychophysical data of five consecutive runs in one eye. Each run followed a QUEST procedure with 20 trials. (**e**) Psychometric function fit to the data (about 100 trials). Acuity thresholds were estimated at 62.5% correct responses. (**f**) Exemplary retinal images (upper rows) and corresponding cone activation patterns (lower rows) of one experimental run (20 trials from top left to bottom right). Cone activation patterns are shown for a representative single frame. See ***Videos 1 and 2*** for a real-time video representation.

reject the long-standing hypothesis about the individual limits of vision. This will help to understand the fundamental physiological limitations of the visual system and will have important implications for clinical studies of retinal health.

Results

Resolution is finer than single cone sampling limits

We investigated the limitations of the photoreceptor packing density on individual visual resolution acuity by overcoming the optical aberrations of the eye with adaptive optics scanning laser ophthalmoscopy (AOSLO), while simultaneously performing psychophysical measurements and recording the

fixational retinal motion (***Figure 1a, b and c***). In a four-alternative forced-choice task, 16 healthy participants indicated the orientation of an E-optotype while inspecting the stimulus with their individually preferred fraction of foveolar photoreceptors. These cone photoreceptors were simultaneously imaged and it was later identified which cells contributed to resolving the stimulus (***Figure 1c and f***). A psychometric fit to the data expressed as percentage correct from 100 trials was used to compute visual acuity thresholds (see online Methods and ***Figure 1d and e***). In this near diffraction-limited testing condition, participants reached visual acuity thresholds between 20.6 and 28.5 arcsec (mean ± SD: 24.1±2.4 arcsec), which compares to 20/8 vision (logMAR = –0.4). All participants reached thresholds better than 20/10 vision (logMAR = –0.3), the last line of a typical clinical Snellen chart or projectors of acuity optotypes that are used in clinical as well as optometric daily routine.

Cone densities at the cone density centroid (CDC) ranged between 10,692 and 16,997 cones/deg^2, with an average density of 13,640 cones/deg^2 (Average peak cone density, PCD: 13,944 cones/deg^2, range: 10,823–17,309 cones/deg^2), comparable to previous reports (***Cava et al., 2020***; ***Putnam et al., 2005***; ***Wang et al., 2019***; ***Wells-Gray et al., 2016***; ***Wilk et al., 2017***; ***Zhang et al., 2015***). The median sampling cone density ranged between 10,297 and 16,104 cones/deg^2 (mean: 13,149 cones/deg^2). Two experimental runs of the eyes with the highest and lowest sampling density are exemplarily shown in ***Videos 1 and 2***. The two foveolar cone mosaic images were also visualized and overlayed with a Snellen E stimulus at average threshold size (***Figure 2a***). A static, theoretical prediction given by the Nyquist sampling limit would assume the high-density retina where each single cone diameter is smaller than the Snellen E's gap or bar is able to resolve the stimulus, whereas the low-density retina fails in identifying the correct orientation (schematic representation in ***Figure 2b***). However, for our 788 nm testing condition, all participants reached individual resolution thresholds well below their Nyquist limit predicted by the spacing between rows of cones (***Figure 2c and d***). On average, visual acuity thresholds exceeded this theoretical prediction by 20% and 16% in dominant and non-dominant eyes, respectively. When participants performed the same resolution task with a longer infrared wavelength (840 nm) imaging background, the absolute thresholds were slightly higher and thus closer to the Nyquist limit. Visual acuity thresholds were on average 7% below and 2% above the Nyquist limit for dominant and non-dominant eyes, respectively. These absolute visual acuity thresholds were the only case where noteworthy differences arose between the 788 nm and 840 nm experimental conditions. For all other analyses, we found qualitatively similar results for either wavelength and therefore only report the 788 nm results throughout the manuscript.

For the first time, we could measure the direct relation between the individual foveolar cone photoreceptor sampling density and participant's visual resolution thresholds. We found the diffraction-limited visual acuity thresholds to be strongly correlated to the foveolar sampling density in dominant as well as fellow eyes (***Figure 2d***). The higher the cone density, the smaller the visual stimulus that could be resolved. The degree of correlation slightly differed for dominant (r^2=0.45, p=0.005) and non-dominant eyes (r^2=0.28, p=0.036), suggesting that up to 45% of the variance in inter-subject visual acuity can be explained by the individual cone sampling densities. Overall, participants reached significantly lower thresholds with their dominant eyes (average: 1.5 arcsec, SD ±1.1; paired t-test, p<0.001). Nevertheless, visual acuity thresholds were strongly correlated between dominant and

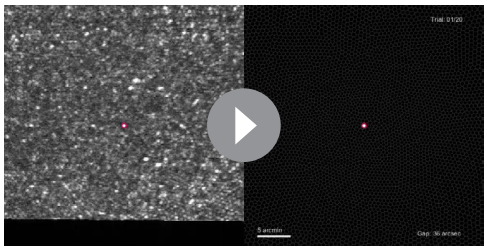

Video 1. Video recordings of one experimental run in the eye with highest sampling density. All successive single trial videos (left) and the Voronoi mosaic of cells colored with their respective amount of cone activation (right).
https://elifesciences.org/articles/98648/figures#video1

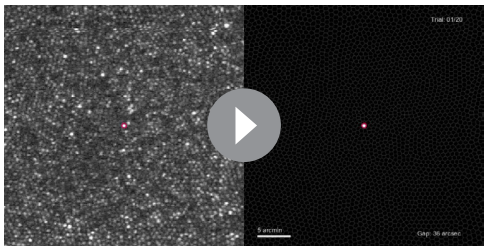

Video 2. Video recordings of one experimental run in the eye with lowest sampling density. All successive single trial videos (left) and the Voronoi mosaic of cells colored with their respective amount of cone activation (right).
https://elifesciences.org/articles/98648/figures#video2

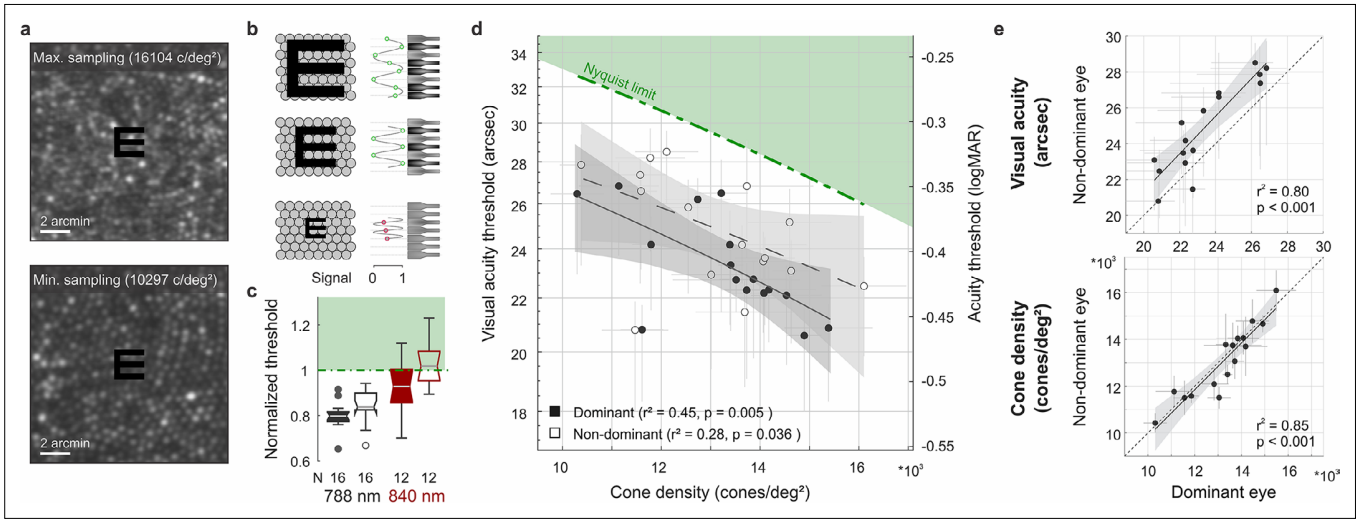

Figure 2. Visual acuity depends on foveolar sampling capacity. (**a**) Foveolar cone mosaics of the two eyes with highest and lowest cone densities, overlayed with the physical stimulus at an average threshold size (24 arcsec). (**b**) Nyquist limit: critical details equaling or larger than the spacing of cones are resolvable. (**c**) Visual acuity thresholds measured with 788 or 840 nm infrared light, normalized to the eyes' Nyquist limits. (**d**) Correlation between participant's individual visual acuity thresholds and cone density. Thresholds exceeded the Nyquist sampling limit and were significantly lower in eyes with higher cone densities. Dominant eyes are shown as filled, and non-dominant eyes as open markers. The gray horizontal and vertical bars at each point represent standard deviations of sampling cone density and the 95% confidence intervals for acuity thresholds. The theoretical Nyquist limit is represented by a dashed green line. (**e**) Correlation between dominant and non-dominant eyes in visual acuity (top) and cone density (bottom). Dominant eyes reached, on average, 1.5 arcmin lower thresholds than non-dominant eyes, whereas cone density (at the retinal locations that sampled the stimulus) was very similar between fellow eyes.

non-dominant eyes (r^2=0.80, p<0.001, ***Figure 2e***). To test whether the effect of different absolute thresholds might be explained by underlying differences in the sampling cone density, fellow eye densities were compared to each other. Sampling densities had a very strong correlation between fellow eyes (r^2=0.85, p<0.001, ***Figure 2e***), but did not differ between right and left eyes (p=0.38) nor when grouping them according to ocular dominance (p=0.88). This compares well with previous studies that also showed strong correlations between fellow eyes regarding both anatomical (***Cava et al., 2020***) as well as functional (***Reiniger et al., 2021***) characteristics. Dominant eyes had a median of 78 cones/deg^2 higher densities compared to their fellow eyes. To account for the 1.5 arcsec difference in acuity thresholds, a much higher density difference of about 1500 cones/deg^2 would have been needed. Based on these results, we conclude that the spatial arrangement of foveal cones can only partially predict resolution acuity. In the following, we show that ocular motion and its associated temporal modulations also influence visual resolution.

Ocular drift is an active sampling mechanism

As the eye drifts, a visual stimulus projected onto the retina is processed as a spatiotemporal luminance flow. The stimulus itself as well as the extent of drift motion determine the characteristics of modulation. By analyzing the exact retinal locations sampling the stimulus we show the impact of the traveled path length first (***Figure 3***), followed by the direction of drift motion and its relation to anatomical and functional landmarks (***Figure 4***). In our experiments, we revealed that participants kept coming back to the same few hundreds of cone photoreceptors (***Figure 3a*** and ***Figure 3—figure supplement 1***). To focus on the characteristics and implications of drift eye motion, trials containing microsaccades during stimulus presentation were excluded from the analyses. During the short stimulus duration, however, microsaccades rarely occurred, as participants tend to suppress their microsaccades, likely because they can be detrimental to fine-scale discrimination (***Bowers et al., 2021***; ***Intoy et al., 2021***). Drift motion patterns varied greatly across, but also within participants. Examples of drift motion paths for the eyes that performed the smallest and largest drift motion, on average, show a great variability in shapes as well as extent of motion (***Figure 3b***). In our analyses, we chose the drift length (sum of piecewise vector lengths) as the prime metric to describe the ocular drift motion,

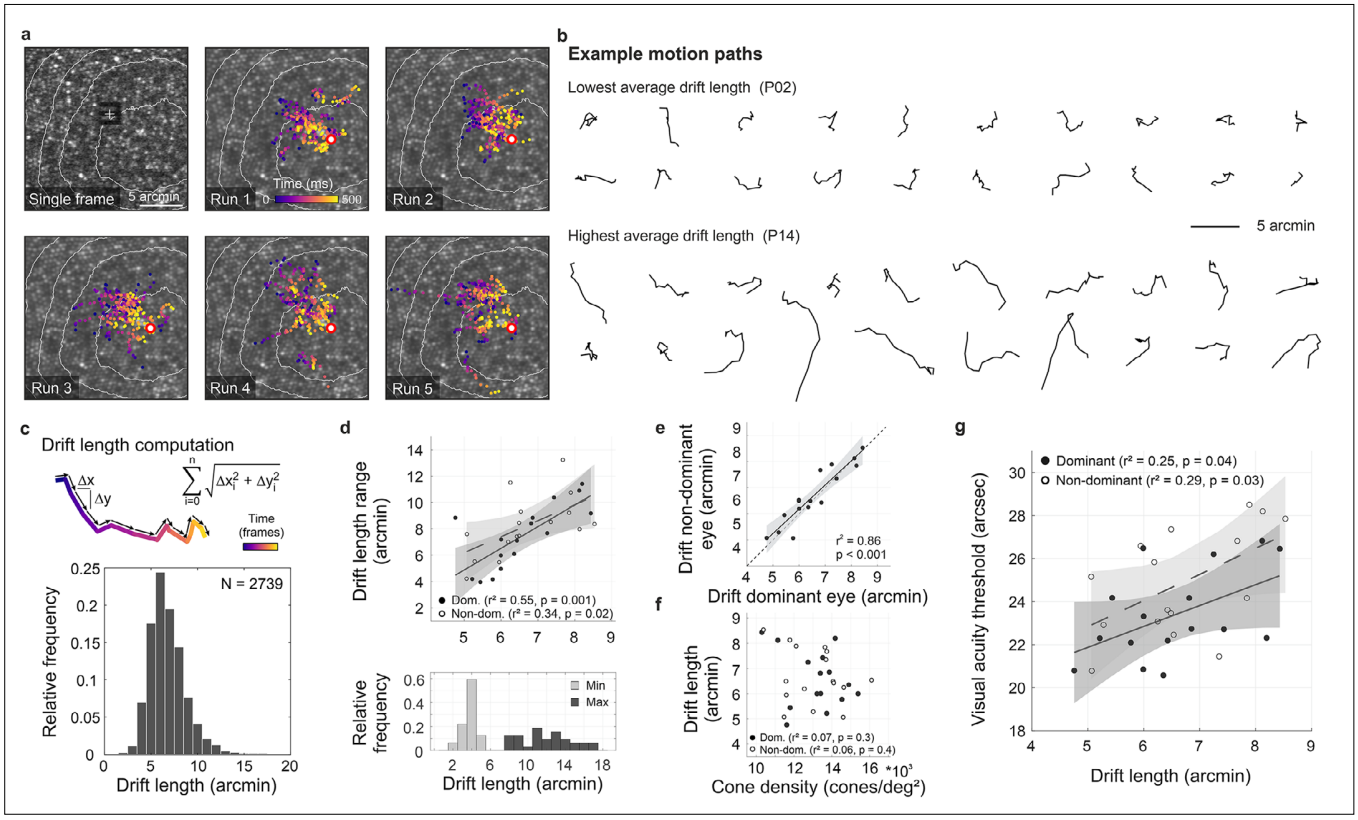

Figure 3. Fixational drift and the contribution to visual acuity. (**a**) Ocular drift during stimulus presentation (participant 16, left eye). Single adaptive optics scanning laser ophthalmoscopy (AOSLO) frame captured during Snellen E presentation (top left) and all single stimulus positions (colored dots) of five experimental runs shown on the corresponding cone mosaic (panels 2–6). White iso-lines delimit cone density percentile areas (90th to 50th percentile visible). Time is represented by color from stimulus onset to offset (purple to yellow). Individual drift trajectories for all eyes are shown in ***Figure 3—figure supplement 1***. (**b**) Individual motion traces highlighting intra- and inter-subject drift variability. Traces are from one run in the participant with the lowest (upper rows) and highest (lower rows) average drift lengths. (**c**) Computation of drift length as a sum of interframe motion vectors (top) and the relative frequency of occurrences among all participants and trials (bottom). (**d**) Median drift length and drift length range showed a moderate correlation in dominant as well as non-dominant eyes (top). The minimum drift length was similar between participants (3.8±0.8 arcmin) whereas the maximum length varied about three times as much (12.0±2.7 arcmin). (**e**) Drift lengths in fellow eyes had a very strong correlation. (**f**) Cone density and drift length did not show a significant correlation in dominant or non-dominant eyes. (**g**) The median drift length had a moderate correlation with visual acuity threshold in dominant as well as non-dominant eyes. Dominant eyes are indicated by filled, non-dominant eyes by open markers.

The online version of this article includes the following figure supplement(s) for figure 3:

Figure supplement 1. Drift trajectories on foveolar mosaics.

because the randomness underlying alternative metrics of drift eye movements becomes increasingly questionable (see also Discussion). Across all participants and experimental trials, drift lengths ranged between 2.5 and 17.2 arcmin, with a median length of 6.5 arcmin (which corresponds to a velocity of 5–34.5 arcmin/s, median: 13 arcmin/s, ***Figure 3c***). The drift lengths are slightly smaller than in previous non-AO studies, which is attributable to the viewing situation. The participants were looking at a very small imaging field within a completely dark periphery without distracting structures or stimuli. The smallest drift movement performed was similar among eyes (range: 2.5–5.4 arcmin), whereas the largest individual drifts differed more than three times as much (range: 7.7–17.2 arcmin). Therefore, the individual drift span was rather driven by the larger drift lengths of an eye and there was a strong correlation between median drift length and drift range (dominant eyes: r^2=0.55, p=0.002, non-dominant eyes: r^2=0.34, p=0.02, ***Figure 3d***).

Between fellow eyes, which were measured consecutively, drift lengths had a very strong correlation (r^2=0.86, p<0.001, ***Figure 3e***) with no significant difference between eyes (paired t-test, p=0.2). The median drift lengths of all eyes varied between 4.8 and 8.5 arcmin (mean ± SD: 6.6±1.1 arcmin). Individual visual acuity thresholds were significantly correlated with drift lengths (dominant: r^2=0.25,

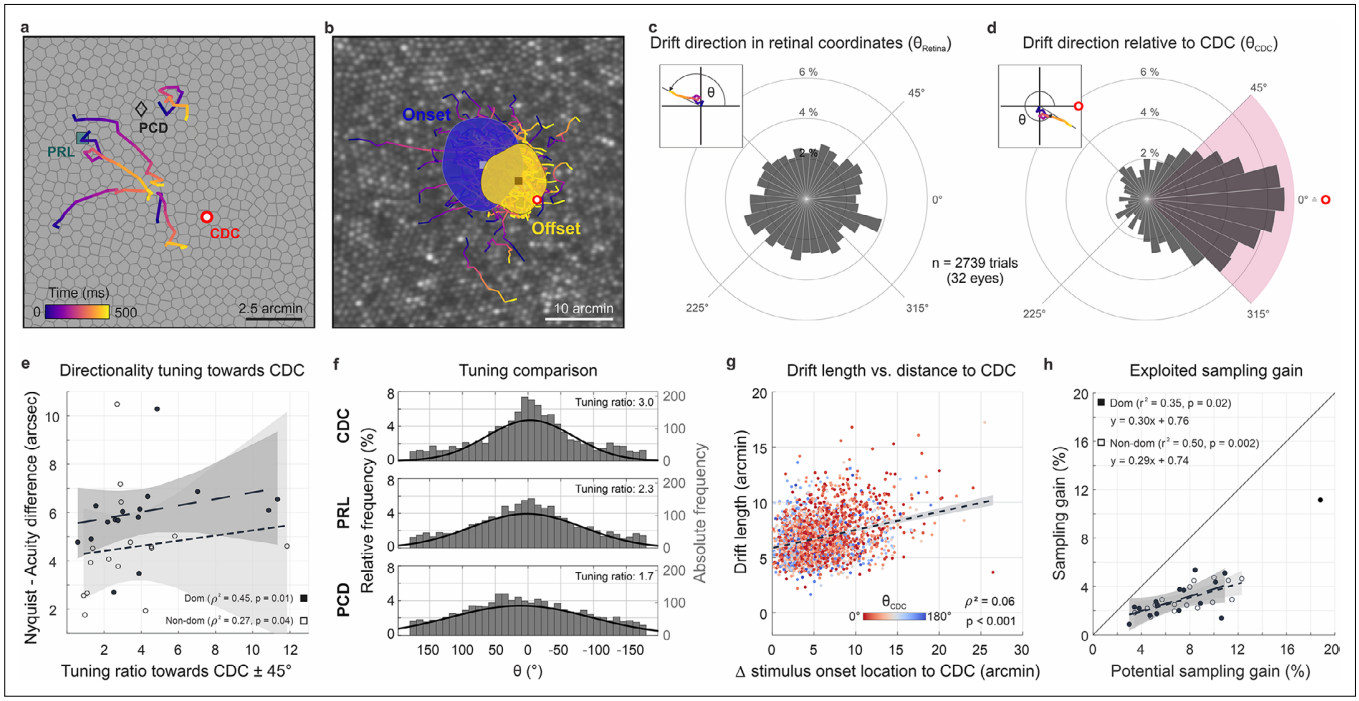

Figure 4. Drift moves stimuli to higher cone density areas. (**a**) Five exemplary motion traces relative to cone density centroid (CDC), preferred retinal locus (PRL), and peak cone density (PCD) location on the Voronoi tessellated cone mosaic of one participant. (**b**) All single trial motion traces of one eye are shown on the corresponding cone mosaic (95 trials containing drift only). One-SD isoline areas (ISOA) are shown for all stimulus onset (blue) and offset (yellow) locations, indicating a trend of directional drift towards higher cone densities during 500 ms stimulus presentation. (**c**) Polar histogram of all individual motion traces (n=2739) shows the relative frequency of motion angles, θ_{Retina}, between the start (coordinate center) and end of motion in retinal coordinates. The inset indicates θ sign. (**d**) Same data as in c, where θ_{CDC} was computed relative to the line connecting drift start location and CDC, see inset. The pink quarter indicates the angular space used for the computation of the tuning ratio. For more details on the drift directionality of individual eyes, see ***Figure 1***. (**e**) The difference between the acuity threshold and Nyquist limit showed a significant trend to be larger for stronger directionality tuning. The tuning ratio was computed as the ratio between the relative frequency of intra-participant drift motion towards the CDC (±45 deg) and the average of drift motion towards the remaining three quadrants. (**f**) Relative frequency of drift direction relative to CDC (top), PRL (middle), and PCD (bottom), respectively. For more details on the temporal progression of drift directionality, see ***Figure 2***. (**g**) Across all participants and trials, drift length correlated with stimulus onset distance from CDC. There was no clear effect of stimulus onset distance on motion directionality (data color corresponding to θ_{CDC}). (**h**) The achieved sampling gain due to the performed drift motion is significantly correlated to the potential sampling gain in individuals. In both dominant and non-dominant eyes the potential sampling gain is on average exploited by 30%, respectively. Due to shifting the CDC towards the stimulus, participants had different PRLs for a sustained fixation task and the visual resolution task (see ***Figure 3***).

The online version of this article includes the following figure supplement(s) for figure 4:

Figure supplement 1. Individual drift directionality.

Figure supplement 2. Time course of drift directionality.

Figure supplement 3. Different retinal locations used in a fixation or resolution task.

p=0.04; non-dominant: r^2=0.29, p=0.03, ***Figure 3g***), with a trend towards better visual acuity for small ocular drift motion. On a photoreceptor resolved scale, this confirms recent findings which showed individual acuity thresholds to be correlated with the drift motion during a non-AO acuity task, closely related to the drift measured in a sustained fixation task (***Clark et al., 2022***).

Considering the previously shown correlation between visual acuity and sampling cone density, one could assume those two aspects to go along with an increase of ocular drift for lower cone densities, whereas higher densities potentially need less drift to translate the stimulus over the same number of cones. However, we don't find the drift motion to be tuned in a way to always let the stimulus slip across a similar number of cones. There was no significant correlation between cone densities and drift length (***Figure 3f***, dominant: r^2=0.07, p=0.3; non-dominant: r^2=0.06, p=0.4). Also, we do observe similar drift lengths across stimulus sizes. We note, however, that in all our experimental trials, stimulus sizes were quite similar. If drift length tuning existed, it may have been more pronounced with

a larger dispersion of stimulus sizes. In the following, we show that drift direction is indeed tuned to optimize sampling.

Drift is adaptive and directed

Ocular drift has long been assumed to be a persistent jittery motion that follows random trajectories. Recent work showed that the amount of drift can vary and may be adapted to the task that has to be performed (***Clark et al., 2022***; ***Intoy and Rucci, 2020***). We here investigated if, beyond this, humans are able to actively tune their ocular drift direction to exploit their prime spatial retinal processing properties. We, therefore, registered the individual drift motion trajectories with the photoreceptor mosaic, tracked them from the retinal location where the stimulus turned on (onset) to where it turned off after 500 ms (offset), and related these trajectories to foveolar landmarks (***Figure 4a and b***). Because of the individual retinal locations used for fixation before stimulus onset, we registered that, across all eyes, drift motion occurred towards all directions during stimulus inspection, and no general trend in drift eye movements towards a particular cardinal direction across participants occurred (***Figure 4c***). Individual eyes, however, showed different drift behavior mostly directed toward one or two of the four quadrants. All four cardinal directions were represented. Participant $P8_{right}$, for example, drifted towards the nasal or superior fovea in 90% of all trials. $P14_{right}$, on the other hand, drifted towards the temporal fovea in 75% of all trials.

When the frame of reference was rotated in each trial to register the motion from the onset location relative to the CDC, we found a clear directional bias in which the drift was likely to move the stimulus closer to the CDC. The drift directionality was evaluated by measuring the relative angle between drift onset to drift offset and drift onset to CDC. We observed a strong trend of drift directionality; 49% of all drift episodes moved the stimulus towards the CDC ± 45° (***Figure 4d***). The directionality was not pronounced directly after stimulus onset but increased with presentation duration (Rayleigh test for circular non-uniformity, $p<0.001$ for all conditions, see ***Figure 4—figure supplement 2***). Among eyes, the individual fractions ranged between 16 and 80% of trials. Only two eyes drifted towards the CDC less frequently than given by chance (***Figure 4—figure supplement 1***). We computed the directionality tuning as the ratio of relative drift towards the CDC ± 45° (purple quadrant in ***Figure 4d***) and the mean relative drift towards the three other quadrants. A ratio of 1 indicated the same relative frequency of drift towards all cardinal directions, whereas for a tuning ratio of 2 the retina moved the CDC towards the stimulus twice as often compared to each of the other three cardinal directions. The directionality tuning ratios ranged between 0.6 and 11.8 with a median value of 3. Directionality tuning ratios had a significant effect on how much the resolution threshold exceeded the Nyquist limit. Participants with highly tuned drift reached larger differences between the Nyquist limit and their visual acuity threshold (dominant eyes: $r^2=0.45$, $p=0.01$; non-dominant eyes: $r^2=0.27$, $p=0.04$, ***Figure 4e***). Drift directionality was mostly similar between eyes, and if intra-ocular differences occurred, they were not related to ocular dominance. Also, we did not observe an effect of training on drift directionality: one of the two trained observers had a very strong drift directionality (7 and 11.8 in the dominant and non-dominant eye, respectively) while the other one exhibited a tuning ratio below average (2.1 and 2.3 in the dominant and non-dominant eye, respectively).

Next to the CDC, two other foveolar landmarks are often reported as anchor locations describing the center of the fovea. We here show that the CDC has the strongest relevance with respect to drift tuning. When relating the drift trajectories to the preferred retinal locus of fixation (PRL) or the location of peak cone density (PCD), we found a weaker approximation towards both. The retinae moved the stimulus towards the PRL or PCD

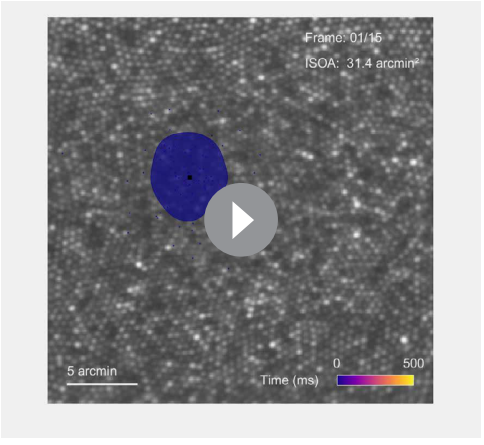

Video 3. Decrease of ISOA across trials during the 500 ms stimulus presentation. The area of stimulus onsets between trials shows a stronger variation than the area of stimulus offsets.
https://elifesciences.org/articles/98648/figures#video3

location in 42% or 35% of all trials, respectively (***Figure 4f***). Therefore, the observed directionality was strongest towards the CDC. In a considerable number of trials, the stimulus onset was further displaced from all of the three retinal locations and, therefore, a directed drift motion resulted in an approximation towards CDC as well as PRL and PCD. Also, in some eyes, two or all of these retinal locations lay very close together, which results in very similar effects. Nevertheless, in some eyes with particularly stable fixation that had at least a few arcmin distances between their PRL and CDC we repeatedly observed a stimulus onset close to PRL followed by a directional drift towards CDC with a resulting stimulus offset closer to the CDC. Across participants, this also resulted in a significant reduction of the isoline contour area (ISOA) size between stimulus onset and offset (p=0.02, ***Figure 3—figure supplement 1***, ***Figure 4b*** and ***Video 3***). The median ISOA for stimulus onset locations was 92.5 arcmin^2 which was reduced to 68.2 arcmin^2 for stimulus offset locations. This decrease in size of the area of all retinal landing points supports the view of a certain retinal cone or a very small area of a few arcmin^2 to be the target region of the drift eye motion in a resolution task.

When we looked at how much the individual drift trajectory decreased the distance from either location, the median distance convergence (onset/offset distance) towards CDC, PRL, and PCD was about 12%, 7%, and 3%, respectively. While no participant had an average convergence of more than 30% towards PRL or PCD, the maximum convergence ratio towards CDC was about 50%. An adaptive drift behavior was also found in the relative drift lengths exhibited in each stimulus presentation. Although the individual drift lengths could vary substantially from trial to trial, we found that, across all participants and experimental trials, eyes exhibited significantly larger drift lengths when the stimulus onset location was further away from the CDC (ρ^2=0.06, p<0.001, ***Figure 4g***). The onset distance was not correlated with drift directionality (***Figure 4g***). Across all trials, the average sampling cone density increased between stimulus onset and offset for most of the participants. This sampling gain was computed as the ratio between the maximum sampling density during the trial and the sampling density at the stimulus onset location. The sampling gain was significantly correlated with the potential retinal sampling gain of individuals in dominant (r^2=0.35, p=0.02) as well as non-dominant eyes (r^2=0.50, p=0.002, ***Figure 4h***). Observers exploited on average 30% of their potential sampling gain in both fellow eyes. Interestingly, one observer combined all the previously described sampling features particularly strong in his dominant eye (P08_R). It had a steep cone density gradient, exhibited strong directional tuning towards the CDC, and had large drift lengths for stimulus onsets far from the CDC. This eye was excluded from the sampling gain analysis because fixation behavior differed by more than 4 standard deviations from the group average.

Discussion

By using synchronous adaptive optics imaging and visual stimulation of the foveola, we find that the human visual system is capable of resolving spatial orientation of E optotypes smaller than a single photoreceptor diameter and uncover a fixational eye motor behavior that optimizes retinal sampling in accordance with the individual photoreceptor mosaic.

Spatial vision, and in particular visual acuity, is the most tested and used performance metric with a close relation to everyday vision. It provides the main behavioral outcome for clinical studies of vision. Measured in daily routine or clinical studies, the best corrected visual acuity of young and healthy adults is usually between 20/20 and 20/12.5 (60 and 37.5 arcsec) (***Reiniger et al., 2019***; ***Rossi et al., 2007***). Even if lower order aberrations are corrected by e.g., glasses or contact lenses, higher order aberrations inherently blur the retinal image, depending on their magnitude (***Reiniger et al., 2019***). Adaptive optics induce a close-to-diffraction limited optical correction, where the optical improvement is significantly correlated with an increase in visual acuity thresholds (***Marcos et al., 2008***). By correcting aberrations with AOSLO, we measured Snellen-E thresholds that were up to half the size (between 20/10 and 20/6.9; 30–20.6 arcsec) compared to the natural viewing condition. This is slightly lower than previously presented data (***Rossi et al., 2007***), very likely because of the different wavelengths used for experimentation (***Figure 2c***). It might be surprising to learn that the neural machinery of human vision is able to resolve such tiny stimuli, because natural viewing is blurred by the eye's optics. Even though observers are, to some degree, adapted to their own aberrations (***Artal et al., 2004***), the best subjective image quality is seen when on average 88% of the aberrations are corrected (***Chen et al., 2007***). This may indicate that, under normal viewing conditions, optical aberrations and not cone topography may play the dominant role in limiting the eye's acuity.

By removing most aberrations in our experiments, we can study in how far resolution thresholds are linked to or limited by the optimized but at the same time individual morphology of the human foveola. While in the periphery, midget retinal ganglion cell sampling dominates resolution, resolution of the foveal center was estimated to be governed by the cone sampling limit (***Rossi and Roorda, 2010***; ***Williams, 1985***). By first-time direct experimental validation in the same participants, we here confirm the hypothesis that the individual spacing of cones can predict the resolution capacity of our foveola when optical influences are bypassed (***Figure 2***). We found that the individual spatial arrangement of cones was highly correlated to the visual acuity of participants and explains up to 45% of its variance (***Figure 2d***). Eyes with higher foveolar sampling capacity reached lower thresholds than eyes with less densely packed cone photoreceptors. Moreover, all participants reached resolution thresholds that exceeded the static Nyquist sampling limit when tested with near-infrared, 788 nm light. Natural vision is comprised of multiwavelength stimuli, thus, using 788 nm in isolation is at the top end of our retinal sensitivity. In the first part of our study, participants also performed experiments with 840 nm light. Thresholds were rather approximating the Nyquist limit with this longer near-infrared wavelength (***Figure 2c***). The L- and M-cone photopigment absorbance for 840 nm is about 1.4 log unit lower than for 788 nm (***Stockman and Rider, 2023***). The decreased cone sensitivity combined with a larger Airy-Disk size of about 7% are likely to be detrimental for the longer, 840 nm, wavelength. We would expect a potential for even lower thresholds for shorter wavelengths.

Otherwise, a potential for lower thresholds is only expected in eyes with higher angular cone densities. Perhaps contrary at first sight, this could potentially be the case for observers with higher myopia. Myopic eyes, despite retinal stretching, generally have a higher angular sampling density in and around the foveola, compared to emmetropes (***Wang et al., 2019***). Therefore, we would expect acuity thresholds to be lower for myopic participants, in the case that (a) angular cone density is increased like previously suggested and (b) AO correction and display resolution are still sufficient to completely resolve the foveolar cone mosaic. Psychophysical data for more participants with higher myopia and longer axial lengths would be needed to verify this assumption.

Theoretical predictions of the Nyquist resolution limit imply stationary sampling. If the retinal image is under-sampled, aliasing occurs at the frequency of the receptor mosaic, which may obscure the original image, especially its orientation (compare example snapshots in ***Figure 1f***). While prior knowledge of the stimulus has been shown to theoretically help to de-alias under-sampled signals even in a static condition (***Ruderman and Bialek, 1992***), we believe that retinal image motion plays a significant role in deciphering orientation at the limits of spatial sampling. Fixational eye movements continuously modulate the luminance flow on individual cones and postreceptoral neuronal activity. Drift motion has long been presumed as a random jitter, a result of the limited precision of the oculomotor system (***Cornsweet, 1956***; ***Ditchburn and Ginsborg, 1953***). More recent work revealed that drift motion is neither random (***Rucci and Poletti, 2015***) nor detrimental due to the introduction of noise (***Burak et al., 2010***; ***Pitkow et al., 2007***), but rather a fine-tuned motion, beneficial for psychophysical measures of visual acuity in the parafovea (***Ratnam et al., 2017***) as well as foveola (***Intoy and Rucci, 2020***). As also observed in other sensory organs (***Ahissar and Arieli, 2001***), neurons in the visual system are strongly selective not just for spatial patterns, but also for temporally changing stimuli (***Ahissar and Arieli, 2012***), a finding that is also supported by computational modeling, suggesting that the visual system may utilize principles comparable to those used in computational imaging for achieving super-resolution via camera motion (***Anderson et al., 2020***). Within the past decades, the interdisciplinary term 'geometrical super-resolution' which is devoted to the filtering properties of sensor systems has become common (***Zalevsky, 2011***). These resolution advantages may be achieved in the visual system by incorporating mechanisms that allow for the recognition of positional differences smaller than a single cell. That such mechanism exists is exemplified in a phenomenon known as hyperacuity. Fine localization discriminations of only a few seconds of arc are performed by identification of the centroid of the retinal light distributions (***Westheimer and McKee, 1977***) of the involved pattern components. In a diffraction-limited resolution task, the visual system seems to be able to translate the temporal luminance modulation in individual photoreceptors by ocular drift to additional spatial information about the stimulus position and shape. Contrary, the indirect suppression of natural fixational eye motion by retinal stabilization techniques impairs visual acuity outside the foveolar center (***Intoy and Rucci, 2020***; ***Rucci et al., 2007***). For prolonged static stimulus presentations, retinal spiking decays over time, while drift motion keeps

the luminance change active, continuously refreshes the receptive field input, and sustains neuronal activity (***Kuang et al., 2012***).

We found a significant correlation between drift motion and visual acuity thresholds between individuals, indicating that drift motion may be one of the key elements in reaching sub-cone resolution thresholds. Interestingly, acuity improved for smaller fixational drift and decreased in participants who exhibited larger drift motion, on average. The fact that less drift is beneficial to reach the lowest possible acuity thresholds reflects the characteristics of spatiotemporal luminance changes introduced by smaller or larger drift motion. Smaller drifts induce luminance changes with higher spatial frequencies and models of retinal ganglion cell activity suggest a higher contrast sensitivity for high spatial frequency motion and less for low spatial frequencies compared to a static retina (***Kuang et al., 2012***; ***Rucci and Victor, 2015***). This is supported by other recent work which also showed that visual acuity thresholds can even be predicted from drift magnitudes measured in a sustained fixation task (***Clark et al., 2022***).

There is evidence that fixational eye motion might have systematic components in primates. A previous study in macaque monkeys revealed a systematic directional drift response only a few dozens of milliseconds after various visual transients (***Malevich et al., 2020***). In our study, we reveal that a certain drift directionality can not only be triggered by particular visual transients, but that human observers are capable of adapting their drift direction to enact an oculomotor strategy that takes advantage of the maximum resolution capacity provided within the retina. Our participants precisely moved their eyes to have the stimulus slip across the most densely packed cone cells within their foveola. We hereby shed light on a mechanism that is potentially particularly active during fine discrimination tasks. This confirms that drift can be quickly adjusted in a continuous closed-loop control (***Gruber and Ahissar, 2020***), while, as other recent work suggests, being at the same time able to quickly switch to an open-loop process, as specific task knowledge influences the dominant orientation of drift, even in the sudden absence of visual information (***Lin et al., 2023***). Yet, the underlying neuronal control of drift motion remains not fully understood. Recent work suggested, based on brainstem recordings in rhesus monkeys, that the origin can be found mostly upstream of the ocular motoneurons. It can likely be explained as diffusion in the oculomotor integrator which is mainly driven by noise, but additionally affected by mechanisms within the visual motor pathway (e.g. feedback mechanisms) (***Ben-Shushan et al., 2022***). An incorporation of a visual feedback loop to that model was shown to modulate the statistics of eye motion, given a time lag of about 100 ms (mainly due to synaptic processing delays, of order 60–80ms ***Malevich et al., 2020***). This fits our results well. Our presentation time of 500 ms sufficed for a modulation of the fixational drift motion towards retinal areas of higher cone sampling (also see ***Figure 4—figure supplements 1–3***). Our data supports the view that some aspects of the statistics of drift motion can be influenced by the visual task (***Ben-Shushan et al., 2022***; ***Intoy and Rucci, 2020***; ***Malevich et al., 2020***; ***Zhao et al., 2023***). The superior colliculus seems to play a major role in modulating drift motion in a feedback loop to visual inputs (***Hafed et al., 2021***). It's not only involved in controlling large eye motions (***Bergeron et al., 2003***) and microsaccades (***Hafed et al., 2009***), but also reflects neural responses to fixational drift that are likely a result of sensory input (C.-Y. ***Chen et al., 2019***).

So, even though the CDC is displaced from the PRL in a way to be beneficial for natural binocular vision (***Reiniger et al., 2021***), constant visual feedback allows to adapt the drift direction and, therefore, also the task-related PRL. Commonly, the term PRL is used for describing the retinal location that is preferably used in fixational tasks. It is still a matter of debate what factors drive the development of this very reproducible (***Reiniger et al., 2021***) retinal location and in how far it might provide enhanced visual function. Sensitivity to small light spots in the foveola seems to be rather plateau-like and not particularly pronounced at the PRL (***Domdei et al., 2021***). As recently shown, the PRL slightly differs between different tasks but has a larger interindividual variability (***Bowers et al., 2021***). The here shown results indicate that also when measuring visual resolution, the PRL is not necessarily the center of the sampling drift motion. The directional drift motion leads to a shift of the preferred retinal location for a resolution task towards the CDC (***Figure 4—figure supplement 3*** and ***Video 3***). Previous work that compared active versus passive fixation did not show a systematic offset in a similar experimental setup. However, 5 out of 8 participants also shifted their PRL in a Snellen E task closer to the CDC compared to the PRL for fixating a static disk stimulus (***Bowers et al., 2021***), the conditions that are best comparable to our study. The main difference to

our visual acuity experiments was that automatically paced random time intervals between presentations (0.5–1.5 s) were applied to not allow the participants to anticipate the next trial whereas in our study, participants self-paced the stimulus output to be able to prepare and focus for the next trial. It might be that this extremely fine-tuned usage of the visual feedback loop can only be kept active for rather short time intervals. By shifting the stimulus towards the CDC in 50% of cases, the potential sampling gain within individual eyes was exploited by 30%, on average, which goes along with a cone density increase of 3% or 285 cones/deg^2. Even though this increase in cone density alone would not account for the difference between acuity thresholds and the Nyquist limit, this and the simultaneous spatiotemporal luminance modulation contribute to achieving sub-cone visual acuity thresholds.

Between fellow eyes, we found very strong correlations for all the measured parameters. While drift lengths and directionality, as well as cone densities are very symmetric between dominant and non-dominant eyes (***Figures 2e and 3e***), significantly lower acuity thresholds of 1.5 arcsec, on average, were observed in the dominant eyes of participants (***Figure 2e***). The dominant eyes' visual input has a tendency to be preferred during binocular viewing, but has not been shown to exhibit relevant differences in visual function in healthy eyes with low refractive errors (***Ehrenstein et al., 2005***; ***Zhou et al., 2017***). Partially this may be due to limited accuracy in the mainly used clinical methods (e.g. Snellen Chart or projection have ~10 arcsec steps between optotype rows). This very fine binocular difference between eyes emphasizes that some remaining factors which especially comprise the neural postprocessing steps, also play an important role and may facilitate the slight functional advantage of dominant eyes.

For clinical studies of retinal health and in new therapeutical approaches, photoreceptor health and visual acuity can be related to other more standard clinical measures as OCT-derived measures of outer segment length or retinal thickness which have been shown to serve for estimates of cone density (***Domdei et al., 2023***). Therefore, building a larger dataset on photoreceptor-resolved foveolar maps and associated visual function measures may help to, on the one hand, better understand the interplay between structural and functional changes to draw conclusions about disease progression, intervention efficiency, or the interpretation of retinal imaging data in studies aimed at vision restoration. On the other hand, a detailed examination of psychophysical measures with knowledge about the exact neural sampling characteristics offers a great potential to answer further questions about e.g., resolution limits in myopia, the effect of image stabilization in the very center of the foveola, or implications for binocular viewing that could previously only be hypothesized. The awareness of the oculomotor system being able to finely adjust the drift motion behavior for a particular task may guide future interpretation of fixational eye motion.

Materials and methods

Participants

A total of 38 participants with White ethnicity underwent a preliminary screening where ocular biometry, ophthalmologic status, fixational eye motion, and adaptive optics correction as well as foveolar image quality were tested. From those, 20 participants with normal ophthalmologic status, resolvable foveolar cones, and ocular anatomy that allowed for a 7 mm pupil aperture during experimentation were chosen for subsequent examination. All 6 male and 14 female observers (17 adults [age: 18–42], three children [age: 10, 12, and 14]) had no or only mild refractive errors (SE:±2.5 diopters). The children and 15 adults were naïve participants and two adults were experienced observers. More detailed cone topography and fixational eye motion characteristics of the here studied population have been shown previously (***Reiniger et al., 2021***). The experiments were conducted under two different light conditions (16 participants 788 nm, 12 participants 840 nm). Eight participants took part in both experimental conditions. We mainly report the data acquired for the 788 nm condition in this manuscript and show 840 nm data for comparison where noteworthy differences arise.

Written informed consent was obtained from each participant and all experimental procedures adhered to the tenets of the Declaration of Helsinki, in accordance with the guidelines of the independent ethics committee of the medical faculty at the Rheinische Friedrich-Wilhelms-Universität of Bonn.

Ocular dominance

Ocular dominance was determined by a Miles Test prior to pupil dilation and visual acuity testing. The experimenter stood at a distance of 6 m in front of the participants and asked them to form a small opening between their thumbs and forefingers with both hands. The participant was then asked to extend their arms in front of them to look through the formed hole in the experimenter's face with both eyes open. This procedure was conducted three to five times to determine the dominant (=uncovered) eye in a 3/3 or at least 3/5 condition.

AOSLO retinal imaging

In vivo images of the complete foveolar cone mosaic were recorded using a custom-built adaptive optics scanning laser ophthalmoscope (AOSLO). The general setup of the AOSLO has been described previously (***Roorda et al., 2002***) and pertinent differences as well as the method of determination of the preferred retinal locus of fixation (PRL) have been described in a recent publication (***Reiniger et al., 2021***).

In brief, the front end of the AOSLO was equipped with three *f*=500 mm focal telescopes. These telescopes were specifically designed for point-scanning an adaptive optics-corrected focal light spot across the retina, ensuring diffraction-limited resolution in both incident and reflected beams. The system incorporated a magnetic actuator-driven deformable mirror (DM97-07, 7.2 mm pupil diameter, ALPAO, Montbonnot-Saint-Martin, France) positioned in a retinal conjugate plane. The deformable mirror was controlled by the wavefront error signals from a 25×25 lenslet Shack Hartmann sensor (SHSCam AR-S-150-GE, Optocraft GmbH, Erlangen, Germany) in closed-loop. Imaging and wavefront correction utilized wavelengths of either 788 nm (±12 nm) or 840 nm (±12 nm) light, achieved through serial dichroic and bandpass filtering of a supercontinuum source (SuperK Extreme EXR-15, NKT Photonics, Birkerød, Denmark). The imaging field of view was 0.85×0.85 degrees of visual angle. The digital lateral resolution was about 0.1 arcmin, the size of one pixel in the recorded videos and images. Light reflected from the retina was detected by a photomultiplier tube (PMT, H7422-50, Hamamatsu Photonics, Hamamatsu, Japan), positioned behind a confocal pinhole (Pinhole diameter = 20 mm, equivalent to 0.47 (840 nm) and 0.5 (788 nm) Airy disk diameters). Continuous sampling of the PMT signal was carried out using a field programmable gate array (FPGA), resulting in a 512x512-pixel video at 30 Hz (600 pixels per degree of visual angle). Through rapid acousto-optic intensity modulation of the imaging lights, the square AOSLO imaging field was used as a retinal display, where each pixel could be individually controlled to produce the visual stimuli.

Cone map generation and computation of sampling characteristics

The best PRL videos acquired were selected to create spatially registered, high signal-to-noise ratio images of the foveal center, which served as master retinal images for cone labeling as well as referencing of stimulus motion trajectories. This study includes only participants for whom the master retinal image was of sufficient quality to label all cones across the image. Cone centers were identified and labeled semi-manually, as previously described (***Cunefare et al., 2017***; ***Reiniger et al., 2021***). Cone density was computed in two different ways. First, for deriving landmark metrics of the foveolar cone map, we then computed Voronoi tessellation, estimating a patch with a certain area for each individual cone and summed the nearest 150 cone patches around each image pixel. The number of cells was divided by the resulting area to derive a pixel-resolved map of cone densities. Based on this map, the peak cone density (PCD) is defined as the highest cone density value of the map with its according retinal location. The cone density centroid (CDC) is computed as the weighted centroid of the 20th percentile of the highest cone densities within the map. We refer to the CDC as the anatomical center and the anchor for further spatial analyses in this study. The CDC has been shown to be a more robust and reproducible metric to describe the anatomical center than the more routinely reported PCD. While the PCD has value in reporting its quantity, namely the maximum cone density of a retina, using it as a landmark is however not advised, for it is too vulnerable against small changes in the analysis of cone density (***Reiniger et al., 2021***; ***Wynne et al., 2022***).

Second, for analyzing the relation between individual sampling limits and resolution acuity, cone density was computed based on the cone cells contributing to the sampling process. To identify the cones interacting in stimulus sampling, a simple model of cone light capture was employed. Each cone was described by an associated light acceptance aperture with its diameter estimated as 48% of

the average spacing between the cone and all of its neighbors. The efficiency of the aperture along its diameter was approximated as Gaussian profiles. Also, a model of the stimulus retinal image was computed by convolving the eye's point spread function (diffraction limited at 788 nm for a 7 mm pupil) with the stimulus bitmap. The complete two-dimensional model of cone apertures was then multiplied by models of the presented stimuli to arrive at the cone-level light distribution based on the different stimulus positions, sizes, and orientations. The light distribution within each cone was integrated across the entire cone aperture. This value was then normalized to the degree to which the aperture was filled. Cone stimulation was considered to be maximal if the entire aperture was filled. Using this method, a cone activation pattern could be generated for each point in time (e.g. ***Figure 1f***). To arrive at a task-related cone density estimate for each frame (sampling cone density), the number of cones identified to interact with the stimulus was divided by their summed cone area. In the presented analyses, the median sampling density of all trials is analyzed and standard deviations are shown as gray lines (***Figure 2d and e***). This stimulus-related cone density was chosen to closely represent the sampling process; however, the results do not qualitatively differ from using the cone density map based on the 150 nearest cones.

We assumed a perfect hexagonal cell mosaic to estimate the average inter-cone-distance (ICD) between neighboring cells and to compute the theoretical Nyquist sampling limit, which is based on the spacing between rows of cones, and given by $\mathrm{N} = \frac{\sqrt{3}}{2} \times \mathrm{ICD}$.

Experimental procedures

For psychophysical acuity testing, participants reported the orientation of a Snellen-E stimulus in a four-alternative forced-choice (four AFC) task under unrestricted eye motion. Psychophysical experiments were performed monocularly in both eyes. The non-dominant eye was tested first and the dominant eye after a 15–30 min break. This protocol was chosen because with pilot experiments in seven participants (which were performed in a random order) less time was needed and hence less fatigue was reported by the participants when the second eye was the dominant one. In these pilot experiments, the same qualitative difference of acuity thresholds between non-dominant and dominant were found.

Mydriasis and cycloplegia were established by two drops of 1% tropicamide, instilled into the eyelid about 25 and 20 min prior to experiments. If experimentation took longer than 40 min, another drop of tropicamide was instilled. A customized dental impression mold (bite bar) was used to immobilize and adjust the head position and thus to align the participant's eye in front of the imaging system to ensure optimal adaptive optics correction and image quality. The participants were encouraged to take breaks at any time. We found that proper resting is one of the most crucial factors during the rather complex AOSLO experimentation. Frequent breaks ensure constant, high-level compliance and excellent image quality as the basis for artefact-free and reproducible results.

Before recording experimental runs, each participant performed three test runs to get used to the test procedure and the appearance of the stimuli. The stimuli were displayed as 'off-stimuli' on the infrared background by switching the displayed intensity via an acousto-optic modulator (***Poonja et al., 2005***) (AOM, TEM-250-50-10-840-2FP, Brimrose, Sparks Glencoe, MD, USA) (***Figure 1a***). Because of ocular diffraction, the stimulus contrast varied between 0.61 and 0.80 for an 18 arcsec versus 36 arcsec gap-sized stimulus (three and six pixels of the scanning raster, respectively). The visual acuity testing followed the Bayesian adaptive procedure QUEST (***Brainard, 1997***; ***Pelli, 1997***; ***Watson and Pelli, 1983***). Stimulus progression was self-paced by the participant. The stimuli were presented for 500 ms to avoid limitations by insufficient temporal summation (***McAnany, 2014***). Around each trial, a 1 s AOSLO video was recorded, with the stimulation onset at around 300 ms after video onset. Visual acuity thresholds were estimated by pooling results from 5 consecutively run staircases, with each containing 20 trials. A psychometric function was fitted using *psignifit4* (***Schütt et al., 2016***) to derive threshold estimates for further analysis. The expected threshold variance is described and visualized by the 95% confidence interval (***Figures 1d, e , and 2d***).

Video processing and eye motion analysis

The AOSLO used a raster scanning technique where each frame was acquired over time. The recorded videos were stabilized after psychophysical testing using custom settings within the *MATLAB*-based stabilization software from Stevenson et al. (***Stevenson and Roorda, 2005***). To acquire eye traces at

higher temporal resolution than the 30 Hz frame rate, each frame of the AOSLO movie is broken into 32 horizontal strips of 16 pixels height and cross-correlated against a reference frame. The reference frame was generally chosen automatically and exchanged by a manually chosen frame in cases weres stabilization failed despite good overall image quality. This method allowed the extraction of eye motion traces at temporal frequencies up to 960 Hz.

The frame-wise (30 Hz) stimulus position was encoded as a white cross marker in each video. As single-strip alignments can have small errors due to noise in the strip or retinal torsion (particularly affecting the horizontal motion estimate) (***Hofmann et al., 2022***), we compute the average offsets from the cross-containing strip and two previous/subsequent strips. These steps yielded more accurate trajectories in retinal coordinates for every trial. All individual trial AOSLO frames and the corresponding trajectories are then referenced to the single master retinal image used for cone map generation.

To quantify the retinal motion across the stimulus, drift length was defined as the concatenated vector sum of all frame-wise motion vectors within the 500 ms stimulus duration (see also ***Figure 3c***). Trials that contained microsaccades or blinks during stimulus presentation were excluded from further analyses. Microsaccade occurrence varied highly between participants (mean ± SD: 14±10% of trials, range: 2-41%). If not stated differently, we here report the median drift length of all trials for individual eyes (e.g. of all traces shown in ***Figure 3a***). To quantify drift direction, the angle between each trajectory's starting coordinate (coordinate center in ***Figure 4c***) and end coordinate was computed. To check for potential motion bias, the drift angles were first analyzed in retinal coordinates (***Figure 4c***), and then as the relative angle, $\theta_{CDC,}$ formed between the drift vector and the line connecting the retinal onset location and the CDC (***Figure 4d***). To compare directionality towards other locations of interest, the same was done for PRL and PCD locations (***Figure 4f***).

Statistical information

All statistical analyses were conducted using custom-written MATLAB code and significance levels were set at 0.05. To assess the normal distribution of the dataset, a two-sided Shapiro–Wilk test was employed. This test is recognized to be appropriate for small sample sizes. The paired samples t-test was utilized to assess whether there were significant differences between the means of normally distributed paired observations. For non-parametric data, the Wilcoxon Signed-Rank test was employed. Linear correlations were computed to examine the relationships between variables. For variables demonstrating normal distribution, Pearson's correlation coefficient was employed, while for non-normally distributed data, Spearman's rank correlation coefficient was utilized. Pearson's correlation is sensitive to linear relationships, assuming bivariate normality, whereas Spearman's correlation is a non-parametric measure suitable for monotonic relationships and is robust against outliers and non-normal distributions.

Acknowledgements

This work is supported by the German Research Foundation, Emmy Noether-Program HA5323/5-1; Carl Zeiss Foundation, HC-AOSLO; Novartis Pharma GmbH, EYENovative research award, and the Open Access Publication Fund of the University of Bonn.

Additional information

Funding

Funder	Grant reference number	Author
Deutsche Forschungsgemeinschaft	HA5323/5-1	Wolf M Harmening
Carl Zeiss Foundation	HC-AOSLO	Wolf M Harmening
Novartis Pharma GmbH	EYENovative research award	Jenny L Witten

Funder	Grant reference number	Author
University of Bonn	Open Access Publication Fund	Jenny L Witten

The funders had no role in study design, data collection and interpretation, or the decision to submit the work for publication.

Author contributions

Jenny L Witten, Conceptualization, Resources, Data curation, Software, Formal analysis, Investigation, Visualization, Methodology, Writing – original draft, Project administration, Writing – review and editing; Veronika Lukyanova, Resources, Software, Formal analysis; Wolf M Harmening, Conceptualization, Resources, Supervision, Funding acquisition, Validation, Writing – original draft, Project administration, Writing – review and editing

Author ORCIDs

Jenny L Witten https://orcid.org/0000-0001-7500-7053
Veronika Lukyanova https://orcid.org/0009-0008-3682-7225
Wolf M Harmening https://orcid.org/0000-0001-7053-1198

Ethics

Participants gave written informed consent before the experiments. All studies complied with the Declaration of Helsinki in its latest version and were approved by the Ethics Committee of the medical faculty at the Rheinische Friedrich-Wilhelms-Universität of Bonn (reference number: 2018-09).

Peer review material

Reviewer #1 (Public review): https://doi.org/10.7554/eLife.98648.3.sa1
Reviewer #2 (Public review): https://doi.org/10.7554/eLife.98648.3.sa2
Reviewer #3 (Public review): https://doi.org/10.7554/eLife.98648.3.sa3
Author response https://doi.org/10.7554/eLife.98648.3.sa4

Additional files

Supplementary files

- MDAR checklist

Data availability

The following data are publicly available for download at Mendeley Data: 1. All original cone mosaic images and cone coordinates. 2. Retinal locations of CDC, PRL and PCD. 3. Fixational eye motion trajectories. 4. MATLAB code that can be used to plot the data on the original image.

The following dataset was generated:

Author(s)	Year	Dataset title	Dataset URL	Database and Identifier
Witten JL, Lukyanova V, Harmening W	2024	Data from: Sub-cone visual resolution by active, adaptive sampling in the human foveola	https://data.mendeley.com/datasets/zp6d5w8kdv/1	Mendeley Data, 10.17632/zp6d5w8kdv.1

References

Ahissar E, Arieli A. 2001. Figuring space by time. *Neuron* **32**:185–201. DOI: https://doi.org/10.1016/s0896-6273(01)00466-4, PMID: 11683990

Ahissar E, Arieli A. 2012. Seeing via miniature eye movements: a dynamic hypothesis for vision. *Frontiers in Computational Neuroscience* **6**:89. DOI: https://doi.org/10.3389/fncom.2012.00089, PMID: 23162458

Anderson AG, Ratnam K, Roorda A, Olshausen BA. 2020. High-acuity vision from retinal image motion. *Journal of Vision* **20**:34. DOI: https://doi.org/10.1167/jov.20.7.34, PMID: 32735342

Artal P, Chen L, Fernández EJ, Singer B, Manzanera S, Williams DR. 2004. Neural compensation for the eye's optical aberrations. *Journal of Vision* **4**:281–287. DOI: https://doi.org/10.1167/4.4.4, PMID: 15134475

Ben-Shushan N, Shaham N, Joshua M, Burak Y. 2022. Fixational drift is driven by diffusive dynamics in central neural circuitry. *Nature Communications* **13**:1697. DOI: https://doi.org/10.1038/s41467-022-29201-y, PMID: 35361753

Bergeron A, Matsuo S, Guitton D. 2003. Superior colliculus encodes distance to target, not saccade amplitude, in multi-step gaze shifts. *Nature Neuroscience* **6**:404–413. DOI: https://doi.org/10.1038/nn1027

Bohigian GM. 2008. An ancient eye test--using the stars. *Survey of Ophthalmology* **53**:536–539. DOI: https://doi.org/10.1016/j.survophthal.2008.06.009, PMID: 18929764

Bowers NR, Gautier J, Lin S, Roorda A. 2021. Fixational eye movements in passive versus active sustained fixation tasks. *Journal of Vision* **21**:1–16. DOI: https://doi.org/10.1167/jov.21.11.16

Brainard DH. 1997. The psychophysics toolbox. *Spatial Vision* **10**:433–436. DOI: https://doi.org/10.1163/156856897X00357, PMID: 9176952

Burak Y, Rokni U, Meister M, Sompolinsky H. 2010. Bayesian model of dynamic image stabilization in the visual system. *PNAS* **107**:19525–19530. DOI: https://doi.org/10.1073/pnas.1006076107

Campbell FW, Green DG. 1965. Optical and retinal factors affecting visual resolution. *The Journal of Physiology* **181**:576–593. DOI: https://doi.org/10.1113/jphysiol.1965.sp007784, PMID: 5880378

Cava JA, Allphin MT, Mastey RR, Gaffney M, Linderman RE, Cooper RF, Carroll J. 2020. Assessing interocular symmetry of the foveal cone mosaic. *Investigative Ophthalmology & Visual Science* **61**:23. DOI: https://doi.org/10.1167/iovs.61.14.23, PMID: 33331861

Caves EM, Brandley NC, Johnsen S. 2018. Visual acuity and the evolution of signals. *Trends in Ecology & Evolution* **33**:358–372. DOI: https://doi.org/10.1016/j.tree.2018.03.001

Chen L, Artal P, Gutierrez D, Williams DR. 2007. Neural compensation for the best aberration correction. *Journal of Vision* **7**:9. DOI: https://doi.org/10.1167/7.10.9, PMID: 17997678

Chen CY, Hoffmann KP, Distler C, Hafed ZM. 2019. The foveal visual representation of the primate superior colliculus. *Current Biology* **29**:2109–2119. DOI: https://doi.org/10.1016/j.cub.2019.05.040, PMID: 31257138

Cherici C, Kuang X, Poletti M, Rucci M. 2012. Precision of sustained fixation in trained and untrained observers. *Journal of Vision* **12**:1–16. DOI: https://doi.org/10.1167/12.6.31, PMID: 22728680

Clark AM, Intoy J, Rucci M, Poletti M. 2022. Eye drift during fixation predicts visual acuity. *PNAS* **119**:e2200256119. DOI: https://doi.org/10.1073/pnas.2200256119, PMID: 36442088

Cornsweet TN. 1956. Determination of the stimuli for involuntary drifts and saccadic eye movements. *Journal of the Optical Society of America* **46**:987–993. DOI: https://doi.org/10.1364/josa.46.000987, PMID: 13367941

Cunefare D, Fang L, Cooper RF, Dubra A, Carroll J, Farsiu S. 2017. Open source software for automatic detection of cone photoreceptors in adaptive optics ophthalmoscopy using convolutional neural networks. *Scientific Reports* **7**:6620. DOI: https://doi.org/10.1038/s41598-017-07103-0, PMID: 28747737

Curcio CA, Packer O, Kalina RE. 1987. A whole mount method for sequential analysis of photoreceptor and ganglion cell topography in a single retina. *Vision Research* **27**:9–15. DOI: https://doi.org/10.1016/0042-6989(87)90137-4, PMID: 3303679

Curcio CA, Sloan KR, Kalina RE, Hendrickson AE. 1990. Human photoreceptor topography. *The Journal of Comparative Neurology* **292**:497–523. DOI: https://doi.org/10.1002/cne.902920402, PMID: 2324310

Ditchburn RW, Ginsborg BL. 1953. Involuntary eye movements during fixation. *The Journal of Physiology* **119**:1–17. DOI: https://doi.org/10.1113/jphysiol.1953.sp004824, PMID: 13035713

Domdei N, Reiniger JL, Holz FG, Harmening WM. 2021. The relationship between visual sensitivity and eccentricity, cone density and outer segment length in the human foveola. *Investigative Ophthalmology & Visual Science* **62**:31. DOI: https://doi.org/10.1167/iovs.62.9.31, PMID: 34289495

Domdei N, Ameln J, Gutnikov A, Witten JL, Holz FG, Wahl S, Harmening WM. 2023. cone density is correlated to outer segment length and retinal thickness in the human foveola. *Investigative Ophthalmology & Visual Science* **64**:11. DOI: https://doi.org/10.1167/iovs.64.15.11, PMID: 38064229

Ehrenstein WH, Arnold-Schulz-Gahmen BE, Jaschinski W. 2005. Eye preference within the context of binocular functions. *Graefe's Archive for Clinical and Experimental Ophthalmology* **243**:926–932. DOI: https://doi.org/10.1007/s00417-005-1128-7

Gruber LZ, Ahissar E. 2020. Closed loop motor-sensory dynamics in human vision. *PLOS ONE* **15**:e0240660. DOI: https://doi.org/10.1371/journal.pone.0240660, PMID: 33057398

Hafed ZM, Goffart L, Krauzlis RJ. 2009. A neural mechanism for microsaccade generation in the primate superior colliculus. *Science* **323**:940–943. DOI: https://doi.org/10.1126/science.1166112, PMID: 19213919

Hafed ZM, Chen CY, Tian X, Baumann MP, Zhang T. 2021. Active vision at the foveal scale in the primate superior colliculus. *Journal of Neurophysiology* **125**:1121–1138. DOI: https://doi.org/10.1152/jn.00724.2020, PMID: 33534661

Hendrickson AE, Yuodelis C. 1984. The morphological development of the human fovea. *Ophthalmology* **91**:603–612. DOI: https://doi.org/10.1016/s0161-6420(84)34247-6, PMID: 6462623

Herrmann CJJ, Metzler R, Engbert R. 2017. A self-avoiding walk with neural delays as a model of fixational eye movements. *Scientific Reports* **7**:12958. DOI: https://doi.org/10.1038/s41598-017-13489-8, PMID: 29021548

Hirsch J, Curcio CA. 1989. The spatial resolution capacity of human foveal retina. *Vision Research* **29**:1095–1101. DOI: https://doi.org/10.1016/0042-6989(89)90058-8, PMID: 2617858

Hofmann J, Domdei L, Jainta S, Harmening WM. 2022. Assessment of binocular fixational eye movements including cyclotorsion with split-field binocular scanning laser ophthalmoscopy. *Journal of Vision* **22**:5. DOI: https://doi.org/10.1167/jov.22.10.5, PMID: 36069941

Intoy J, Rucci M. 2020. Finely tuned eye movements enhance visual acuity. *Nature Communications* **11**:795. DOI: https://doi.org/10.1038/s41467-020-14616-2, PMID: 32034165

Intoy J, Mostofi N, Rucci M. 2021. Fast and nonuniform dynamics of perisaccadic vision in the central fovea. *PNAS* **118**:e2101259118. DOI: https://doi.org/10.1073/pnas.2101259118, PMID: 34497123

Kaplan E, Benardete E. 2001. The dynamics of primate retinal ganglion cells. *Progress in Brain Research* **134**:17–34. DOI: https://doi.org/10.1016/s0079-6123(01)34003-7, PMID: 11702542

Ko HK, Poletti M, Rucci M. 2010. Microsaccades precisely relocate gaze in a high visual acuity task. *Nature Neuroscience* **13**:1549–1553. DOI: https://doi.org/10.1038/nn.2663, PMID: 21037583

Krauskopf J, Cornsweet TN, Riggs LA. 1960. Analysis of eye movements during monocular and binocular fixation. *Journal of the Optical Society of America* **50**:572–578. DOI: https://doi.org/10.1364/josa.50.000572, PMID: 14411808

Kuang X, Poletti M, Victor JD, Rucci M. 2012. Temporal encoding of spatial information during active visual fixation. *Current Biology* **22**:510–514. DOI: https://doi.org/10.1016/j.cub.2012.01.050, PMID: 22342751

Lin YC, Intoy J, Clark AM, Rucci M, Victor JD. 2023. Cognitive influences on fixational eye movements. *Current Biology* **33**:1606–1612. DOI: https://doi.org/10.1016/j.cub.2023.03.026, PMID: 37015221

Malevich T, Buonocore A, Hafed ZM. 2020. Rapid stimulus-driven modulation of slow ocular position drifts. *eLife* **9**:e57595. DOI: https://doi.org/10.7554/eLife.57595, PMID: 32758358

Marcos S, Sawides L, Gambra E, Dorronsoro C. 2008. Influence of adaptive-optics ocular aberration correction on visual acuity at different luminances and contrast polarities. *Journal of Vision* **8**:1. DOI: https://doi.org/10.1167/8.13.1, PMID: 19146331

McAnany JJ. 2014. The effect of exposure duration on visual acuity for letter optotypes and gratings. *Vision Research* **105**:86–91. DOI: https://doi.org/10.1016/j.visres.2014.08.024, PMID: 25281413

Nagano T. 1980. Temporal sensitivity of the human visual system to sinusoidal gratings. *Journal of the Optical Society of America* **70**:711–716. DOI: https://doi.org/10.1364/josa.70.000711, PMID: 7400873

Pelli DG. 1997. The videotoolbox software for visual psychophysics: transforming numbers into movies. *Spatial Vision* **10**:437–442 PMID: 9176953.

Pitkow X, Sompolinsky H, Meister M. 2007. A neural computation for visual acuity in the presence of eye movements. *PLOS Biology* **5**:e331. DOI: https://doi.org/10.1371/journal.pbio.0050331, PMID: 18162043

Poonja S, Patel S, Henry L, Roorda A. 2005. Dynamic visual stimulus presentation in an adaptive optics scanning laser ophthalmoscope. *Journal of Refractive Surgery* **21**:S575–S580. DOI: https://doi.org/10.3928/1081-597X-20050901-30, PMID: 16209464

Putnam NM, Hofer HJ, Doble N, Chen L, Carroll J, Williams DR. 2005. The locus of fixation and the foveal cone mosaic. *Journal of Vision* **5**:632–639. DOI: https://doi.org/10.1167/5.7.3, PMID: 16231998

Ratnam K, Domdei N, Harmening WM, Roorda A. 2017. Benefits of retinal image motion at the limits of spatial vision. *Journal of Vision* **17**:30. DOI: https://doi.org/10.1167/17.1.30, PMID: 28129414

Reiniger JL, Lobecke AC, Sabesan R, Bach M, Verbakel F, de Brabander J, Holz FG, Berendschot T, Harmening WM. 2019. Habitual higher order aberrations affect landolt but not vernier acuity. *Journal of Vision* **19**:11. DOI: https://doi.org/10.1167/19.5.11, PMID: 31100127

Reiniger JL, Domdei N, Holz FG, Harmening WM. 2021. Human gaze is systematically offset from the center of cone topography. *Current Biology* **31**:4188–4193. DOI: https://doi.org/10.1016/j.cub.2021.07.005, PMID: 34343479

Rolfs M. 2009. Microsaccades: small steps on a long way. *Vision Research* **49**:2415–2441. DOI: https://doi.org/10.1016/j.visres.2009.08.010

Roorda A, Romero-Borja F, Donnelly Iii W, Queener H, Hebert T, Campbell M. 2002. Adaptive optics scanning laser ophthalmoscopy. *Optics Express* **10**:405–412. DOI: https://doi.org/10.1364/oe.10.000405, PMID: 19436374

Rossi EA, Weiser P, Tarrant J, Roorda A. 2007. Visual performance in emmetropia and low myopia after correction of high-order aberrations. *Journal of Vision* **7**:14. DOI: https://doi.org/10.1167/7.8.14, PMID: 17685821

Rossi EA, Roorda A. 2010. The relationship between visual resolution and cone spacing in the human fovea. *Nature Neuroscience* **13**:156–157. DOI: https://doi.org/10.1038/nn.2465, PMID: 20023654

Rossi EA, Chung M, Dubra A, Hunter JJ, Merigan WH, Williams DR. 2011. Imaging retinal mosaics in the living eye. *Eye* **25**:301–308. DOI: https://doi.org/10.1038/eye.2010.221, PMID: 21390064

Rucci M, Iovin R, Poletti M, Santini F. 2007. Miniature eye movements enhance fine spatial detail. *Nature* **447**:851–854. DOI: https://doi.org/10.1038/nature05866, PMID: 17568745

Rucci M, Poletti M. 2015. Control and functions of fixational eye movements. *Annual Review of Vision Science* **1**:499–518. DOI: https://doi.org/10.1146/annurev-vision-082114-035742, PMID: 27795997

Rucci M, Victor JD. 2015. The unsteady eye: an information-processing stage, not a bug. *Trends in Neurosciences* **38**:195–206. DOI: https://doi.org/10.1016/j.tins.2015.01.005, PMID: 25698649

Ruderman DL, Bialek W. 1992. Seeing beyond the nyquist limit. *Neural Computation* **4**:682–690. DOI: https://doi.org/10.1162/neco.1992.4.5.682

Schütt HH, Harmeling S, Macke JH, Wichmann FA. 2016. Painfree and accurate Bayesian estimation of psychometric functions for (potentially) overdispersed data. *Vision Research* **122**:105–123. DOI: https://doi.org/10.1016/j.visres.2016.02.002, PMID: 27013261

Stevenson SB, Roorda A. 2005. Correcting for miniature eye movements in high-resolution scanning laser ophthalmoscopy. *Ophthalmic Technologies XV* **1**:145–151. DOI: https://doi.org/10.1117/12.591190

Stockman A, Rider AT. 2023. Formulae for generating standard and individual human cone spectral sensitivities. *Color Research and Application* **48**:818–840. DOI: https://doi.org/10.1002/col.22879, PMID: 38504724

Syrbe S, Kuhrt H, Gärtner U, Habermann G, Wiedemann P, Bringmann A, Reichenbach A. 2018. Müller glial cells of the primate foveola: an electron microscopical study. *Experimental Eye Research* **167**:110–117. DOI: https://doi.org/10.1016/j.exer.2017.12.004, PMID: 29242027

Tuten WS, Harmening WM. 2021. Foveal vision. *Current Biology* **31**:R701–R703. DOI: https://doi.org/10.1016/j.cub.2021.03.097, PMID: 34102113

Wang Y, Bensaid N, Tiruveedhula P, Ma J, Ravikumar S, Roorda A. 2019. Human foveal cone photoreceptor topography and its dependence on eye length. *eLife* **8**:e47148. DOI: https://doi.org/10.7554/eLife.47148, PMID: 31348002

Watson AB, Pelli DG. 1983. QUEST: a bayesian adaptive psychometric method. *Perception & Psychophysics* **33**:113–120. DOI: https://doi.org/10.3758/BF03202828

Wells-Gray EM, Choi SS, Bries A, Doble N. 2016. Variation in rod and cone density from the fovea to the mid-periphery in healthy human retinas using adaptive optics scanning laser ophthalmoscopy. *Eye* **30**:1135–1143. DOI: https://doi.org/10.1038/eye.2016.107, PMID: 27229708

Westheimer G. 1975. Editorial: visual acuity and hyperacuity. *Investigative Ophthalmology* **14**:570–572. DOI: https://doi.org/10.1097/00006324-198708000-00002, PMID: 1150397

Westheimer G, McKee SP. 1977. Spatial configurations for visual hyperacuity. *Vision Research* **17**:941–947. DOI: https://doi.org/10.1016/0042-6989(77)90069-4, PMID: 595400

Westheimer G. 2012. Optical superresolution and visual hyperacuity. *Progress in Retinal and Eye Research* **31**:467–480. DOI: https://doi.org/10.1016/j.preteyeres.2012.05.001, PMID: 22634484

Wilk MA, Dubis AM, Cooper RF, Summerfelt P, Dubra A, Carroll J. 2017. Assessing the spatial relationship between fixation and foveal specializations. *Vision Research* **132**:53–61. DOI: https://doi.org/10.1016/j.visres.2016.05.001, PMID: 27286921

Williams DR. 1985. Aliasing in human foveal vision. *Vision Research* **25**:195–205. DOI: https://doi.org/10.1016/0042-6989(85)90113-0, PMID: 4013088

Williams DR, Coletta NJ. 1987. Cone spacing and the visual resolution limit. *Journal of the Optical Society of America A* **4**:1514. DOI: https://doi.org/10.1364/JOSAA.4.001514

Wynne N, Cava JA, Gaffney M, Heitkotter H, Scheidt A, Reiniger JL, Grieshop J, Yang K, Harmening WM, Cooper RF, Carroll J. 2022. Intergrader agreement of foveal cone topography measured using adaptive optics scanning light ophthalmoscopy. *Biomedical Optics Express* **13**:4445–4454. DOI: https://doi.org/10.1364/BOE.460821, PMID: 36032569

Zalevsky Z. 2011. Exceeding the diffraction and the geometric limits of imaging systems: A review. Dolev S, Oltean M (Eds). *Optical Supercomputing 2010. Lecture Notes in Computer Science*. Springer-Verlag. p. 119–130. DOI: https://doi.org/10.1007/978-3-642-22494-2_13

Zhang T, Godara P, Blanco ER, Griffin RL, Wang X, Curcio CA, Zhang Y. 2015. Variability in human cone topography assessed by adaptive optics scanning laser ophthalmoscopy. *American Journal of Ophthalmology* **160**:290–300. DOI: https://doi.org/10.1016/j.ajo.2015.04.034

Zhang C, Kim YJ, Silverstein AR, Hoshino A, Reh TA, Dacey DM, Wong RO. 2020. Circuit reorganization shapes the developing human foveal midget connectome toward single-cone resolution. *Neuron* **108**:905–918. DOI: https://doi.org/10.1016/j.neuron.2020.09.014, PMID: 33027639

Zhao Z, Ahissar E, Victor JD, Rucci M. 2023. Inferring visual space from ultra-fine extra-retinal knowledge of gaze position. *Nature Communications* **14**:269. DOI: https://doi.org/10.1038/s41467-023-35834-4, PMID: 36650146

Zhou D, Ni N, Ni A, Chen Q, Hu DN, Zhou J. 2017. Association of visual acuity with ocular dominance in 2045 myopic patients. *Current Eye Research* **42**:1155–1159. DOI: https://doi.org/10.1080/02713683.2017.1297464, PMID: 28494159

eLife

RESEARCH ARTICLE

Figures and figure supplements

Sub-cone visual resolution by active, adaptive sampling in the human foveola

Jenny L Witten *et al*.

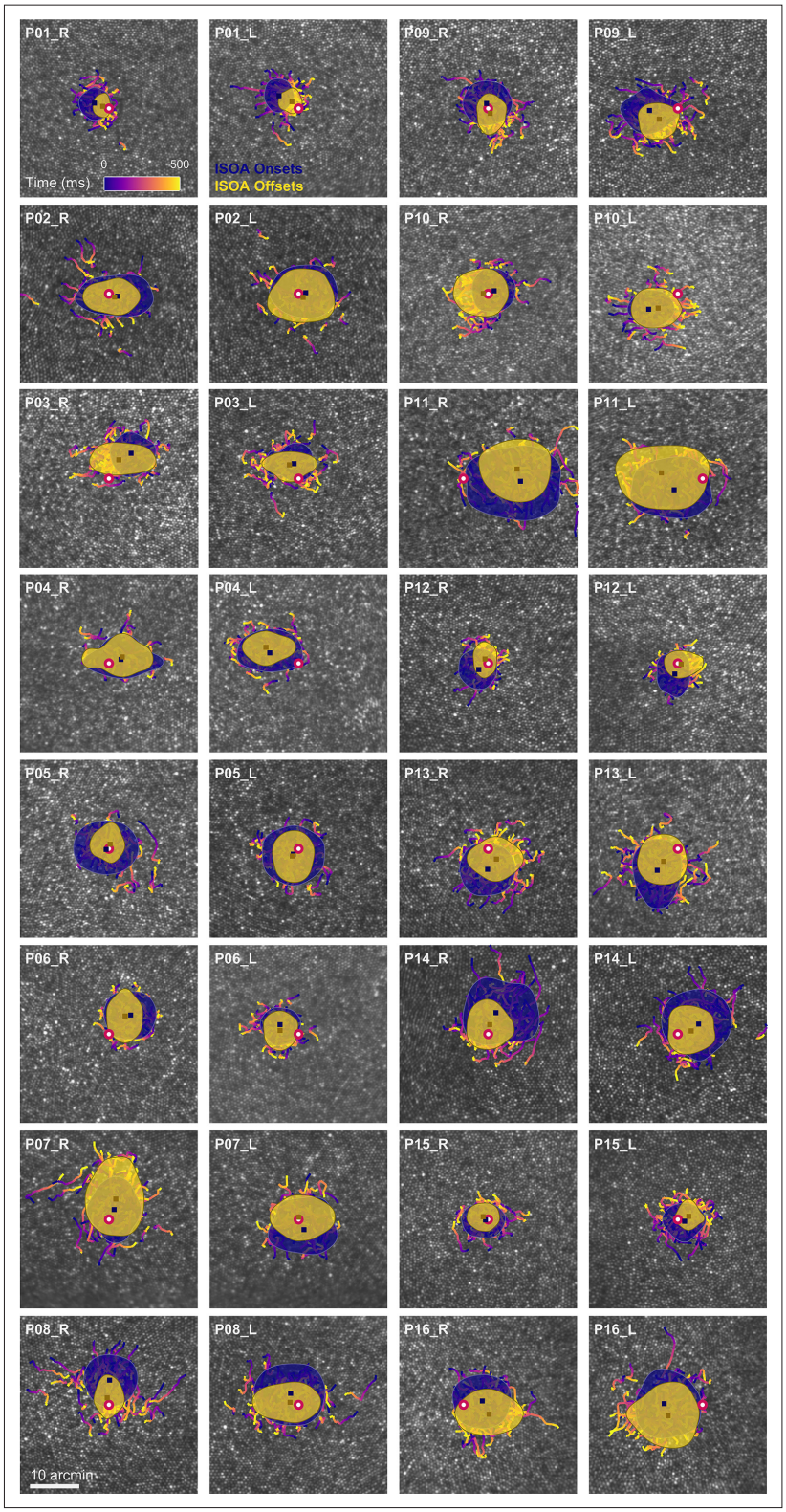

Figure 3—figure supplement 1. Drift trajectories on foveolar mosaics. Participants (P01-16) are sorted according to acuity thresholds in their dominant eye (best to worst). All single trial motion traces are shown on the corresponding cone mosaic, color-coded by elapsed time. One-SD isoline areas (ISOA) are shown for all stimulus onset (blue) and offset (yellow) locations. The medians of all onset and offset locations are shown as blue and yellow squares, respectively. The cone density centroid (CDC) is indicated by a red circle with white fill.

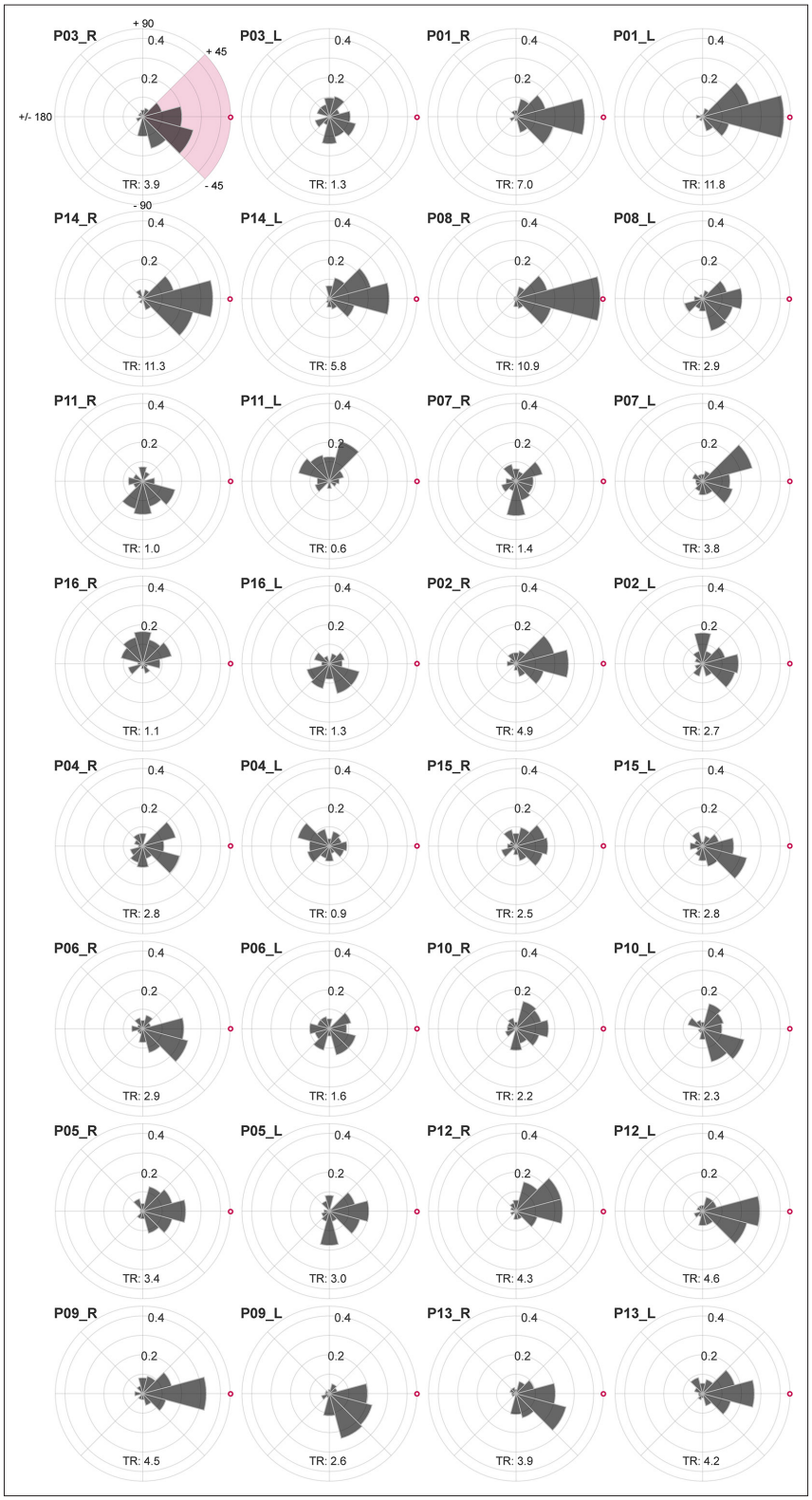

Figure 4—figure supplement 1. Individual drift directionality. Sorted according to their dominant eyes cone density centroid (CDC) to preferred retinal locus (PRL) distance (largest to smallest) eyes drift directionality is shown relative to the CDC. The CDC is indicated by a red circle with white fill. Participant numbers (P01 to P16) are assigned based on the dominant eye's visual acuity threshold (best to worst). The upper left plot shows the angular

Figure 4—figure supplement 1 continued on next page

Figure 4—figure supplement 1 continued

labels exemplarily for all eyes. The tuning ratio was computed as the ratio between the relative frequency of intra-participant drift motion towards the CDC (±45 deg), indicated by the pink quarter, and the average of drift motion towards the remaining three quadrants.

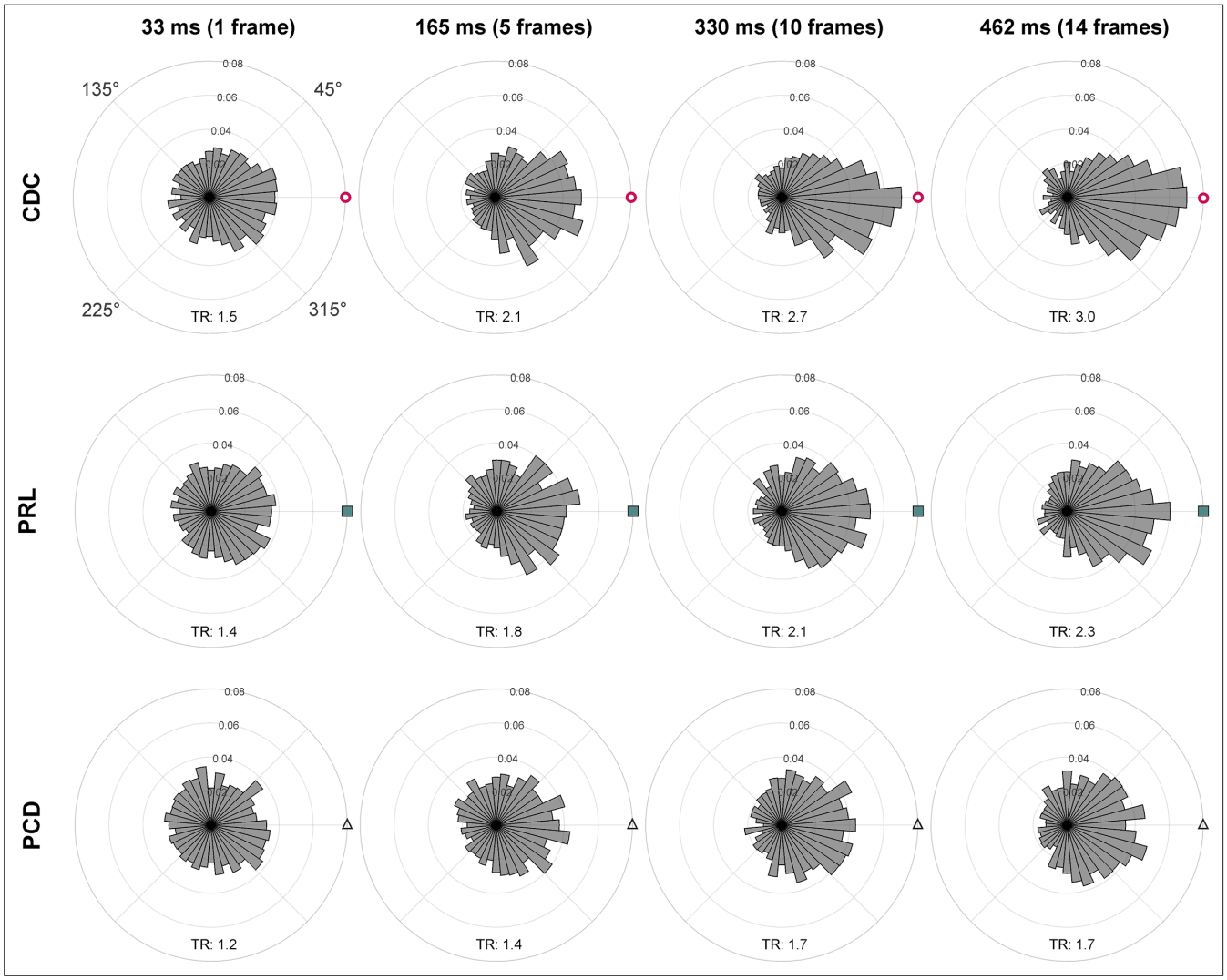

Figure 4—figure supplement 2. Time course of drift directionality. The angles θ cone density centroid (CDC), θ preferred retinal locus (PRL), and θ peak cone density (PCD) for all eyes were computed over time, relative to the stimulus onset, and are shown after 33 ms (one frame), 165 ms (five frames), 330 ms (10 frames), and 462 ms (14 frames). The respective tuning ratio (TR) is shown in the bottom part of each subplot. The tuning ratio was computed as the ratio between the relative frequency of inter-participant drift motion towards the CDC (±45 deg) and the average of drift motion towards the remaining three quadrants. For all cases, the circular data are not distributed uniformly around the circle (Rayleigh test, $p<0.001$, with increasing significance for longer durations). The distributions were compared against each other by the Kolmogorov-Smirnov test. Only CDC vs. PRL (33 ms) and PRL vs. PCD (33 ms) show no statistically significant difference. The distribution towards CDC compared to PCD is significantly different for 33 ms ($p=0.002$). For all other time points, all distributions are significantly different from each other, with increasing significance for longer durations (for 462 ms, all $p<0.001$).

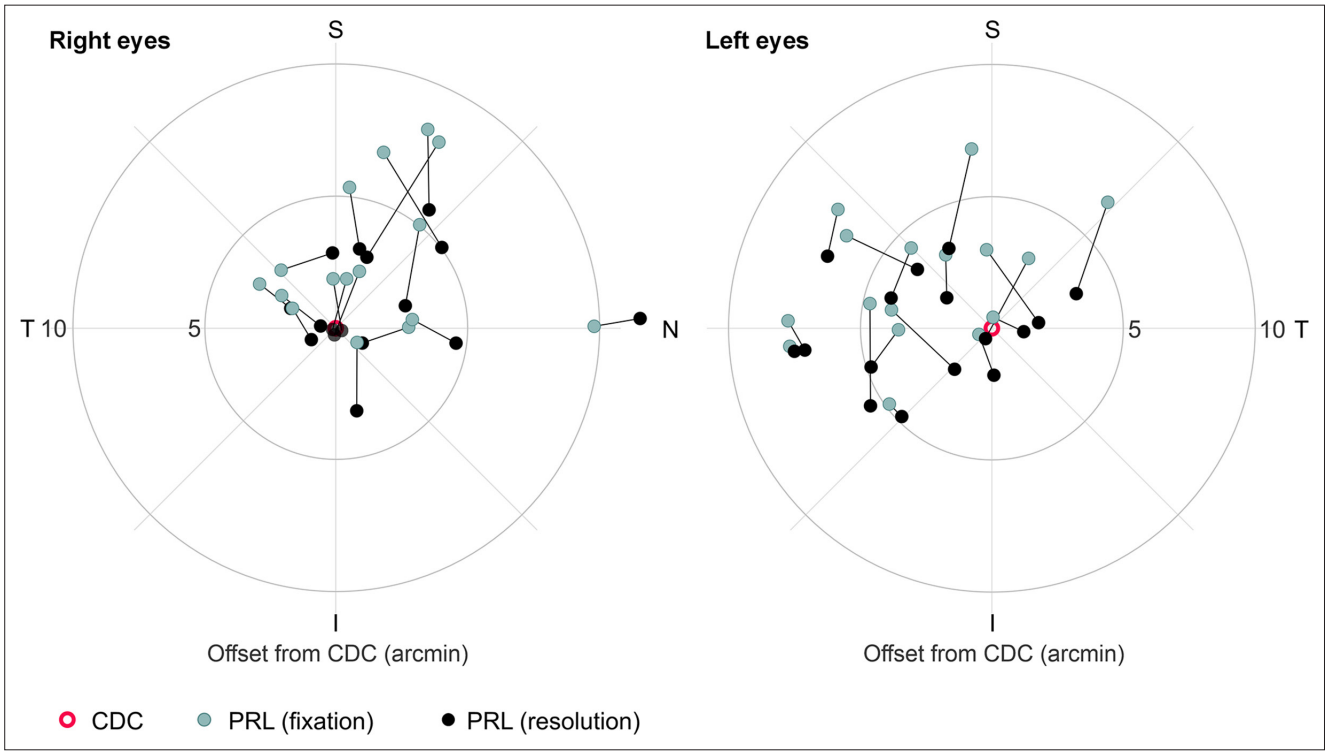

Figure 4—figure supplement 3. Different retinal locations used in a fixation or resolution task. Median preferred retinal locus (PRL) locations of all participants' right and left eyes plotted in retinal coordinates relative to the cone density centroid (CDC). Retinal locations are plotted in teal for the fixation task and in black for the resolution task. A black line connects the retinal locations of the same participant.

4 Discussion with references

Human vision represents an intricate balance between optical, anatomical, and neural factors, which together shape the extraordinary spatial resolution capabilities of the fovea. While the human eye is often regarded as one of the most advanced visual systems in nature, it is not without fundamental constraints. In my thesis, I investigated the extent to which these constraints - stemming from optical imperfections, photoreceptor organization, and dynamic visual processing - limit visual resolution, as well as the mechanisms that mitigate these limitations. The main findings of the three scientific projects, which are further discussed in the following sections, can be individually summarized as:
(1) Visual resolution acuity, but not discrimination acuity, is affected by small inter-individual differences in HOA of the eye's optics.
(2) Human developed a strategy to ensure the overlap of high cell density areas in the binocular visual field by systematically displacing the topographical center of cone distribution and the retinal locus preferably used in a fixation task from each other.
(3) Visual resolution thresholds can exceed the theoretical static sampling limit, given by the size of cones, by targeted eye movements, making use of closed-loop feedback mechanisms within the oculomotor system.

4.1 The limit of visual resolution

Since the visual sense plays the dominant role in how humans perceive and interact with the world (Rock and Harris 1967; Calvert et al. 2004), it seems to be intuitive to scrutinize it's limits and the mechanisms behind it's precision (see 2.3.1). The influence of the optical quality of the eye on visual functions, especially resolution, have been well studied. While it is indisputable that LOA have an influence on habitual visual acuity, it has been shown in publication 1 of this thesis, that also minor imperfections, like HOA, which cannot be corrected by glasses or contact lenses, significantly influenced visual resolution acuity. The average visual acuity under natural viewing conditions, and correction of only LOA was 45.1 arcsec (SD: 7 arcsec), similar to other work (Rossi et al. 2007). At natural pupil sizes, reduced acuity thresholds were observed for decreased retinal image quality. Thus, even small amounts of optical deterioration impact resolution acuity (Marsack et al. 2004;

Watson and Ahumada 2008), but optical quality alone cannot explain the wide variation of observed visual acuity thresholds, even for similar amounts of aberrations. Other factors that influence resolution acuity are the density of cone photoreceptors and ganglion cells, intraocular scatter, cortical processing, and neural adaptation (Artal 2015; Artal et al. 2004; Hou et al. 2017; Jiang et al. 2017; Rossi and Roorda 2010; Wang et al. 2018).

Even though observers were shown to be neurally adapted to their own aberrations (Artal et al. 2004), the perceived image quality is best when approximately 88 % of the aberrations are corrected (Chen et al. 2007). This indicates, that the visual system could be able to resolve smaller details than those which are typically present on the retina when optical aberrations were absent. Applying AOSLO in project 2 and 3 allowed to bypass the optical aberrations and offered a direct and noninvasive view on the photoreceptor mosaic *in vivo*. To achieve a sufficient resolution for resolving even the most densely packed cone photoreceptors in the foveola, the field of view is typically as small as 1 deg, roughly 1/3 of a millimeter where about 10,000 cones can be identified. The highest individual cone densities within the foveola count roughly 10,000 to 20,000 cones/deg² or 140,000 to 220,000 cones/mm², which has been confirmed in numerous studies (Putnam et al. 2005; Li et al. 2010; Zhang et al. 2015; Cooper et al. 2016; Wells-Gray et al. 2016; Wilk et al. 2017; Wang et al. 2019; Cava et al. 2020; Ameln et al. 2025), conducted mostly within the last decade, after technological advances in adaptive optics imaging made it possible to visualize the foveolar cones in a larger variety of eyes (Williams et al. 2023).

If we follow the hypothesis and assume that the spacing of the cone photoreceptors would impose the fundamental resolution limit when bypassing the optics of the eye, the observed average packing density of 13,149 cones/deg² in publication 3 would relate to an acuity threshold of 29.2 arcsec. However, in the AOSLO based diffraction-limited visual acuity testing thresholds even decreased to 24.1 arcsec, on average (SD: 2.4 arcsec), and therefore exceeded the theoretical prediction of the cones Nyquist limit. At the same time, visual acuity thresholds were highly correlated with individual cone densities and up to 45 % of the variance in visual acuity could be explained by cone density. Thus, the cell spacing itself does not impose the fundamental limitation for resolution, but plays a major role for it. By their position within the retinal array, the photoreceptors explicitly encode space and the spatial relationships are mapped to equal areas within V1 (Hubel

and Wiesel 1974; Schira et al. 2007). The cortical representations of the cones within the foveola in V2 and V3 are even larger than in V1, indicating rather increased than reduced neural processing power for the centermost part of the visual field (Schira et al. 2009). However, the information must already be present in the sensory neurons. Since during natural vision the spatial relationship between the stimulus and the photoreceptor mosaic is never static, additional important information might be provided by the variability in cell activity due to the continuously occurring fixational eye movements.

4.2 The role of fixational eye movements at the foveal scale

Even though they happen unconsciously, ever present subtle eye movements transverse the retinal image of a stimulus across several dozens of photoreceptor cells per second, while attempting to maintain stable fixation. It has only recently become possible to investigate the direct interaction between a fixated target and the photoreceptors of the foveola that are naturally used to sample it. Publication 2 of this thesis revealed a small but distinct systematic offset between the preferred retinal location for fixation (PRL) and the topographical center of the foveola. This mirror symmetrical offset between fellow eyes ensures a horizontal overlap of the areas with highest cone density in the binocular visual field and displaces the areas of highest sampling density to be slightly superior to a fixated object. This retinal location corresponds to a part of the visual field which is usually more distant and therefore contains smaller spatial details.

In the third publication of this thesis it was observed that this behavior changes for a diffraction-limited high resolution task. In this case, the retina traverses the stimulus with a directional drift motion with which it shifts the most densely packed cone photoreceptors towards the critical details that are to be sampled. The amount of drift motion significantly correlated with visual acuity thresholds, suggesting drift to play a key role in achieving sub-cone resolution thresholds. The important role of active sampling is also supported when modeling visual acuity based on retinal spiking activity (Nghiem et al. 2025). From this observation it can be concluded that the human visual system is capable of translating the temporal luminance information in individual photoreceptors that originate from ocular drift, to additional knowledge of high spatial frequency stimuli - the fine spatial features of an image. It has been shown that the absence of retinal image motion, attempted

by stabilization of stimuli to a certain retinal location, impairs visual acuity outside the foveolar center (Rucci et al. 2007; Ratnam et al. 2017; Intoy and Rucci 2020). When natural eye movements are indirectly suppressed, retinal spiking decays over time (Burak et al. 2010). In contrast, drift sustains neural activity by keeping the receptoral luminance change active (Kuang et al. 2012; Nghiem et al. 2025). Based on the findings of this thesis and given that neurons in the retina and early visual system are rather insensitive to an unchanging input (Purpura et al. 1990), an impairment in visual acuity thresholds would be expected for image stabilization in the foveola, too. However, under diffraction-limited experimental conditions this could not yet be shown, since the 1-to-1 connectivity between foveolar cones and midget retinal ganglion cells (mRGCs) (Zhang et al. 2020) requires an instant and perfect stabilization, which currently available techniques cannot provide. Tiny stabilization inaccuracies of a few image pixels, which in the case of the here described AOSLO relate to 10 - 20 arcsec of variation between frames, result in concatenate motion path lengths that are only slightly shorter than during habitual drift motion (average path lengths: stabilized: 4.5 arcmin, habitual: 6.5 arcmin). This not intended jitter is sufficient for inducing a luminance variation that makes it possible to integrate temporal dynamics for unattenuated perception of spatial details (Lukyanova et al. 2025). One degree outside the foveal center, it has also been shown that resolution thresholds did not differ whether the participants sample the stimulus with their habitual fixational eye motion or a manipulated motion path with similar motion statistics, whereas thresholds were reduced when the stimulus position was stabilized on the retina (Ratnam et al. 2017). This likely differs between the foveolar center and 1 deg eccentricity, as the cones and receptive fields are significantly larger at 1 deg. Thus the stabilization is accurate enough to induce no or very minor luminance variation at 1 deg retinal eccentricity, while the same amount of remaining jitter induces a resolvable spatiotemporal luminance signal in the most central foveal cone photoreceptors.

Even though perhaps not intuitive at first sight, it has been shown that participants who performed smaller fixational drift had better visual acuity, while performance decreased for larger drift motion (Clark et al. 2022). This is likely due to the fact that the luminance changes induced by smaller drift entail higher spatial frequencies, which better fits the retinal ganglion cell activity, producing a higher contrast sensitivity (Kuang et al. 2012;

Rucci and Victor 2015). To support this sampling behavior, microsaccades, which can be detrimental to fine-scale discrimination (Bridgeman and Palca 1980), can be suppressed for a few hundreds of milliseconds (Intoy et al. 2021; Bowers et al. 2021). Publication 3 shows that this time duration also sufficed to make use of a visual feedback mechanism which enacted an oculomotor strategy that precisely drifted the eyes to have the stimulus slip towards the most densely packed cones within the foveola. The visual system was capable of modulating the statistics of eye motion with a short time lag of about 100 ms (60-80 ms due to synaptic processing delays, Malevich et al. 2020) (Ben-Shushan et al. 2022).

Thus, as in other senses (Ahissar and Arieli 2001), visual processing relies on temporal neural strategies to extract and represent spatial information, thereby independent of whether the temporal information results from external motion of an object or eye movements (Snodderly et al. 2001). It was observed that fixational drift and microsaccades underlie strong variations between as well as within participants (Bowers et al. 2021; Clark et al. 2022), at the same time, they can be adapted to various different demands, such as maintaining fixation (Intoy and Rucci 2020), reducing redundant information (Kuang et al. 2012; Rucci and Victor 2015), compensating head movements (Aytekin et al. 2014; Poletti et al. 2015), or resolving a tiny detail (Ko et al. 2010). To meet all the different requirements that accompany these tasks, drift has been shown to be capable of both, being quickly adjusted in a continuous closed-loop control (Ahissar and Arieli 2012; Gruber and Ahissar 2020), as well as quickly switching to an open-loop process (Lin et al. 2023). Therefore, it might be the right time to fully jettison the view of fixational eye movements being detrimental and to be ignored or overcome by the visual system and instead replace retinal movements "induce smearing" by "induce adaptability and precision" to visual processing.

4.3 Hyperacute perception

The ability of sensory systems to resolve details beyond the physical limits of sensory receptors is referred to as hyperacuity. Visual hyperacuity is most typically measured as the offset between a pair of lines (Vernier acuity), which is roughly 10 times smaller than the spacing of the most central foveal cones. It depends on the ability of the neural visual system to identify and interpret small differences in the spatial patterns of retinal light

distributions (Westheimer and McKee 1977; Morgan and Aiba 1985). In publication 1 it could be shown that this hyperacute discrimination is unaffected by the habitual HOA of the eye's optics. This is also the case for other small-scale retinal image degradation, while threshold variation is also highly dependent on the chosen stimulus parameters, such as gap size (Williams et al. 1984). The notion of this ability being dependent on the neural averaging of photoreceptor signals across multiple locations stimulated due to miniature eye movements has already been suggested by Hering 1899, referring to experimental observations of such small discrimination angles from Volkmann 1836. Now, almost 2 centuries later, the results of this thesis demonstrate that sub-cell differentiation can also be achieved in a visual resolution task. When individual photoreceptors can be visualized and stimulated *in vivo*, enabled by correcting LOA and HOA, hyperacuity features of the visual system can be directly observed while the most central foveal cones traverse a small letter optotype.

Physiological and computational models of the mechanisms behind hyperacuity (Findlay 1973; Geisler 1984), identified small movements to be of prime importance for this fine-scale discrimination (Jiang et al. 2017) and show Vernier acuity not to be some miraculous singularity, but an intrinsic property of the neural networks encoding sensory information (Ahissar and Arieli 2001; Westheimer 2009). Thus, hyperacuity phenomena have also been observed in other senses and species. Similar to increased visual detail discrimination by fine-scale eye movements, also rats vibrissal systems can reach a hyperacuity level in an active process. Rats move their whiskers to improve horizontal object localization, resulting in acuities finer than the inter-vibrissal spacing (Knutsen et al. 2006; Ahissar and Knutsen 2016). Also visual hyperacuity (Vernier acuity) has been observed in other species, such as monkeys (Kiorpes et al. 1993), cats (Murphy and Mitchell 1991), rats (Seymoure and Juraska 1997), and birds (Harmening et al. 2007). Strong evidence for mechanisms that translate temporal into spatial information have even been found in insects compound eyes. Fruit flies (Drosophila), who do not move their eyes, induce microsaccadic sampling by contracting their photoreceptors due to light impulses (Juusola et al. 2017). Their rabomers move inside their photoreceptors which moves and narrows the cells receptive fields. The photoreceptors refractory sampling and photomechanical contractions therefore improve the fly eyes spatiotemporal image resolution 4-10 times

beyond the optical limit. Thus, also Drosophila achieves a kind of hyperacute vision by encoding space in time (Kemppainen et al. 2022a; Kemppainen et al. 2022b). However, there is big differences in the speed of such beneficial receptor movements. In Drosophila, microsaccadic sampling seems to be beneficial for visual information capture, whereas the current view in human eyes is that microsaccades rather contribute to the visual process by relocating gaze (Ko et al. 2010), but are mostly suppressed when it comes to high resolution demands (Bowers et al. 2021). For high acuity, in turn, rather slow drift movements are beneficial (Clark et al. 2022, publication 3). Assuming that both visual systems would in general benefit from similar temporal information, a potential reason might be the dependence of an information gain or loss on the visual task. Drosophilas behavior is primarily driven by basic biological needs for which a good orientation in their environment is crucial. When considering studies in human that rather demand orientation than detail examination, the spatial (e.g., saccade amplitude) as well as temporal viewing characteristics (e.g., fixation duration or saccade frequency) also change clearly (Mills et al. 2011; McCamy et al. 2014). Generally previous work, based on video eyetrackers, showed that smaller targets elicit less overall fixational eye movements than larger targets (Hirasawa et al. 2016; McCamy et al. 2013).

Moreover, the visual system's hierarchical structure allows it to integrate both low-level sensory input and high-level contextual information (Hubel and Wiesel 1962), facilitating functions ranging from motion detection to reading and face recognition. Recent findings suggest that individual differences in those tasks may have practical implications, as higher-level perceptual tasks like reading have been linked to Vernier acuity. Specifically, Vernier acuity may play a role in the early stages of hierarchical letter and word processing, as psychophysical thresholds in these tasks were found to correlate with the processing of Chinese characters (Tan et al. 2018). Vernier targets have also been shown to more effectively characterize the magnitude of acuity loss in amblyopic eyes compared to VEP grating acuity, based on visually evoked potentials (VEP) (Hou et al. 2018). Thus, the precision of the mechanisms behind hyperacute visual perception makes hyperacuity an indispensable measure for further understanding of neural mechanisms and feedback mechanisms of sub-cell-size spatial vision as well as an important, yet underrepresented, biomarker for retinal disease diagnoses (Hu et al. 2021).

4.4 Clinical relevance

Impaired visual function can lead to significant restraints in everyday life. Therefore, the awareness of deficits within the visual system in a very early stage is essential for selecting an adequate treatment. In visual screening, a particular focus is usually put on the function of the foveola, as a good visual resolution of small details is highly advantageous for nearly all tasks in our daily routine from reading small text to identifying faces from large distance.

The resolution of tiny details depends in the first instance on the individual ocular optics and second on the cone photoreceptor packing density in the center of the fovea. As the foveolar cone density is significantly correlated with visual resolution thresholds (publication 3), it should be possible to anticipate a potential foveolar cone loss from high resolution visual acuity thresholds or vice versa estimate visual acuity based on cone photoreceptor arrangement. However, to date, AO ophthalmoscopy is not integrated into standard ophthalmic care and it is clinical practice to terminate visual acuity testing when 20/20 vision (1 arcmin critical details) is confirmed. Therefore, significant cone loss was predicted to be necessary to cause measurable reductions in visual function (Geller et al. 1992). Retinopathia pigmentosa (RP) patients remained 20/20 vision until their cone density was decreased by about 40 to 50 % (Foote et al. 2018), while objective cone regularity metrics (i.e. number of neighbors regularity) could already detect a significant deviation from normal when cones were reduced by 10 % (Cooper et al. 2016). To be able to detect small changes in foveolar cone density by just doing functional clinical testing it would be at least necessary to measure visual acuity as far as possible, typically 20/10 vision (30 arcsec). If AOSLO high resolution imaging and visual acuity testing could be conducted more routinely in clinical practice, structural changes and functional vision loss within the foveola could be detected much earlier than with conventional clinical measurement methods, where declined visual acuity is detected rather late during the progression of a variety of retinal disease, such as RP, Stargardt's disease, diabetic retinopathy and glaucoma. However, the impact of AO on image optimization is critically limited by the patients ocular optics (e.g. cataract, but also tearfilm) as well as the ability to maintain stable fixation (e.g. reduced in different retinal degenerative diseases), which hampers the routine use of AOSLO in the clinic. Even though attempts have been made to link *in vivo* photoreceptor structure and visual function in diseased eyes (such as RP, Foote

et al. 2018), yet, no study directly measured the photoreceptor resolved resolution limits in retinal disease. The knowledge gained based on AO imaging of retinal disease has still not reached a level to alter decisions regarding patient care, which appears to be the most crucial point for it's use in clinical routine (Morgan et al. 2023). There are attempts though, to e.g. develop simple image processing routines to improve the automated identification of generic image features, especially in pathological retinas (Kalitzeos et al. 2024) to facilitate this process.

In a different, more simple but therefore much more accessible approach in clinical routine, hyperacuity thresholds could serve as an alternative functional biomarker to visual acuity, as they are unaffected by small-scale image degradation (Williams et al. 1984, publication 1). Vernier acuity has been explored as a measure of retinal or neural visual function when optical media opacities are present. Additionally, it has been proven to be a more sensitive marker than grating acuity for the detection and monitoring of several disease, such as cortical visual impairments in children (Skoczenski and Good 2004), amblyopia, glaucoma, and retinopathia pigmentosa. While it is not routinely measured in clinical practice (Hu et al. 2021), this currently results in investigations of new testing methods (Rabin et al. 2024) to facilitate the straightforward use of hyperacuity in clinical routine.

More in general, medical diagnostic changes towards very early disease detection, preferably even before its first symptoms occur. For neurodegenerative disease (e.g. Alzheimer's or Parkinson's disease) there are already well known biomarkers that allow for identification of the disease condition long before the first apparent clinical symptoms (Sperling et al. 2014; Shao et al. 2024). Such biomarkers can identify individuals who have biological evidence of the disease, but clinicians and researchers may not easily use them on a large scale. Alternatively, functional ocular biomarkers like the analysis of eye movements can provide an indirect link to neuronal and cognitive functioning, due to their accuracy, affordability, and ease of use. Various paradigms of eye movements have already been proven to be potential biomarkers for cognitive disorders, such as Alzheimer's disease (Opwonya et al. 2022) or Schizophrenia (Hutton and Ettinger 2006). Deepening the understanding about how exactly the healthy eye moves in a variety of tasks as well as the interaction between photoreceptor structure and fixational eye movements can al-

low to detect additional early biomarkers for cognitive disorders and retinal degenerative disease.

Facing towards the next decades, when medical data will be more digitalized, tracked more individually and their analyses automatized, this work provides a piece of knowledge about the mechanisms connecting visual perception, anatomical constraints and visuomotor control which can help to build crucial synapses within the network for linking functional and molecular biomarkers to a variety of diseases.

4.5 Discussion references

Ahissar, E. and Arieli, A. Figuring space by time. *Neuron*. 2001; 32 (2): pp. 185–201

Ahissar, E. and Arieli, A. Seeing via Miniature Eye Movements: A Dynamic Hypothesis for Vision. *Front. Comput. Neurosci.* 2012; 6 (11): pp. 1 –27

Ahissar, E. and Knutsen, P. M. (2016). Vibrissal Location Coding. In: *Sch. Touch*. Ed. by T. Prescott, E. Ahissar, and E. Izhikevich. Paris: Atlantis Press, pp. 725–735.

Ameln, J., Lukyanova, V., Witten, J. L., Gutnikov, A., Holz, F. G., and Harmening, W. M. The in-vivo cone photoreceptor topography of the normal human foveola. *Press*. 2025;:

Artal, P. Image Formation in the Living Human Eye. *Annu. Rev. Vis. Sci.* 2015; 1: pp. 1–17

Artal, P., Chen, L., Fernández, E. J., Singer, B., Manzanera, S., and Williams, D. R. Neural compensation for the eye's optical aberrations. *J. Vis.* 2004; 4 (4): p. 4

Aytekin, M., Victor, J. D., and Rucci, M. The visual input to the retina during natural head-free fixation. *J. Neurosci.* 2014; 34 (38): pp. 12701–12715

Ben-Shushan, N., Shaham, N., Joshua, M., and Burak, Y. Fixational drift is driven by diffusive dynamics in central neural circuitry. *Nat. Commun.* 2022; 13 (1): p. 1697

Bowers, N. R., Gautier, J., Lin, S., and Roorda, A. Fixational eye movements in passive versus active sustained fixation tasks. *J. Vis.* 2021; 21 (11): pp. 1 –16

Bridgeman, B. and Palca, J. The role of microsaccades in high acuity observational tasks. *Vision Res.* 1980; 20 (9): pp. 813–817

Burak, Y., Rokni, U., Meister, M., and Sompolinsky, H. Bayesian model of dynamic image stabilization in the visual system. *Proc. Natl. Acad. Sci. U. S. A.* 2010; 107 (45): pp. 19525–19530

Calvert, G. A., Spence, C., and Stein, B. E. The Handbook of Multisensory Processes: MIT Press, 2004

Cava, J. A., Allphin, M. T., Mastey, R. R., Gaffney, M., Linderman, R. E., Cooper, R. F., and Carroll, J. Assessing Interocular Symmetry of the Foveal Cone Mosaic. *Investig. Opthalmology & Vis. Sci.* 2020; 61 (14): pp. 1–11

Chen, L., Artal, P., Gutierrez, D., and Williams, D. R. Neural compensation for the best aberration correction. *J. Vis.* 2007; 7 (2007): pp. 1–9

Clark, A. M., Intoy, J., Rucci, M., and Poletti, M. Eye drift during fixation predicts visual acuity. *Proc. Natl. Acad. Sci. U. S. A.* 2022; 119 (49): pp. 1–10

Cooper, R. F., Wilk, M. A., Tarima, S., and Carroll, J. Evaluating Descriptive Metrics of the Human Cone Mosaic. *Investig. Opthalmology & Vis. Sci.* 2016; 57 (7): pp. 2992–3001

Findlay, J. M. Feature detectors and vernier acuity. *Nature*. 1973; 241 (5385): pp. 135–137

Foote, K. G., Loumou, P., Griffin, S., Qin, J., Ratnam, K., Porco, T. C., Roorda, A., and Duncan, J. L. Relationship Between Foveal Cone Structure and Visual Acuity Measured With Adaptive Optics Scanning Laser Ophthalmoscopy in Retinal Degeneration. *Investig. Opthalmology & Vis. Sci.* 2018; 59 (8): p. 3385

Geisler, W. S. Physical limits of acuity and hyperacuity. *J. Opt. Soc. Am. A.* 1984; 1 (7): pp. 775–82

Geller, A. M., Sieving, P. A., and Green, D. G. Effect on grating identification of sampling with degenerate arrays. *J. Opt. Soc. Am. A*. 1992; 9 (3): pp. 472–477

Gruber, L. Z. and Ahissar, E. Closed loop motor-sensory dynamics in human vision. *PLoS One*. 2020; 15 (10 October): pp. 1–18

Harmening, W. M., Göbbels, K., and Wagner, H. Vernier acuity in barn owls. *Vision Res.* 2007; 47 (7): pp. 1020–1026

Hering, E. (1899). Ueber die Grenzen der Sehschärfe [On the limits of visual acuity]. In: *Berichte über die Verhandlungen der Königlich-Sächsischen Gesellschaft der Wissenschaften zu Leipzig. Math. Classe; Naturwissenschaftlicher Teil, 51*. Leipzig, Germany: Georg Thieme, pp. 16–24.

Hirasawa, K., Okano, K., Koshiji, R., Funaki, W., and Shoji, N. Smaller Fixation Target Size Is Associated with More Stable Fixation and Less Variance in Threshold Sensitivity. *PLoS One*. 2016; 11 (11): e0165046

Hou, C., Good, W. V., and Norcia, A. M. Detection of amblyopia using sweep VEP vernier and grating acuity. *Investig. Ophthalmol. Vis. Sci.* 2018; 59 (3): pp. 1435–1442

Hou, C., Kim, Y.-J., and Verghese, P. Cortical sources of Vernier acuity in the human visual system: An EEG-source imaging study. *J. Vis.* 2017; 17 (6): pp. 1–12

Hu, M. L., Ayton, L. N., and Jolly, J. K. The clinical use of Vernier acuity: Resolution of the visual cortex is more than meets the eye. *Front. Neurosci.* 2021; 15 (October): pp. 1–12

Hubel, D. H. and Wiesel, T. N. Receptive fields, binocular interaction and functional architecture in the cat's visual cortex. *J. Physiol.* 1962; 160 (1): pp. 106–154

Hubel, D. H. and Wiesel, T. N. Uniformity of monkey striate cortex: A parallel relationship between field size, scatter, and magnification factor. *J. Comp. Neurol.* 1974; 158 (3): pp. 295–305

Hutton, S. B. and Ettinger, U. The antisaccade task as a research tool in psychopathology: A critical review. *Psychophysiology*. 2006; 43 (3): pp. 302–313

Intoy, J., Mostofi, N., and Rucci, M. Fast and nonuniform dynamics of perisaccadic vision in the central fovea. *Proc. Natl. Acad. Sci. U. S. A.* 2021; 118 (37):

Intoy, J. and Rucci, M. Finely tuned eye movements enhance visual acuity. *Nat. Commun.* 2020; 11 (1): pp. 1–11

Jiang, H., Cottaris, N., Golden, J., Brainard, D., Farrell, J. E., and Wandell, B. A. Simulating retinal encoding: factors influencing Vernier acuity. *Electron. Imaging*. 2017; 29 (14): pp. 177–181

Juusola, M., Dau, A., Song, Z., Solanki, N., Rien, D., Jaciuch, D., Dongre, S. A., Blanchard, F., De Polavieja, G. G., Hardie, R. C., and Takalo, J. Microsaccadic sampling of moving image information provides Drosophila hyperacute vision. *Elife*. 2017; 6: pp. 1–149

Kalitzeos, A., Michaelides, M., and Dubra, A. Minimum intensity projection of embossed quadrant-detection images for improved photoreceptor mosaic visualisation. *Front. Ophthalmol.* 2024; 4 (March): pp. 1–7

Kemppainen, J., Mansour, N., Takalo, J., and Juusola, M. High-speed imaging of light-induced photoreceptor microsaccades in compound eyes. *Commun. Biol.* 2022; 5 (1): pp. 1–16

Kemppainen, J., Scales, B., Razban Haghighi, K., Takalo, J., Mansour, N., McManus, J., Leko, G., Saari, P., Hurcomb, J., Antohi, A., Suuronen, J.-P., Blanchard, F., Hardie, R. C., Song, Z., Hampton, M., Eckermann, M., Westermeier, F., Frohn, J., Hoekstra, H., Lee, C.-H., Huttula, M., Mokso, R., and Juusola, M. Binocular mirror-symmetric microsaccadic sampling enables Drosophila hyperacute 3D vision. *Proc. Natl. Acad. Sci. U. S. A.* 2022; 119 (12): pp. 1–12

Kiorpes, L., Kiper, D. C., and Movshon, J. A. Contrast sensitivity and vernier acuity in amblyopic monkeys. *Vision Res.* 1993; 33 (16): pp. 2301–2311

Knutsen, P. M., Pietr, M., and Ahissar, E. Haptic object localization in the vibrissal system: Behavior and performance. *J. Neurosci.* 2006; 26 (33): pp. 8451–8454

Ko, H. K., Poletti, M., and Rucci, M. Microsaccades precisely relocate gaze in a high visual acuity task. *Nat. Neurosci.* 2010; 13 (12): pp. 1549–1554

Kuang, X., Poletti, M., Victor, J. D., and Rucci, M. Temporal encoding of spatial information during active visual fixation. *Curr. Biol.* 2012; 22 (6): pp. 510–514

Li, K. Y., Tiruveedhula, P., and Roorda, A. Intersubject variability of foveal cone photoreceptor density in relation to eye length. *Investig. Ophthalmol. Vis. Sci.* 2010; 51 (12): pp. 6858–6867

Lin, Y.-C., Intoy, J., Clark, A. M., Rucci, M., and Victor, J. D. Cognitive influences on fixational eye movements. *Curr. Biol.* 2023; 33 (8): pp. 1606–1612

Lukyanova, V., Gutnikov, A., Witten, J. L., and Harmening, W. Minimal retinal slip required for maximum visual acuity. *Press*. 2025;:

Malevich, T., Buonocore, A., and Hafed, Z. M. Rapid stimulus-driven modulation of slow ocular position drifts. *Elife*. 2020; 9: pp. 1–21

Marsack, J. D., Thibos, L. N., and Applegate, R. A. Metrics of optical quality derived from wave aberrations predict visual performance. *J. Vis.* 2004; 4 (4): p. 8

McCamy, M. B., Jazi, A. N., Otero-Millan, J., Macknik, S. L., and Martinez-Conde, S. The effects of fixation target size and luminance on microsaccades and square-wave jerks. *PeerJ*. 2013; e9 (1): pp. 1–12

McCamy, M. B., Otero-Millan, J., Di Stasi, L. L., Macknik, S. L., and Martinez-Conde, S. Highly informative natural scene regions increase microsaccade production during visual scanning. *J. Neurosci.* 2014; 34 (8): pp. 2956–2966

Mills, M., Hollingworth, A., Van der Stigchel, S., Hoffman, L., and Dodd, M. D. Examining the influence of task set on eye movements and fixations. *J. Vis.* 2011; 11 (8): pp. 1–15

Morgan, J. I. W., Chui, T. Y. P., and Grieve, K. Twenty-five years of clinical applications using adaptive optics ophthalmoscopy [Invited]. *Biomed. Opt. Express*. 2023; 14 (1): pp. 387–428

Morgan, M. J. and Aiba, T. S. Vernier acuity predicted from changes in the light distribution of the retinal image. *Spat. Vis.* 1985; 1 (2): pp. 151–161

Murphy, K. and Mitchell, D. Vernier acuity of normal and visually deprived cats. *Vis. Res*. 1991; 31 (2): pp. 253–266

Nghiem, T.-A. E., Witten, J. L., Dufour, O., Harmening, W. M., and Azeredo da Silveira, R. Fixational eye movements as active sensation for high visual acuity. *Proc. Natl. Acad. Sci.* 2025; 122 (6): pp. 1–8

Opwonya, J., Doan, D. N. T., Kim, S. G., Kim, J. I., Ku, B., Kim, S., Park, S., and Kim, J. U. Saccadic eye movement in mild cognitive impairment and Alzheimer's disease: A systematic review and meta-analysis. *Neuropsychol. Rev.* 2022; 32 (2): pp. 193–227

Poletti, M., Aytekin, M., and Rucci, M. Head-Eye Coordination at a Microscopic Scale. *Curr. Biol.* 2015; 25 (24): pp. 3253–3259

Purpura, K, Tranchina, D, Kaplan, E, and Shapley, R. M. Light adaptation in the primate retina: analysis of changes in gain and dynamics of monkey retinal ganglion cells. *Vis. Neurosci.* 1990; 4 (1): pp. 75–93

Putnam, N. M., Hofer, H. J., Doble, N., Chen, L., Carroll, J., and Williams, D. R. The locus of fixation and the foveal cone mosaic. *J. Vis.* 2005; 5 (7): pp. 632–639

Rabin, J., Goodroe, K., Hood, A., Duka, C., Dunmon, K., Bouaphavong, D., and Truong, T. Minimum visual acuity: a new cone specific clinical test. *Eye*. 2024; (September): pp. 14–16

Ratnam, K., Domdei, N., Harmening, W. M., and Roorda, A. Benefits of retinal image motion at the limits of spatial vision. *J. Vis.* 2017; 17 (1): pp. 1–11

Rock, I. and Harris, C. S. Vision and touch. *Sci. Am.* 1967; 216 (5): pp. 96–104

Rossi, E. and Roorda, A. The relationship between visual resolution and cone spacing in the human fovea. *Nat Neurosci*. 2010; 13 (2): pp. 156–157

Rossi, E., Weiser, P., Tarrant, J., and Roorda, A. Visual performance in emmetropia and low myopia after correction of high-order aberrations. *J. Vis.* 2007; 7 (8): pp. 1–14

Rucci, M., Iovin, R., Poletti, M., and Santini, F. Miniature eye movements enhance fine spatial detail. *Nature*. 2007; 447 (7146): pp. 851–854

Rucci, M. and Victor, J. D. The unsteady eye: An information-processing stage, not a bug. *Trends Neurosci.* 2015; 38 (4): pp. 195–206

Schira, M. M., Tyler, C. W., Breakspear, M., and Spehar, B. The foveal confluence in human visual cortex. *J. Neurosci.* 2009; 29 (28): pp. 9050–9058

Schira, M. M., Wade, A. R., and Tyler, C. W. Two-dimensional mapping of the central and parafoveal visual field to human visual cortex. *J. Neurophysiol.* 2007; 97 (6): pp. 4284–4295

Seymoure, P. and Juraska, J. M. Vernier and grating acuity in adult hooded rats: the influence of sex. *Behav. Neurosci.* 1997; 111 (4): pp. 792–800

Shao, K., Hu, X., Kleineidam, L., Stark, M., Altenstein, S., Amthauer, H., Boecker, H., Buchert, R., Buerger, K., Butryn, M., Cai, Y., Cai, Y., Cosma, N. C., Chen, G., Chen, Z., Daamen, M., Drzezga, A., Düzel, E., Essler, M., Ewers, M., Fliessbach, K., Gaertner, F. C., Glanz, W., Guo, T., Hansen, N., He, B., Janowitz, D., Kilimann, I., Krause, B. J., Lan, G., Lange, C., Laske, C., Li, Y., Li, R., Liu, L., Lu, J., Meng, F., Munk, M. H., Peters, O., Perneczky, R., Priller, J., Ramirez, A., Rauchmann, B. S., Reimold, M., Rominger, A., Rostamzadeh, A., Roy-Kluth, N., Schneider, A., Spottke, A., Spruth, E. J., Sun, P., Teipel, S., Wang, X., Wei, M., Wei, Y., Wiltfang, J., Yan, S., Yang, J., Yu, X., Zhang, M., Zhang, L., Wagner, M., Jessen, F., Han, Y., and Kuhn, E. Amyloid and SCD jointly predict cognitive decline across Chinese and German cohorts. *Alzheimer's Dement.* 2024; 20 (9): pp. 5926–5939

Skoczenski, A. M. and Good, W. V. Vernier acuity is selectively affected in infants and children with cortical visual impairment. *Dev. Med. & Child Neurol.* 2004; 46 (8): pp. 526–532

Snodderly, D. M., Kagan, I., and Moshe, G. Selective activation of visual cortex neurons by fixational eye movements: Implications for neural coding. *Vis. Neurosci.* 2001; 18 (2): pp. 259–277

Sperling, R., Mormino, E., and Johnson, K. The evolution of preclinical Alzheimer's disease: Implications for prevention trials. *Neuron*. 2014; 84 (3): pp. 608–622

Tan, Y., Tong, X., Chen, W., Weng, X., He, S., and Zhao, J. Vernier but not grating acuity contributes to an early stage of visual word processing. *Neurosc Bull.* 2018; 34 (3): pp. 517–526

Volkmann, A. W. Neue Beiträge zur Physiologie des Gesichtssinnes: Breitkopf und Härtel, 1836

Wang, Y., Bensaid, N., Tiruveedhula, P., Ma, J., Ravikumar, S., and Roorda, A. Human foveal cone photoreceptor topography and its dependence on eye length. *Elife*. 2019; 8: pp. 1–21

Wang, Y., Bensaid, N., Tiruveedhula, P., Ma, J., Roorda, A., and Ravikumar, S. (2018). The Relationship between Cone Density and Axial Length: CAL Study. In: *Annu. Meet. Assoc. Res. Vis. Ophthalmol.* Berkeley, California, United States.

Watson, A. B. and Ahumada, A. J. Predicting visual acuity from wavefront aberrations. *J. Vis.* 2008; 8 (4): pp. 1–19

Wells-Gray, E. M., Choi, S. S., Bries, A., and Doble, N. Variation in rod and cone density from the fovea to the mid-periphery in healthy human retinas using adaptive optics scanning laser ophthalmoscopy. *Eye*. 2016; 30 (8): pp. 1135–1143

Westheimer, G. Visual acuity: information theory, retinal image structure and resolution thresholds. *Prog. Retin. Eye Res.* 2009; 28 (3): pp. 178–86

Westheimer, G. and McKee, S. P. Spatial configurations for visual hyperacuity. *Vision Res.* 1977; 17 (8): pp. 941–947

Wilk, M. A., Dubis, A. M., Cooper, R. F., Summerfelt, P., Dubra, A., and Carroll, J. Assessing the spatial relationship between fixation and foveal specializations. *Vision Res.* 2017; 132: pp. 53–61

Williams, D. R., Burns, S. A., Miller, D. T., and Roorda, A. Evolution of adaptive optics retinal imaging [Invited]. *Biomed. Opt. Express*. 2023; 14 (3): pp. 1307–1338

Williams, R. A., Enoch, J. M., and Essock, E. A. The resistance of selected hyperacuity configurations to retinal image degradation. *Investig. Ophthalmol. Vis. Sci.* 1984; 25 (4): pp. 389–399

Zhang, C., Kim, Y. J., Silverstein, A. R., Hoshino, A., Reh, T. A., Dacey, D. M., and Wong, R. O. Circuit reorganization shapes the developing human foveal midget connectome toward single-cone resolution. *Neuron*. 2020; 108 (5): pp. 905–918

Zhang, T., Godara, P., Blanco, E. R., Griffin, R. L., Wang, X., Curcio, C. A., and Zhang, Y. Variability in human cone topography assessed by adaptive optics scanning laser ophthalmoscopy. *Am. J. Ophthalmol.* 2015; 160 (2): pp. 290–300

5 Acknowledgement

This PhD thesis is the result of my scientific work at the AO Vision Lab in Bonn. I would like to take this opportunity to thank some people for their valuable support during my scientific journey.

First of all, I want to thank my supervisor Dr. Wolf Harmening. Thank you for convincing me to start a PhD, for your continuous support and feedback. Your energetic and optimistic nature has always provided a positive atmosphere and a sense of "anything is doable". Also, I feel like your inventive scientific mindset and my in the beginning sometimes a bit too realistic approach to next steps, together made a good mixture for new and finally feasible ideas. Working in your lab and everything it involved not only has enriched my scientific skills but also challenged and expanded some personal qualities.

I would like to thank Prof. Henning Boecker for agreeing to be the second supervisor for my thesis and Prof. Frank G. Holz for being a part of the committee and for the opportunity to work on those interesting projects and write the thesis in his eye hospital. I also want to thank Prof. Ulrich Ettinger for completing the committee and for contributing another perspective on the analysis of eye movements.

I want to thank Prof. Andrew Metha and Philipp Bedggood for being very welcoming and giving me another perspective into the "AO world" during my 2 months research stay in your lab in Melbourne. Thanks for giving me an overall unforgettable time in Australia, which gave me a lot of new insights and motivation.

Many thanks to Dr. Niklas Domdei for moving the first stones out of the way before I started in the lab and for being the one who provided a different perspective.

I want to thank Veronika Lukyanova, my first female colleague, for enriching the second part of this journey scientifically and personally.

I also want to thank all AO Vision Lab members: Michael Linden, Lennart Domdei, Julius Ameln, Aleksandr Gutnikov, and Maximilian Freiberg not only for intellectual support, but for making it an overall unforgettable time.

Many thanks to the whole "Augenkeller"-Team: Johanna Meyer, Sarah Schmidt, Kirsten Harmening, Janine Marx, Claudine Strack, Mona Senner and Petra Larsen, Sarah Kunze, Julia Pawlik, Kritika Sharma, Rouhollah Habibey, and Johannes Striebel for scientific ex-

change, but also for the many great events and experiences inside and outside the laboratory, which helped to create a great working atmosphere and which I will always enjoy to look back to.

I want to thank Prof. Peter Baumbach, Prof. Ulrich Schiefer, Prof. Annemarie Buser and Prof. Annette Limberger for being professionally great and always approachable teachers who paved the way with their motivating and inspiring personalities.

I also want to thank Johanne Forkel, a very good friend, who was a mental support and endlessly understanding, and Judith Ungewiß, who were former study colleagues, with whom together I did the first steps towards scientific working during our smaller scientific project works for the Bachelor and Master degree.

A special thank you to my parents, grandparents, husband, and son for your continuous support in so many ways and open ears, for making time when we did not have it, and for always making me feel that you believe in me without doubt!

Last but definitely not least, I want to thank all participants of my PhD projects for their time, patience, and motivation in the often time-consuming experiment sessions.

Thank you all!

6 Statement

The work contained in this thesis has not been previously submitted for a degree or diploma at any higher education institution. To the best of my knowledge and belief, the thesis contains no material previously published or written by another person except where due references are made.

UNIVERSITÄT BONN

ukb universitäts klinikum bonn

Faculty of Medicine – University of Bonn
PhD doctoral examination procedure

For the publication for which the doctoral student is the lead author, the doctoral student must have undertaken the **predominant share** of **the planning of the academic work, data collection, evaluation, and interpretation**, and have written the **first version of the manuscript himself**.

For the publications for which the doctoral student is a co-author, the doctoral student must have taken on a significant share of the **planning of the academic work, data collection, evaluation and interpretation**. Relevant proof of the work carried out by the doctoral student is to be submitted to the publisher (sections 6(3), 7(1)).

Thesis title: Precision and limits of human vision - How visual resolution depends on ocular optics and spatiotemporal sampling characteristics of the foveolar photoreceptor mosaic

The doctoral student, Jenny Lorén Witten (nee Reiniger), has authored the above-mentioned doctoral thesis in the Department of Ophthalmology under the supervision of *Dr. Wolf M. Harmening* .

Please specify your **own share of work** as well as the share of work taken on by **others** in **each publication**, using the following criteria.

(One table specifies one publication.)

Title of publication: Habitual higher order aberrations affect Landolt but not Vernier acuity	
Please specify your **own share** in the following areas:	Please specify the **share of others** in the following areas:
Planning of the academic work: 20 %	***Planning of the academic work:*** 80 %
Data collection 0 %	***Data collection*** 100 %
Evaluation 90 %	***Evaluation*** 10 %
Interpretation 90 %	***Interpretation*** 10 %

Please tick the relevant box:

☒ ***The doctoral student is the lead author and has written the first version of the manuscript himself/herself***

☐ ***The doctoral student is a co-author***

Title of publication: Human gaze is systematically offset from the center of cone topography	
Please specify your **own share** in the following areas:	Please specify the **share of others** in the following areas:
Planning of the academic work: 90 %	***Planning of the academic work:*** 10 %
Data collection 100 %	***Data collection*** 0 %
Evaluation 100 %	***Evaluation*** 0 %
Interpretation 90 %	***Interpretation*** 10 %
Please tick the relevant box:	
☒ ***The doctoral student is the lead author and has written the first version of the manuscript himself/herself***	
☐ ***The doctoral student is a co-author***	

Title of publication: Sub cone visual resolution by active, adaptive sampling of the human foveola	
Please specify your **own share** in the following areas:	Please specify the **share of others** in the following areas:
Planning of the academic work: 90 %	***Planning of the academic work:*** 10 %
Data collection 100 %	***Data collection*** 0 %
Evaluation 100 %	***Evaluation*** 0 %
Interpretation 90 %	***Interpretation*** 10 %
Please tick the relevant box:	
☒ ***The doctoral student is the lead author and has written the first version of the manuscript himself/herself***	
☐ ***The doctoral student is a co-author***	

Bonn, 02.02.2025

_____	_____	_____
Place, Date	Signature doctoral student	Signature primary supervisor

7 Curriculum vitae

Full name	Jenny Lorén Witten, née Reiniger
Date of birth	February 9, 1991
Nationality	German
PhD Office Address	Department of Ophthalmology University of Bonn Ernst-Abbe-Str. 2 53127 Bonn, Germany
Office Phone	+ 49 (0) 288-287-19818
E-mail	jennylwitten@gmail.com

Education and academic positions

06/2024 – Now	**Carl Zeiss Vision International GmbH**, Tübingen, Germany Researcher in Physiological Optics and Vision Science, Zeiss Vision Science Lab Group Leader: Prof. Siegfried Wahl
05/2017 – Now	**University of Bonn**, Bonn, Germany PhD student, Faculty of Medicine (Supervisor: Dr. Wolf Harmening) Member of the Bonn International Graduate School (BIGS) Neuroscience
03/2016 – 05/2024	**University Eye Hospital Bonn**, Bonn, Germany Research Associate, Adaptive Optics Vision Lab Group Leader: Dr. Wolf Harmening
03/2014 – 02/2016	**Aalen University of Applied Science**, Aalen, Germany Master of Science, Ophthalmic Optics and Psychophysics (grade: 1.3) Joint Master thesis: *Comparative study of visual field size and wearer comfort of progressive addition lenses with individualized designs and standard designs*
09/2009 – 02/2014	**Aalen University of Applied Science**, Aalen, Germany Bachelor of Science, Optometry and Audiology (grade: 1.6)
08/2001 – 07/2009	**Philipp-Melanchthon-Gymnasium**, Herzberg (Elster), Germany High-school diploma (grade: 2.0)

Research experience

10/2019 – 12/2019	**Visiting Research Scholar**, Laboratory of Prof. Andrew Metha, Department of Optometry and Vision Sciences, University of Melbourne, Australia
04/2015 – 05/2015	**Visiting Research Scholar**, Research group of Prof. Chris A. Johnson, Department of Ophthalmology and Visual Sciences, University of Iowa Hospitals and Clinics, Iowa City, USA

Research interests

Ophthalmic optics; Optical, physiological and perceptual characteristics of human vision; Visual neuroscience

PhD methods: Adaptive optics, High-resolution retinal imaging, Visual psychophysics, Behavioral testing

---

Teaching activity

10/2016 – 06/2020	Lectures *Anatomy of the eye* for undergraduate orthoptists, University Eye Hospital Bonn

---

Research grants and awards

2022	Research award for the publication „Human gaze is systematically offset from the center of cone topography“ (Current Biology, September 2021), Stiftung Auge
2020	EYENovative research award, Novartis Pharma GmbH
2019	BM-AXIS stipend for a 2-month research stay in the Department of Optometry and Vision Sciences, University of Melbourne, Australia
2019	The Rank Prize Funds travel grant for participating in the Symposium on Adaptive Optics Retinal Imaging: New Opportunities for Visual Neuroscience, Grasmere, UK
2019	DAAD Travel grant for participating in the Annual Meeting of the Association for Research in Vision and Ophthalmology (ARVO) in Vancouver, Canada
2016	Travel stipend of Heidelberg Engineering GmbH for participating in the Winter School on Medical Optics in Pichl, Austria
2015	PROMOS stipend awarded by the DAAD for an international student internship at the University of Iowa City, Department of Ophthalmology and Visual Sciences, Iowa, USA

Publications

(* denotes equal contributions)

Peer-reviewed journal articles

Nghiem TAE*, **Witten JL ***, Dufour O, Harmening WM & Silveira RA (2025) Fixational eye movements as active sensation for high visual acuity. *PNAS*. *122*(6). doi 10.1073/pnas.2416266122

Witten JL, Lukyanova V & Harmening WM (2024) Sub-cone visual resolution by active, adaptive sampling in the human foveola. *eLife. Oct 29*(13): 1-19. doi 10.7554/eLife.98648

Domdei N, Ameln J, Gutnikov A, **Witten JL**, Holz FG, Wahl S & Harmening WM (2023) Cone density is correlated to outer segment length and retinal thickness in the human foveola. *Invest Ophthalmol Vis Sci*. *64*(15): 1-11. doi 10.1167/iovs.64.15.11

Wynne N, Cava JA, Gaffney M, Heitkotter H, Scheidt A, **Reiniger JL**, Grieshop J, Yang K, Harmening WM, Cooper RF & Carroll J (2022) Intergrader agreement of foveal cone topography measured using adaptive optics scanning light ophthalmoscopy. *Biomed Opt Express*. *13*(8):4445-4454. doi 10.1364/BOE.460821

Ameln J, **Reiniger JL**, Hess K, Holz FG & Harmening WM (2022) Supernormal foveal photoreceptor density in Alport syndrome: A case report. *Eur J Ophthalmol*. *33*(4):NP51-NP54. doi 10.1177/11206721221093197

Reiniger JL, Domdei N, Holz FG, & Harmening WM (2021) Human gaze is systematically offset from the center of cone topography. *Curr Biol*. *31*(18):4188-4193. doi 10.1016/j.cub.2021.07.005

Domdei N, **Reiniger JL**, Holz FG & Harmening WM (2021) The relationship between visual sensitivity and eccentricity, cone density and outer segment length in the human foveola. *Invest Ophthalmol Vis Sci*. *62*(9): 1-16. doi 10.1167/iovs.62.9.31

Domdei N, Linden M, **Reiniger JL**, Holz FG & Harmening WM (2019) Eye tracking-based estimation and compensation of chromatic offsets for multi-wavelength retinal microstimulation with foveal cone precision. *Biomedical Optics Express*. *10*(8): 4126-4141. doi 10.1364/BOE.10.004126

Reiniger JL, Lobecke AC, Sabesan R, Bach M, Verbakel F, de Brabander J, Holz FG, Berendschot TTJM & Harmening WM (2019) Habitual higher order aberrations affect Landolt but not Vernier acuity. *Journal of Vision*.

Domdei N*, Domdei L*, **Reiniger JL**, Linden M, Holz FG, Roorda A, & Harmening WM (2018) Ultra-high contrast retinal display system for single photoreceptor psychophysics. *Biomedical Optics Express*. *9*(1): 157-172. doi 10.1364/BOE.9.000157

Reiniger JL*, Domdei N*, Pfau M, Müller PL, Holz FG, & Harmening WM (2017) Potential of adaptive optics for the diagnostic evaluation of hereditary retinal diseases. *Klinische Monatsblätter Für Augenheilkunde*. *234*(3): 311–319. doi 10.1055/s-0043-100631

Reiniger JL, Domdei N, Holz FG, & Harmening WM (2017) Technical principles of adaptive optics in ophthalmology. *Der Ophthalmologe*. *114*(3): 198–205. doi 10.1007/s00347-017-0440-z

Domdei N, **Reiniger JL**, Pfau M, Charbel Issa P, Holz FG, & Harmening WM (2017) Histology in the living eye: Non-invasive microscopic structure and functional analysis of the retina with adaptive optics. *Der Ophthalmologe. 114*(3): 206–214. doi 10.1007/s00347-016-0411-9

Reiniger JL*, Forkel J*, Muschielok A, Welk A, Seidemann A, & Baumbach P (2017) Personalized progressive addition lenses: Correlation between performance and design. *Optometry and Vision Science*. *94*(2): 208–218. doi 10.1097/OPX.0000000000001016

Conference talks and posters

Jenks SK, **Witten JL**, Moon B, Clark AM, Kapisthalam S, Harmening WM, Poletti M (2023) Asymmetries in fine spatial vision and cone density within the foveola. *Annual Meeting of the Vision Sciences Society (VSS)*, St. Pete Beach, USA

Reiniger JL, Harmening WM (2021) On the relationship between fixation behavior and the cone photoreceptor mosaic. *Young Researcher Vision Camp*, Leibertingen, Germany

Reiniger JL, Harmening WM (2019) Does the foveal photoreceptor mosaic limit visual acuity?. *Symposium on Adaptive Optics Retinal Imaging: New Opportunities for Visual Neuroscience (The Rank Prize Funds)*, Grasmere, UK

Reiniger JL, Domdei N, Linden M, Holz FG, Harmening WM (2019) Relationship between the foveal photoreceptor mosaic and adaptive optics corrected visual acuity. *Annual Meeting of the Association for Research in Vision and Ophthalmology (ARVO)*, Vancouver, Canada

Reiniger JL, Holz FG, Harmening WM (2018) Korrelation zwischen fovealer Rezeptordichte und maximaler Sehschärfe. *Annual Meeting of the German Ophthalmology Society (DOG)*, Bonn, Germany

Reiniger JL, Sheehy C, Domdei N, Holz FG, Roorda A, Harmening WM (2017) Photoreceptor-resolved visual psychophysics with and without adaptive optics. *European Conference on Visual Perception (ECVP)*, Berlin, Germany

Johnson CA, Upadhyaya S, Thapa S, Robin A, **Reiniger JL**, Forkel J (2016) Tablet visual field screening: comparison of test and exam conditions. *International Visual Field and Imaging Symposium (IPS)*, Udine, Italy